Dendritic arithmetic and dynamics for neuromorphic temporal pattern detection

Auteur : Halbach, Quentin
Promoteur(s) : Franci, Alessio
Faculté : Faculté des Sciences appliquées
Diplôme : Master : ingénieur civil électricien, à finalité spécialisée en Neuromorphic Engineering
Année académique : 2023-2024
URI/URL : http://hdl.handle.net/2268.2/20133

Master thesis

in the degree program

Electrical Civil Engineering

Dendritic Arithmetic and Dynamics for Neuromorphic Temporal Pattern Detection

Submitted by

Halbach Quentin

Matr. : S191982

Academic year : 2023-2024

Faculty of Applied Sciences at University of Liege

University supervisor : Franci Alessio

Acknowledgements

I would like to thank my thesis supervisor, Pr. Alessio Franci, for his steadfast support and guidance throughout this research journey. His expertise and insightful feedback have been essential in shaping the direction and depth of this thesis. Pr. Alessio Franci's dedication to my academic and personal growth has been truly inspiring.

I am grateful to my parents for their unwavering support and encouragement throughout my academic journey. Their belief in my abilities has been a constant source of motivation and strength.

A special thank you to my father who not only provided emotional support but also took the time to review my thesis and offer invaluable advice. His keen insights and constructive feedback have been crucial in refining my work and ensuring its clarity and coherence.

Abstract

This thesis investigates the utilization of event-based camera technology to detect motion within a grid of pixels, emphasizing the development of models readily adaptable to neuromorphic circuits. Event-based cameras, renowned for their asynchronous sensing mechanism, offer distinct advantages over conventional frame-based cameras, boasting high temporal resolution and minimal latency. Leveraging this technology, the thesis introduces novel algorithms and methodologies to process the stream of events generated by the camera, with a focus on spatio-temporal filtering to exploit the event-based camera's advantages.

The research begins with an in-depth examination of event-based camera principles, emphasizing the generation of events based on brightness changes, while bypassing detailed hardware functioning as this thesis focuses on the motion detection model's mathematical design. Subsequently, existing movement detection algorithms are reviewed comprehensively, identifying limitations and areas for enhancement within the event-based camera framework.

Building upon this groundwork, the thesis presents innovative approaches for movement detection, tailored to exploit the event-based camera's characteristics and inspired by dendritic spike generation and the non-linear properties of dendrites. Two distinct methodologies are investigated, structured following the organization of dendritic branches, where each dendritic compartment receives events from a specific pixel. The first approach leverages dendritic arithmetic with additive operations, while the second integrates both additive and multiplicative arithmetic operations, mimicking the excitation and inhibition between dendritic compartments. Equilibrium and nullcline analyses are performed to optimize model parameters. Results reveal the first approach's susceptibility to event shape dependency, while the second approach exhibits robustness with minimal dependency on event shape.

Further exploration includes the study of consecutive movement detection and the development of a bidirectional movement detection model using the second approach. Additionally, the extension of the working model to a 2-dimensional setup is conducted to detect 2-dimensional movements effectively.

Validation of proposed methodologies is achieved through extensive simulations, where the limitations of the designed models are investigated, and the range of parameter values under which the models function optimally is determined. These simulations provide insights into the robustness and adaptability of the developed approaches across various environmental conditions and scenarios.

The thesis concludes with discussions on potential applications and implications of the developed movement detection system in domains such as targets of interest tracking or moving obstacles detection. By harnessing event-based camera technology and drawing inspiration from neural computation, this research contributes to advancing movement detection capabilities, laying the foundation for future developments in visual sensing and perception.

Table of Contents

1. Introduction

1.1. Overview of event-based Camera Technology

In recent years, the field of motion detection in visual scenes has witnessed the emergence of a groundbreaking technology known as neuromorphic vision sensors or event-based cameras. Inspired by the biological mechanisms of the human eye and brain, this innovative technology offers a fundamentally different approach to capturing visual information compared to conventional cameras. Consequently, it presents significant advantages in the realm of computer vision, particularly in motion detection, when contrasted with traditional technologies.

Unlike conventional cameras, which capture frames synchronously, event-based cameras operate asynchronously. They detect and transmit changes in pixel intensity in real time, resulting in more efficient frame processing and a reduced volume of data. This asynchronous operation provides several key advantages [1]:

- High-temporal resolution: Event-based cameras can capture rapid motions in the visual scene without succumbing to motion blur. They continuously report changes in the scene on a per-pixel basis as they occur.
- Low power consumption: By transmitting only the brightness changes perceived by the pixels, event-based cameras eliminate redundant data transmission. Consequently, power is consumed only to process changing pixels.
- Low latency: Each pixel of the event-based camera operates independently, transmitting brightness changes as soon as they are detected.
- High dynamic range: Event-based cameras boast a dynamic range exceeding 120 $[dB]$, whereas conventional cameras typically have a dynamic range of around 60 $[dB]$. This allows event-based cameras to capture visual scene information under varying

light intensities.

1.1.1. From frames to events in event-based cameras

Conventional cameras utilize an image acquisition process to capture visual scene information in the form of frames. These cameras are equipped with sensors comprising millions of individual photosensitive elements, or pixels. During the exposure period, light passes through the camera's lens, illuminating the sensor. As photons interact with the sensor's photosensitive elements, they accumulate an electrical charge proportional to the intensity of the incident light. Subsequently, an Analog-to-Digital converter translates this accumulated charge into a digital signal, which is used to construct the digital image [2].

In contrast, event-based cameras, inspired by biological mechanisms, acquire visual information in a fundamentally different manner from traditional cameras. Unlike conventional cameras, which capture frames at a fixed rate synchronized with an external clock, event-based cameras consist of a two-dimensional array of independent pixels. Each pixel responds to changes in scene brightness asynchronously, registering these changes as events instead of continuously measuring brightness at a fixed rate [1].

This asynchronous operation of event-based cameras is rooted in the functioning of individual pixels. Each pixel maintains a log intensity, representing the change in brightness it detects during event transmission, and continually monitors for significant changes in brightness. When the difference exceeds a certain threshold, the pixel transmits an event containing information about its position (x, y), time t, and event polarity.

Consequently, the output of event-based cameras comprises a digital sequence of events transmitted by its pixels, reflecting the magnitude of brightness changes in the scene. Notably, the event transmission rate of this technology varies with the perceived motion velocity, resulting in a higher transmission rate for faster motion.

The difference in the output between a conventional camera and an event-based camera for a rotating black dot can be seen in Figure 1.1.

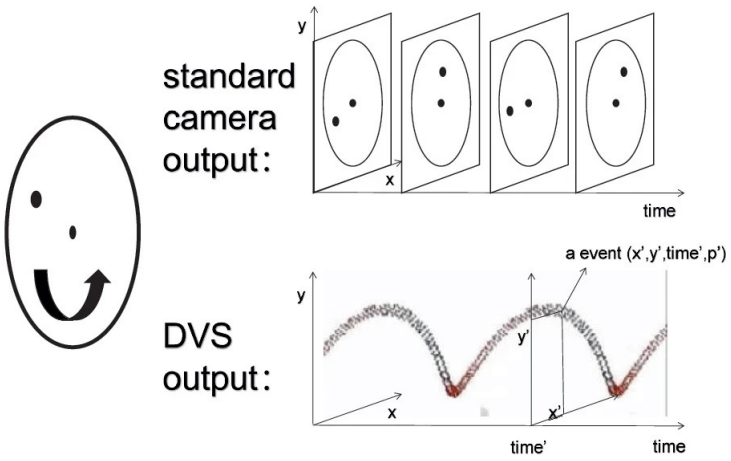

Figure 1.1.: Output comparison between a conventional camera (up) and an event-based camera (down). The conventional camera outputs a frame containing the whole visual scene while the event-based camera outputs only the rotating black dot (events). [3]

A comparison between the frame obtained using event-based cameras and the one using conventional cameras is shown in Figure 1.2.

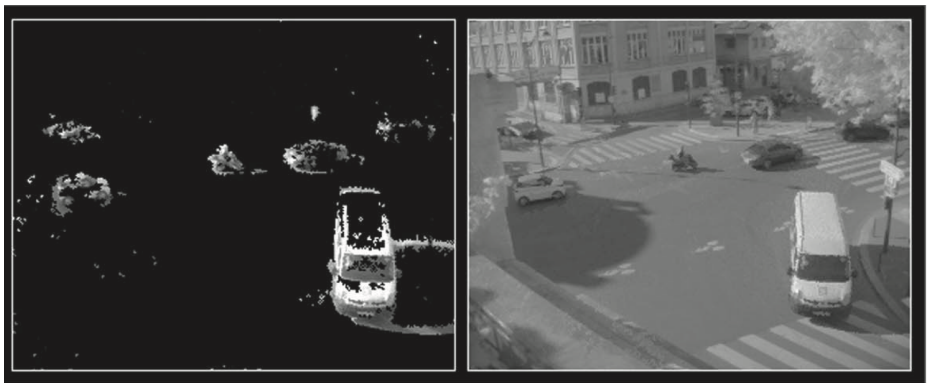

Figure 1.2.: Comparison of the frame obtained by an event-based camera (left) and by a conventional camera (right). Only parts of the visual scene having high brightness changes are detected by the event-based camera. [4]

1.1.2. Video feature extraction as temporal event pattern detection

Traditional motion detection algorithms applied to images captured by conventional cameras rely on background subtraction techniques. These algorithms are commonly employed to identify motion in videos recorded by stationary cameras. The underlying principle of

background subtraction involves analyzing the disparity between the current frame and a reference frame, known as the "background frame," which represents the visual scene without any moving objects. This reference frame is regularly updated to accommodate variations in scene luminance. However, these algorithms necessitate the analysis of each frame in the video to detect potential object motions, which can be inefficient, particularly in scenes with minimal changes [5].

These conventional algorithms are inherently limited by the synchronous nature of frame acquisition in conventional cameras. They consume considerable computational resources and suffer from a lack of temporal resolution due to their reliance on frame-based processing.

In contrast, to address the shortcomings of conventional cameras and associated algorithms, this master's thesis introduces innovative methodologies and algorithms to effectively process the stream of events generated by event-based cameras for motion detection in visual scenes.

The motion detection algorithms developed in this thesis fully leverage the advantages offered by event-based cameras. These cameras are better suited for efficient motion detection, as asynchronous computing inherently retains temporal information without the necessity to explicitly encode time. When an object moves within the field of view of an event-based camera, pixels along the motion trajectory detect variations in brightness and generate corresponding events. These events, temporally separated in the direction of motion, form a temporal event pattern. An illustration is provided in Figure 1.3.

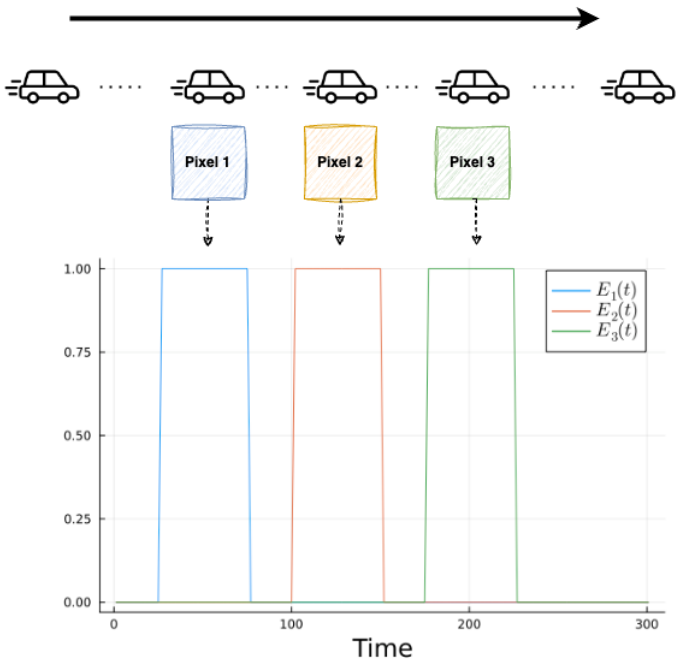

Figure 1.3.: Illustration of a constructed temporal events pattern generated by three consecutive pixels in the motion direction. E_i is the event generated by the pixel i. The moving car symbolizes the linear motion.

The algorithm proposed in this thesis diverges from traditional motion detection algorithms by focusing solely on the constructed temporal event pattern. The core principle of the algorithm's model is to assign mathematical units to each pixel, which receive events generated by their respective pixels and produce a response only if the preceding pixels have generated events in the correct order corresponding to the object's motion.

The algorithm proposed in this thesis diverges from traditional motion detection algorithms by focusing solely on the constructed temporal event pattern. The core principle of the algorithm is to assign a dendritic compartment to each pixel. The dendritic compartments take as input the events generated by the pixel to which they are connected. A dendritic compartment generates a response to an event only if all preceding compartments have already produced a response for the same object.

The structure of the model can be seen in Figure 2.7 for an array of n pixels.

1.1.3. Neuromorphic Application of Motion Detection in event-based Cameras

A motion detection system leveraging event-based cameras has been practically implemented in neuromorphic circuits, as illustrated in the paper by Milde et al. (2018) [6] . This system employs both additive and multiplicative arithmetic operations in its circuit dynamics, demonstrating a functional application similar to the approach taken in this thesis. The system includes a DPI (Differential Pair Integrator) synapse and a DPI neuron. The innovative aspect of this paper is that the output of the DPI synapse is multiplied by an adaptive gain to serve as the input to the DPI neuron, thereby incorporating multiplicative arithmetic operations alongside additive ones.

This system introduces an innovative method called the spiking elementary motion detector (sEMD) to process event streams from event-based cameras. The sEMD utilizes correlations within the event-based sensor data, particularly estimating the time it takes for an event to traverse the camera's field of view and encoding this information into a burst of spikes.

This encoding strategy is inspired by the notion that the burst's size and duration directly reflect the temporal correlation between adjacent pixels while the number of spikes within a burst is proportional to the speed of the events. Notably, this approach capitalizes on the asynchronous operation inherent in event-based cameras, enabling parallel computation while achieving low power consumption and minimal latencies.

This thesis is therefore a mathematical generalization of the paper [6] using an innovative approach to detect motion in the visual field of an event-based camera. Nonetheless, the system designed in this master thesis remains amenable to neuromorphic implementation.

1.2. Problem formulation

This master's thesis aims to introduce novel methodologies and algorithms for efficiently processing the stream of events generated by event-based cameras to detect motion in visual scenes. These models have to prioritize spatial filtering and should be easily adaptable to neuromorphic circuits to harness the advantages offered by event-based cameras.

The development of models for both one-dimensional and two-dimensional movements will need to be undertaken to identify accurate temporal event patterns. Additionally, the implemented system must be capable of recognizing successive temporal event patterns, indicating the movement of multiple consecutive objects within the event-based camera's field of view.

A thorough analysis of system parameters, such as the width of events generated by pixels and the delays between events in the temporal event pattern, is necessary. This analysis will determine the range of parameter values in which the system operates optimally and results in only true positive detection of motion.

1.3. Outlines

A comprehensive literature review on the biological functioning of neurons and dendrites has been conducted in Chapter 2 to inform the design of the motion detection system in this thesis. The review highlighted the crucial role of the nonlinear properties of dendrites in discriminating temporal input sequences. Specifically, the combination of additive and multiplicative arithmetic operations in dendritic dynamics, along with inherent negative feedback, contributes to these nonlinear properties. The review focused on the mechanisms and sites of dendritic action potential generation, determining that dendritic spikes are produced in distal dendritic regions and propagate towards the soma. It was found that calcium-dependent conductances, along with NMDA (N-methyl-D-aspartate) receptor-dependent conductances, are primarily responsible for generating dendritic action potentials. Additionally, the literature revealed that neurons exhibit inherent directional selectivity, amplifying their response to sequences of stimuli in the preferred direction while nearly completely inhibiting responses to stimuli in the opposite direction.

The designed motion detection system has been implemented using two distinct approaches: one utilizing solely additive arithmetic operations and another, dendritic-inspired, incorporating both additive and multiplicative arithmetic operations. The latter approach has been found to yield superior performance for the motion detection system (see Section 3.3). A comprehensive analysis of system parameters was conducted to identify the optimal parameter value intervals for system functionality. It was determined that the optimal configuration, which results in only true positive detection, involves large time constants and narrow synaptic input widths.

As the dendritic-inspired approach was not suited to detect successive temporal event patterns, an improvement was introduced in Chapter 4 by incorporating slow local negative feedback into the model's dynamics. This enhancement introduced inherent bistability to the model, enabling the system to accurately identify successive input sequences. The incorporation of slow negative feedback is biologically plausible, as slow negative feedback is widespread in neurons and neuronal circuits through various mechanisms and currents.

In Chapter 5, a bidirectional motion detection system was implemented using both slow local negative feedback and reinforced local positive feedback in the dendritic-inspired model's dynamics. This system could make both positive and negative decisions while resetting its state. Consequently, the model accurately distinguished left-to-right and right-to-left temporal event patterns from incorrect ones in consecutive input sequence configurations.

Chapter 6 describes the extension of the system from a one-dimensional to a two-dimensional model, enabling the effective detection of horizontal, vertical, and diagonal motions within a two-dimensional square grid.

Finally, Chapter 7 evaluates the performance of various models in detecting successive input sequences in a one-dimensional configuration. The improved dendritic-inspired model and the bidirectional model successfully identified consecutive input sequences temporally-separated by an in-between sequence delay, while the basic dendritic-inspired model failed to reset its dynamics regardless of the input sequence order.

2. Dendritic Arithmetic for Temporal Pattern Detection

2.1. Electrical Functioning of the Neuron

To fully grasp the concepts explored within this master's thesis, it is essential to conduct a concise analysis of the structure and function of neurons, which play a fundamental role in biology.

Neurons, specialized cells within the nervous system, are responsible for transmitting information through a combination of electrical and chemical signals [7] [8]. These cellular elements are essential to the functioning of vital nervous system components, such as the brain and spinal cord.

The transmission of information via electrical and chemical signals relies on the structural components of neurons. The cell body, or soma, serves as the central part of the neuron, housing the nucleus and biochemical machinery essential for synthesizing proteins and sustaining cellular processes. It integrates incoming signals received from dendrites and generates outgoing signals along the axon. Our focus here is on the regions of the neuron where electrical impulses are initiated and propagated.

The first region of interest are the dendrites, branching extensions from the cell body, acting as the primary sites for signal reception. Indeed, dendrites act as the main physical surface on which the neuron receives incoming signals. They receive signals, typically neurotransmitters, from other neurons or sensory receptors via synapses.

The second region of interest is the axon, extending away from the soma, which serves

as the neuron's output pathway. It conducts signals away from the soma to other parts of the nervous system. These signals, known as action potentials, are electrochemical in nature.

Dendrites and axons exhibit distinct structural characteristics. Dendritic branches cluster near the soma, forming complex structures resembling trees, while axons extend away from the soma to facilitate communication with other neurons.

Axon terminals, located at the ends of axons, establish synapses with dendrites or somas of neighboring neurons. These synapses are specialized junctions where communication between neurons occurs. Synapses consist of the presynaptic membrane of the axon terminal, the synaptic cleft being a tiny gap between neurons and the postsynaptic membrane of the dendrite or soma of the receiving neuron. Chemical messengers, known as neurotransmitters, released from the presynaptic neuron cross the synaptic cleft to bind with receptors on the postsynaptic neuron, thereby facilitating signal transmission.

The structure of a typical neuron from a vertebrate animal can be seen in Figure 2.1.

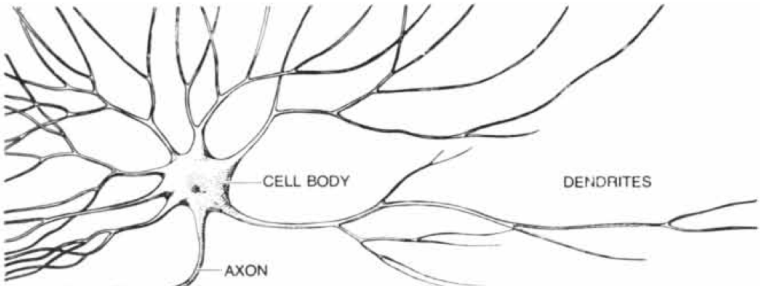

Figure 2.1.: Structure of a vertebrate animal's neuron [7].

2.2. Neuronal Membrane and Ions Channels

The intracellular compartment of the neuron is segregated from the extracellular environment by the plasma membrane, a biological barrier. Such a membrane is composed of two layers of phospholipids molecules arranged in such a way that the membrane is highly impermeable to ions. The neuronal membrane contains several types of proteins including ions pumps as well as ions channels [7].

Due to the non-permeability of the neuronal membrane, the only way for ions to move in and out of the neuron is either by using ions pumps or by going through ions channels. The role of ionic pumps consists in moving ions against concentration gradients in order to maintain adequate concentrations of these ions in the cell. Thus, ion pumps maintain both a voltage disparity and an electric field across this membrane, establishing an initial resting potential [9].

However, ions channels are more interesting for this master thesis as they underlie the mechanism of action potentials. Indeed, they constitute the permeation pathways across the cell membrane. Such proteins can control the width of their pathway in order to whether or not allow the flow of ions through the membrane.

The structure of the cell membrane as well as its most important ions channels are depicted in Figure 2.2.

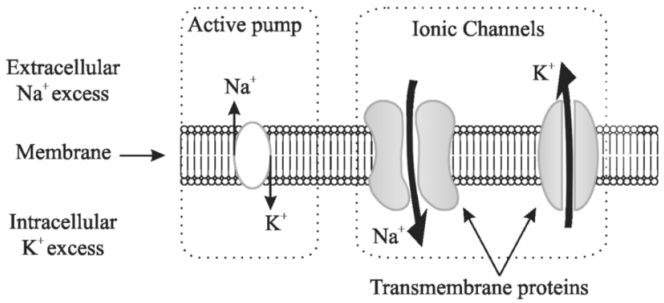

Figure 2.2.: Structure of a neuron membrane. The two mains proteins considered in the membrane are ions pumps and ions channels while the main ions are sodium and potassium. [10]

These transmembrane ionic channels are said to be voltage-gated as their gates open or close depending on the potential applied across the membrane. One key property of ions

channels is their ability to be selectively permeable to one type of ion, typically sodium, calcium, and potassium ions. The principal ions channels involved in the action potential mechanism are sodium and potassium voltage-gated ions channels. Consequently, the neuron's active electrical behavior is facilitated by these voltage-gated ion channels.

Therefore, the passive electrical characteristics of the neuron stem from the capacitive and resistive traits of this membrane.

2.3. Action Potential Generation Mechanism

Before discussing about the different initiation sites of spikes, a definition of the notion of an action potential will be undertaken [9] [7].

An action potential, commonly known as a spike, is an electrical impulse generated by changes in the electric field across the cell membrane. It propagates through the axonal membrane to convey information from the axon to the axonal terminals. Thus, action potentials are crucial for neuronal activity and confer excitability to neurons.

To grasp the mechanism of action potentials, we must first define the equilibrium potential of an ion, which represents a balance between the forces exerted by the concentration gradient and the electrical gradient of that ion. Consequently, there is no net flow of the ion across the membrane at equilibrium.

The generation of action potentials comprises several distinct phases, as illustrated in Figure 2.3.

- Resting phase: During rest, the resting membrane potential typically stays between the equilibrium potentials of sodium and potassium ions, typically around -60 mV.
- Depolarization phase: Upon receiving excitatory current, such as through stimulation, a localized depolarization occurs, leading to the opening of a few voltage-gated sodium channels, reinforcing the depolarization. If the membrane potential surpasses a certain threshold, a rapid recruitment of voltage-gated sodium channels occurs, resulting in a swift depolarization of the membrane potential (from -60 mV to 40 mV). The opening of these channels triggers the opening of additional sodium channels until all are open.
- Repolarization phase: After reaching its peak voltage, two intrinsic mechanisms of ion channels are initiated. Firstly, voltage-gated sodium channels undergo inactivation, reducing their permeability and preventing further inward sodium ion flow. Secondly, voltage-gated potassium channels activate, allowing outward potassium ion flow. Thus, following substantial depolarization, potassium channels activate while sodium channels inactivate, restoring the membrane potential to its resting state.

- Hyperpolarization phase: As the membrane potential hyperpolarizes, potassium channels deactivate by closing their deactivation gate. However, this process is relatively slow, resulting in a refractory period during which potassium channels remain open. This refractory period may cause an overshoot of the resting membrane potential. Notably, during this period, action potentials cannot be generated.

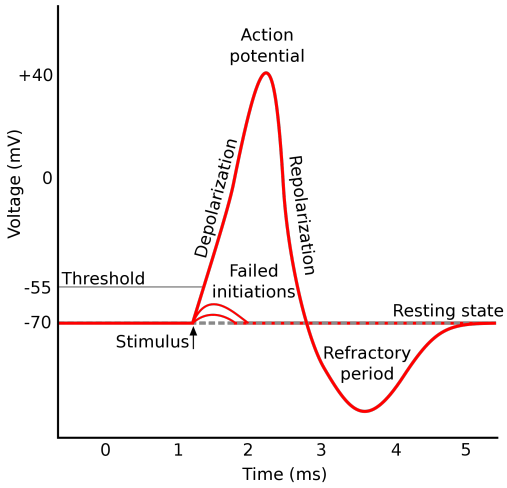

Figure 2.3.: Shape of a typical action potential [11].

2.4. Neuronal Spike Initiation Sites

The literature highlights the existence of two primary types of spikes that can occur within a neuron: somatic and dendritic.

In the case of Purkinje cells [12], large neurons situated in the cerebellar cortex of the brain, studies have revealed the occurrence of spontaneous firing in both the soma and dendrites of the neuron. Somatic spikes have been recognized for a longer duration compared to dendritic spikes, as it was previously believed that action potentials originated near the soma and subsequently invaded the dendrites. Somatic spikes have been extensively studied compared to dendritic spikes, as it was previously believed that action potentials originated near the soma and subsequently invaded the dendrites. However, it has since been discovered that dendrites can exhibit electroresponsiveness in certain neurons, albeit with distinctions from somatic electroresponsiveness. Notably, dendritic action potentials are generated discontinuously, in contrast to the continuous generation of somatic action potentials. Additionally, dendritic currents are primarily induced by voltage-dependent membrane conductance to calcium ions rather than sodium ions, as observed in somatic currents in Purkinje cells.

One of the primary motivations of this master's thesis to focus on the dendritic tree rather than the soma is that dendritic responses result from the summation of multiple components along the dendritic tree. It has been observed that there is a heterogeneous distribution of active membrane properties across the dendritic tree, with multiple regions featuring non-excitable membrane segments. This non-uniform distribution of ionic conductances leads to discontinuous conduction, resulting in dendritic action potentials being generated in a non-continuous manner.

Another reason for prioritizing the study of the dendritic tree is the observation that calcium-dependent action potentials exhibit larger amplitudes in more distal dendritic regions compared to those closer to the soma. This finding was established through experiments involving DC stimulation of Purkinje cells, which enabled the observation of two distinct types of action potentials. Voltage-dependent sodium conductance changes generated fast spikes, primarily noticeable at the soma and propagating towards the dendrites with a strong attenuation. Conversely, slow calcium-dependent spikes were gener-

ated within the dendrites, with their amplitudes significantly greater in distal dendritic locations compared to proximal ones, with only minimal amplitudes observed in the soma.

Such a behavior can be observed in Figure 2.4. On one hand, fast sodium-dependent spikes (in the form of bursts of spikes) are mainly observed at the soma and are attenuated while propagating towards the end of the dendritic branch. On the other hand, calcium-dependent spikes are larger in distal locations of the dendritic branch and quite weak at the soma.

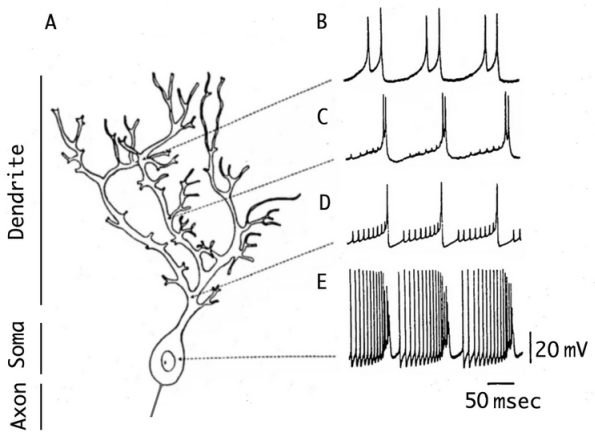

Figure 2.4.: Comparison between somatic and dendritic spikes after a DC depolarization at different dendritic levels. [12]

In addition to calcium ion channels, NMDA (N-methyl-D-aspartate) receptor channels have been identified as contributors to calcium-dependent dendritic spikes [13] [14]. Studies have revealed that NMDA-dependent spikes can be generated in the basal dendrites of pyramidal cells. As a result, NMDA receptors play a crucial role in detecting temporally correlated input sequences within dendrites. An important finding regarding the involvement of NMDA receptors in dendritic spikes is the observed directional preference of input sequences within dendrites. Specifically, it has been observed that when the input sequence progresses from distal to proximal regions, the amplitude of dendritic spikes is greater compared to sequences moving in the opposite direction [15].

In the case of CA1 pyramidal neurons [16], research has demonstrated that synaptic inputs occurring at distal locations of the dendritic tree may lead to initiation of dendritic spikes, whereas inputs at proximal dendritic locations or near the soma typically result

in initiation of axonal spikes. In most neurons, spikes initially arise in the soma in response to synaptic stimulation slightly above the threshold potential, then propagate back into the dendrites with a significant reduction in strength. However, in CA1 pyramidal neurons, sodium-dependent dendritic spikes can be generated with stronger excitatory synaptic inputs.

This master's thesis places particular emphasis on determining whether dendritic spikes are influenced by recent action potentials firing, as part of designing a temporal movement detection system. Studies such as [16] have indicated that dendritic excitability is modulated by early back-propagating spikes, with later back-propagating spikes exerting considerably less influence. This phenomenon can be attributed to the attenuation of back-propagating spikes as they propagate towards distal dendritic regions. Consequently, it has been inferred that dendritic spikes are initiated in distal dendritic regions that are shielded from the effects of attenuated back-propagation.

Furthermore, it has been observed that dendritic spikes can serve as an active mechanism of synaptic integration, enhancing the likelihood of a synaptic input triggering an axonal action potential. However, this function is not entirely reliable, as dendritic spikes generated in distal dendritic regions experience attenuation as they propagate towards the soma. Nonetheless, dendritic spikes remain a significant means of influencing the initiation of axonal action potentials in response to specific synaptic inputs.

An overview of the main ions responsible for somatic and dendritic spikes initiation can be seen in Figure 2.5.

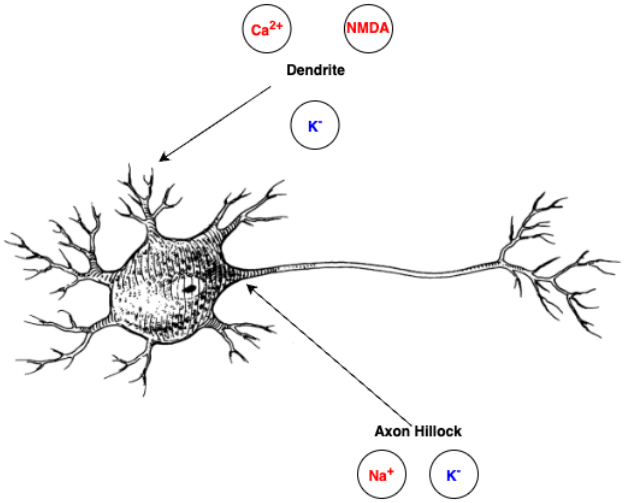

Figure 2.5.: Overview of the main ions responsible for somatic and dendritic spikes initiation. The axon hillock is considered as the earliest site of spike initiation along the axonal segment. The main ions involved in somatic spikes are sodium and potassium ions while calcium and potassium ions are involved in dendritic spikes as well as NMDA molecules. Red ions and molecules have an excitatory effect while blue ions have a inhibitory effect. Modified from [17].

2.5. Dendritic arithmetic Properties

Neuronal arithmetic has been largely studied, especially in [18], [19] and [20]. It usually consists in modifying the output response of a neuron by combining several synaptic inputs in different ways. Two main types of arithmetic operations have been studied in neurons: additive and multiplicative. By combining driving inputs, being excitatory synaptic inputs, with modulatory inputs such as inhibition, the way a neuron transforms its synaptic inputs into an output can be altered.

Such a behavior is essential for the main purpose of this master thesis which is to be able to discriminate temporal input sequences. Therefore, mechanisms underlying the modification of the neuron I-O relationship will be taken as inspiration to create the dendritic activation functions of the temporal pattern detection model. From all possible alterations of the neuron I-O relationship discussed in [18], input modulations will be primarily used to achieve the correct detection of input sequences. Therefore, modulatory inputs will be added to the driving inputs before being conveyed to the dendritic spiking mechanism. This will then allow the dendritic activation function to be either shifted along the x-axis either have its slope, known as neuronal gain, changed.

The usefulness of using additive operations in neurons for detecting inputs sequences is their properties to alter the range of temporal correlations of the synaptic inputs. Therefore, the ability of the desired system to detect inputs sequences with variable delays between the different synaptic inputs can thus be implemented by using additive operations.

Multiplicative operations are crucial in the detection of temporal inputs sequences. Indeed, by tuning the slope of the dendritic activation function of a dendritic compartment, it is possible to achieve an amplified non-linear I-O relationship similar to an AND logical operation. Such a logical operation is very well adapted for the purpose of the implemented system as it enables to inhibit dendritic compartments along the dendritic tree if the different compartments are not activated in the correct order of inputs.

In the scope of this master thesis, the different synaptic inputs are supposed to be temporally correlated as well as spatially segregated. Indeed, the spatial condition is inherent to the fact that the different inputs from the sequence that has to be detected each influ-

ence one compartment along the dendritic tree. As regards the temporal condition, the different inputs have to temporally correlated for a sequence to be correctly detected in an appropriate timescale.

As it has been highlighted in [18], detecting temporally correlated and spatially segregated sequences needs to overcome some difficulties. Indeed, depending on the location of the synaptic inputs over the dendritic tree, the synaptic integration time differs since the membrane time constant is shorter at distal locations of the dendritic tree than at proximal locations (near the soma). However, in this master thesis, such a feature has been overlooked as only interesting dendritic properties for the purpose of the pattern detection are used. The other main difficulty is, as already discussed in previous sections, the attenuation of dendritic action potentials generated at distal locations of the dendritic tree when propagating to the soma. However, sodium as well as calcium conductances can be used to amplify these synaptic inputs in order for the generated dendritic spikes to be larger once they reach the soma. On the other hand, potassium conductances can be used to dampen dendritic excitability and therefore diminish the response to synaptic inputs [20]. These amplification conductances are used as modulatory inputs in the implemented system to tune the amplification of the driving inputs at each dendritic compartment in order to counteract the attenuation of the dendritic spikes.

2.6. Temporal Pattern Detection in Neural Dendrites

Some researches such as [21], [22], [23] and [24] have studied the discrimination of temporal input sequences in biological neurons. Therefore, the system of pattern detection in the scope of this master thesis has been implemented by taking into account inherent properties of cells and dendrites.

It has been observed in ganglion cells that directional selectivity is inherent due to a sequence discrimination in sub-units of the cell [22]. Indeed, a sequence of stimuli caused a greater depolarization in the preferred direction of the cell compared to the one happening in the reverse direction. Such a behavior of the cell seems to be caused by an inherent mechanism that inhibits the response of the cell when the input sequence does not activate its sub-units in its preferred direction. Therefore, an absence of response from the cell was observed when the input sequence was in the reversed direction. This feature is thus taken into account for the implementation of the pattern detection system by using an inhibition-like mechanism that prevents subsequent dendritic compartments along the dendritic tree to generate a response in case the input sequence was not detected in the desired direction. An inhibition of a certain dendritic compartment is therefore applied by the preceding dendritic compartment if the detected movement is not in the preferred direction. Therefore, a crucial feature for sequence discrimination used in the system is an inhibition mechanism that prevent responses of the system to sequences corresponding to a movement in the non-preferred directions.

The implemented system takes mostly its inspiration in dendritic calcium-dependent spikes rather than dendritic sodium-dependent spikes. Indeed, it has been observed in [21] that dendritic calcium-dependent action potentials showed a preferred direction for input sequences. The results of experiments determined that the dendritic calcium-dependent spikes were much larger for input sequences activating dendritic compartments going from distal compartments to the soma rather than the opposed direction. Moreover, the somatic spikes have been observed to be nonlinear as well as growing with the number of dendritic compartments activated along the dendritic tree.

It has been deduced that direction sensitivity in dendrites are mainly caused by the non-linear voltage dependence of NMDA conductance. Such a behavior results from the fact that depending on the order of activation of synaptic inputs in the dendritic compartments, sequences starting from distal locations of the dendritic tree, having a higher impedance, generate a larger depolarization, and thus lead to more activation of NMDA channels compared to other sequences. The system is therefore designed to detect input sequences that are in the preferred direction of a cell which is from distal locations in the dendritic tree towards the soma of the cell. Moreover, this behavior can be abstracted as a multiplicative effect that either excites or inhibits the system's response to input sequences based on their direction of motion.

2.7. Basic System Design

The system designed in the scope of this master thesis consists in modelling a dendritic-like structure of a neuron to represent an array of event-based camera's pixels. The model therefore tries to mimic the functioning of a dendritic branch by representing each considered pixel by a dendritic compartment along the dendritic branch.

A representation of the dendritic compartments along the dendritic branch can be seen in Figure 2.6.

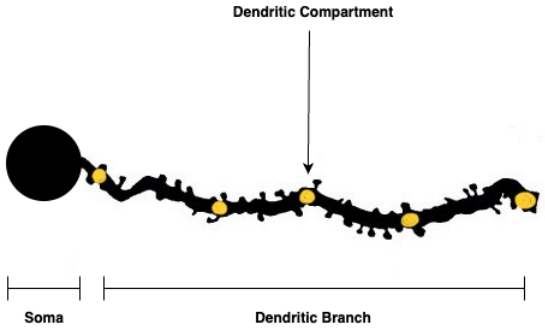

Figure 2.6.: Representation of dendritic compartments along a dendritic branch ending at the soma. The yellow points illustrate the dendritic compartments along the dendritic branch. Modified from [25].

These dendritic compartments are mathematical units represented by the variable $s_i(t)$, being the activation variable of the dendritic compartment i along the dendritic branch. It has been taken as notation that $i = 1$ represents the most distal dendritic compartment of the dendritic branch while $i = n$ stands for the dendritic compartment directly preceding the decision unit equivalent here to the soma of a neuron.

An overview of the system implemented for a dendritic branch composed of three dendritic compartments inspired from Figure 2.6 can be seen in Figure 2.7.

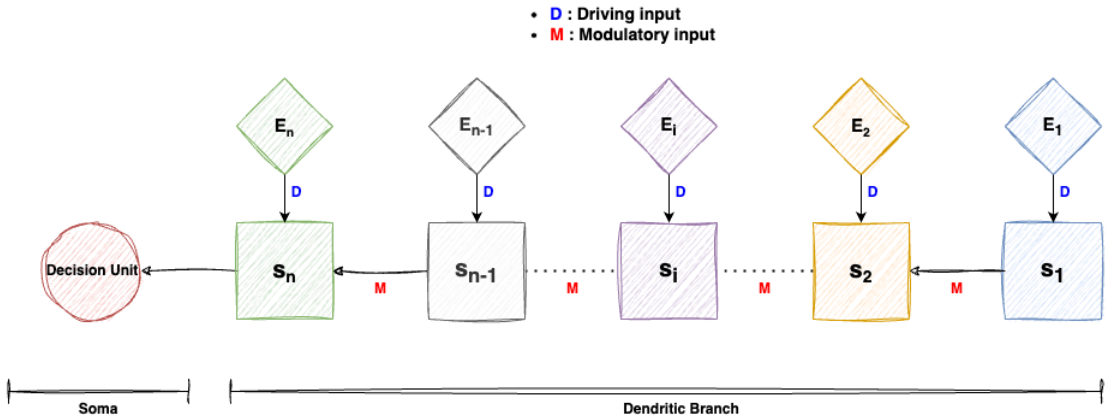

Figure 2.7.: Overview of the structure of the designed system for a dendritic branch composed of n dendritic compartments.

The decision unit, representing the soma of the neuron, acts as a threshold unit that outputs whether or not a correct input sequence has been detected by comparing the activation variable of the preceding dendritic compartment, in this case $s_n(t)$, with a certain threshold. The dendritic branch is therefore composed of all dendritic compartments represented by all s_i with $i \in [1, n]$ and n the number of dendritic compartments composing the dendritic branch.

As discussed in Section 2.5, two types of inputs are used in the implemented system. The driving inputs, being the synaptic inputs, are the events E_i captured by the pixels. Taking this notation into consideration, it follows that all events captured by a certain pixel i are modeled by the variable $E_i(t)$.

The events captured by the pixels have a crucial significance since they lie at the foundation of the model response. These are thus defined as a single pulse composed of an increasing part, a plateau as well as a decreasing part. Indeed, the increasing part represents the object appearing in the receptive field of the pixel while the decreasing part represents the disappearance of the object from the receptive field of the pixel. The width of the plateau is directly representative of the width of the object going through the receptive field of the pixel.

The events are hence defined as follows:

$$E(t, t_0, \text{width}) = \text{pulse}(t, t_0, t_0 + \text{width})$$

Figure 2.8 illustrates an event following the above definition. In view of normalizing the different objects seen by the pixels, it has been decided that events would have a unitary value when an object would be present in the receptive field of a pixel. The effect of the width of the events on the activation variables will be investigated in further sections.

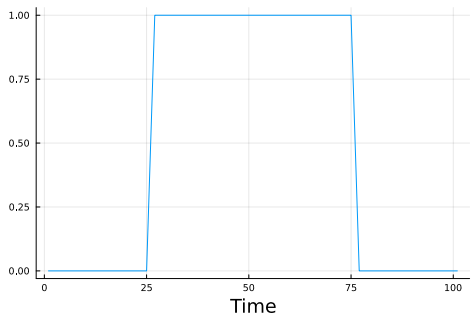

Figure 2.8.: Illustration of the events used as synaptic inputs with $t_0 = 25$ and $width = 50$.

Note that it is assumed for this master thesis that the events E_i of the different dendritic compartments all possess the same width as an object is supposed to have a non-variable perceived width when moving.

As regards the second type of inputs considered by the model, the activation variable of a preceding dendritic compartment is considered as a modulatory input for the current dendritic compartment. These modulatory inputs can either act as excitation or as inhibition depending on the input sequence order. Such a mechanism will be explained in further sections.

In the designed system, driving inputs, modeled by the events E_i, acts as voltage-dependent calcium conductances which are used to generate calcium-dependent dendritic spikes while modulatory inputs either acts as voltage-dependent NMDA conductances when used as excitation either as voltage-dependent potassium conductances when used as inhibition.

3. Dendritic Dynamics for Neuromorphic Temporal Pattern Detection

The implementation of the system to detect whether an input sequence is correct or not has been undertaken using two distinct approaches. The first one uses only additive arithmetic operations between the activation variables of the different dendritic compartments. Therefore, such an approach only uses the basic properties of dendrites and does not fully take advantage of their non-linear properties.

The second approach is neuromorphic-oriented and fully uses the non-linear properties of dendrites by using both additive and multiplicative arithmetic operations. However, the activation variables of the dendritic compartments are not directly multiplied together but are rather used as either excitatory or inhibitory modulatory inputs depending on the state of the preceding dendritic compartment's activation variable..

For both approaches, the model of each dendritic compartment is composed of an integrative unit as well as a non-linear unit. The integrative unit consists in a first-order low-pass filter whose parameter is the time constant τ. The Laplace notation of such a first-order low-pass filter is the following:

$$H(s) = \frac{1}{\tau s + 1}$$

The non-linear unit consists in a sigmoid-like function symbolizing the dendrites non-linear properties and is used to amplify non-linearly the synaptic input fed to the dendritic compartment. The non-linear units' mathematical function is defined in the following sections given that they are different for the two approaches since the function of the first one does

not have a state feedback while the one of the second approach does.

The structure of a dendritic compartment can be seen in Figure 3.1.

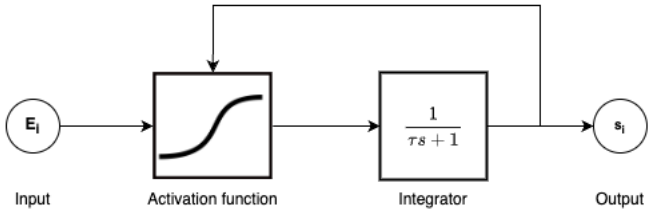

Figure 3.1.: Dendritic compartment structure. The mathematical model of the compartment is composed of a non-linear unit followed by an integrative unit (first order low-pass filter).

It has to be noted that the gain of the sigmoid can be modulated to achieve the desired behavior of the system.

In the following sections, both the effect of the width of the synaptic inputs as well as the delay between the synaptic inputs of the different compartments will be investigated. A study of the effect of these parameters is indeed crucial to design a system having a robustness w.r.t. the temporal correlation of the different synaptic inputs.

All the simulations were performed using the Julia Programming Language [26] with the DifferentialEquations package [27] to solve the different systems of differential equations.

3.1. Naive Approach

The activation function used in the dendritic compartment's response is denoted $S(E, b)$ and is defined as such:

$$S(E, b) = \tanh(E - b) - \tanh(-b)$$

where E denotes the synaptic input of the dendritic compartment and b represents the bias of the activation function. Such an expression of the activation function has been chosen to have a zero input in case the event is null (whatever the value of the bias).

The effect of the bias on the activation function is shown in Figure 3.2.

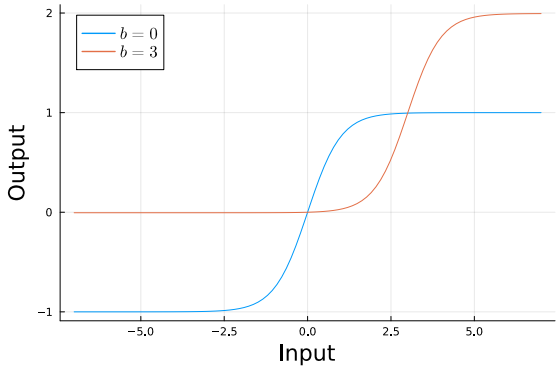

Figure 3.2.: Activation function $S(E\ , b)$ of a dendritic compartment. Increasing the value of the bias b results in a left-upward translation of the activation function. The activation function is always null when no input is fed.

Thus, the bias can be tuned to obtain the desired behaviour for the activation function. Indeed, using a sufficiently large positive bias might make the activation function only be non zero for larger inputs. Such a configuration would mean that the dendritic compartment's response would only take into account its synaptic input if it is significant enough (the significance of the event being tuned by the magnitude of the event to the compartment itself) to influence the response.

It can be observed that the activation function of the naive approach does not depend on the activation variable of the dendritic compartment itself. Therefore, the output of the activation function is non-zero only when the synaptic input of the compartment is non-zero.

Note that the argument E of the activation function S can either represent a single event either a combination of events.

3.1.1. Independent dendritic compartments

A naive approach is to consider the different dendritic compartments independent with one another and in a configuration where their synaptic inputs are also independent with the others.

The interconnections between the different dendritic compartments of the system can be seen in Figure 3.3.

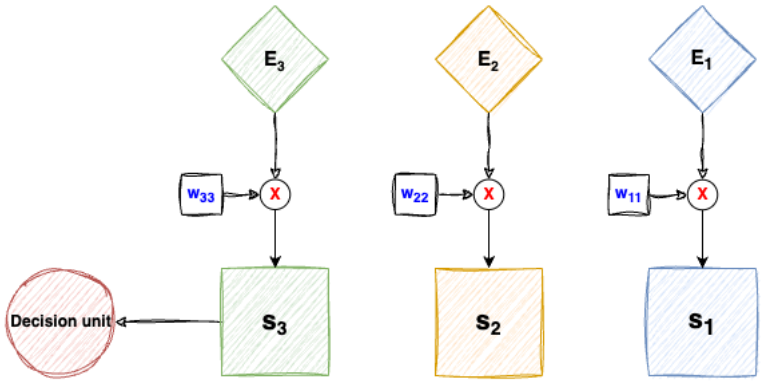

Figure 3.3.: Overview of the structure of the system for a dendritic branch composed of three independent dendritic compartments.

Mathematical model

The system's equations are such that the activation function of a dendritic compartment's response takes into account its own synaptic input. Thus, the system's equations are as follows:

$$\begin{cases} \dot{s}_1(t) = \frac{-s_1(t) \ + \ S(w_{11} \cdot E_1(t) \ , \ b)}{\tau} \\ \dot{s}_2(t) = \frac{-s_2(t) \ + \ S(w_{22} \cdot E_2(t) \ , \ b)}{\tau} \\ \dot{s}_3(t) = \frac{-s_3(t) \ + \ S(w_{33} \cdot E_3(t) \ , \ b)}{\tau} \end{cases}$$

Equilibrium Analysis

An analysis of the different equilibrium of the system at the initial time t_0 has been performed to study the dynamics of the model. The fixed points of the model can be computed for $\dot{s}_i = 0 \ , \forall i$. The system of equations obtained by taking into consideration these conditions as well as the fact that $E_i = 0 \ , \forall i$ is the following:

$$\begin{cases} 0 = -s_1 \\ 0 = -s_2 \\ 0 = -s_3 \end{cases} \tag{3.1}$$

The only fixed point of the system of equations 3.1 can be directly inferred as being $\bar{s} = [0, 0, 0]$.

The Jacobian matrix of this system can be computed the following way:

$$J = \begin{pmatrix} \frac{\partial \dot{s}_1}{\partial s_1} & \cdots & \frac{\partial \dot{s}_1}{\partial s_n} \\ \vdots & \ddots & \vdots \\ \frac{\partial \dot{s}_n}{\partial s_1} & \cdots & \frac{\partial \dot{s}_n}{\partial s_n} \end{pmatrix} \tag{3.2}$$

After computation, the Jacobian matrix is as follows:

$$J = \begin{pmatrix} \frac{-1}{\tau} & 0 & 0 \\ 0 & \frac{-1}{\tau} & 0 \\ 0 & 0 & \frac{-1}{\tau} \end{pmatrix} \tag{3.3}$$

Evaluating the Jacobian matrix at the fixed point $\bar{s} = [0, 0, 0]$ and computing the determinant, one can found the following eigenvalues for the system of equations 3.1.

$$\lambda_i = \frac{-1}{\tau}, \text{ for } i = 1, 2, 3$$

It is direct that the system of equations 3.1 has one eigenvalue of multiplicity 3. The stability of the system can thus be directly inferred by analysing the sign of the eigenvalues of the system leading to a stable fixed point located at $(s_1, s_2, s_3) = (0, 0, 0)$.

The eigenvectors matrix of the system 3.1 is the following:

$$V = \begin{pmatrix} 0 & 0 & 1 \\ 0 & 1 & 0 \\ 1 & 0 & 0 \end{pmatrix} \tag{3.4}$$

Model simulation

The dynamics of an activation variable $s_i(t)$ can be seen in Figure 3.4. As it can observed, it is not possible to detect a movement with such a system dynamics given that all dendritic compartments' response have the same magnitude whatever the order of the input sequence.

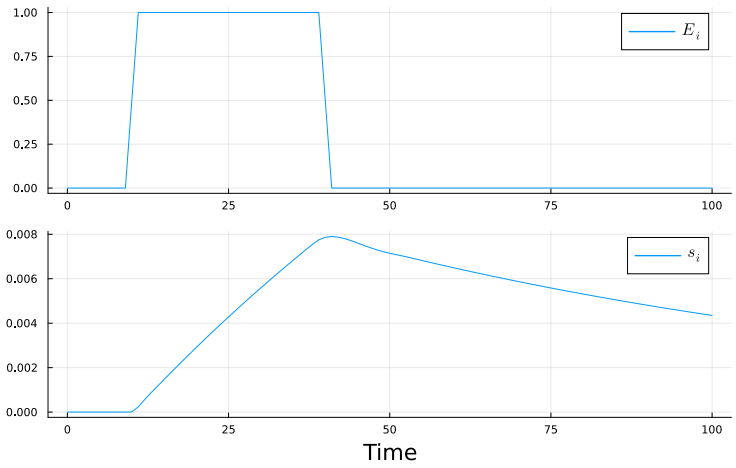

Figure 3.4.: Simulation of the model involving independent dendritic compartments for an event's width of 30.

Such an approach cannot lead to a functioning temporal pattern detection system since a symmetry is inherent to the system. The proof to the inefficiency of this approach is direct.

Starting from the expression of a dendritic compartment's response $\dot{s}_i(t) = \frac{-s_i(t) + S(E,\ b)}{\tau}$,

we find that s_i has the following form:

$$\tau s_i(t) = e^{\frac{-t}{m}} \cdot \int_0^t e^{\frac{\xi}{\tau}} \; S(\xi, b)\, d\xi$$

Hence, considering that the response in the integral is solely influenced by the different events, it becomes evident that the approach is incapable of detecting a difference in the events order (hence it cannot detect a movement from right to left in the dendritic branch). Regardless of the order of events, the integral's outcome will remain unchanged if the integration time encompasses all events, assuming the events have the same magnitude and form.

It is notable that all dendritic compartments responses possess an identical delay and form (all compartments having the same time constant τ). Consequently, it becomes impossible to discern any variations in the order of events.

The effects of the parameters w, b and τ are explained in Table 3.1.

Parameter	Meaning and effect
w	Weight of the synaptic input in the activation function. A large weight will result in a faster saturation of the activation function. However, reaching a certain value of w, the saturation of the hyperbolic tangent will be reached anyway and further incrementing w has no effect.
b	The bias effect has been shown previously in figure 3.2. Increasing b will result in a translation of the hyperbolic tangent to the right and upwards (so that it is either 0 either 2 in saturation for large values of b). Note that $S(0, b) = 0 \ , \ \forall b$. Therefore, increasing b does not affect the output of the activation function when there isn't any input.
τ	The time constant has for effect to affect the speed of the dynamics of the dendritic compartments' response. Therefore, by increasing τ, the compartment's response will have a slower reaction time than low values of τ.

Table 3.1.: Parameters effects.

3.1.2. Coupling of dendritic compartments

Since a system using dendritic compartments in a independent fashion is not sufficient to correctly detect temporal input sequences, the synaptic inputs received by the different compartments will be coupled and additive operations between the compartments will be performed by the model.

The interconnection between the different compartments are shown in Figure 3.5.

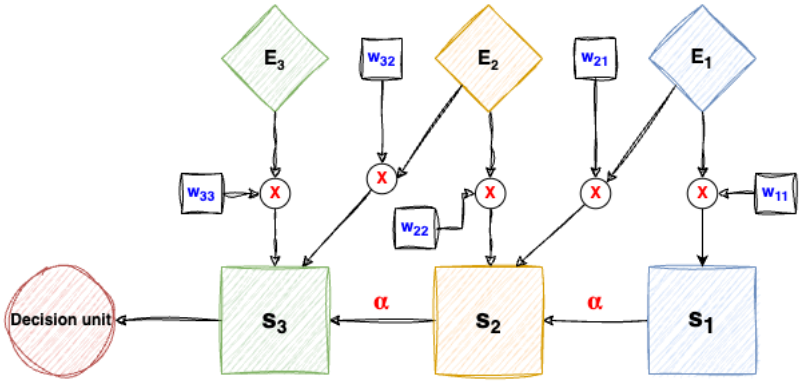

Figure 3.5.: Overview of the structure of the system for coupled compartments involving additive arithmetic operations for a dendritic branch composed of three dendritic compartments.

Mathematical model

The system's equations are such that the activation function of a dendritic compartment takes into account its own synaptic input as well as the synaptic input of the preceding dendritic compartment. Moreover, additive arithmetic operations are used between the current and preceding dendritic compartment. Thus, the system's equations are as follows:

$$\begin{cases} \dot{s}_1(t) = \frac{-s_1(t) \ + \ S(w_{11} \cdot E_1(t) \ , \ b)}{\tau} \\ \dot{s}_2(t) = \frac{-s_2(t) \ + \ S(w_{21} \cdot E_1(t) \ + \ w_{22} \cdot E_2(t) \ , \ b) \ + \ \alpha \cdot s_1(t)}{\tau} \\ \dot{s}_3(t) = \frac{-s_3(t) \ + \ S(w_{32} \cdot E_2(t) \ + \ w_{33} \cdot E_3(t) \ , \ b) \ + \ \alpha \cdot s_2(t)}{\tau} \end{cases} \tag{3.5}$$

The event weights interconnection matrix used for this model is the following:

$$W = \begin{pmatrix} w_{11} & w_{12} & w_{13} \\ w_{21} & w_{22} & w_{23} \\ w_{31} & w_{32} & w_{33} \end{pmatrix} = \begin{pmatrix} 1 & 0 & 0 \\ 1 & 1 & 0 \\ 0 & 1 & 1 \end{pmatrix} \tag{3.6}$$

Several values of the bias b have been studied but a null bias $b = 0$ led to the best performances for this model. A low value of the interconnection parameter α has been chosen as the response would grow too significantly if a large value was taken, leading to a chosen value $\alpha = 2$.

Equilibrium Analysis

The same equilibrium analysis as the one performed in Section 3.1.1 has been conducted for this model and led to the determination of the same eigenvalues and associated eigenvectors.

The system of equations under the conditions introduced in the Section 3.1.1 is as follows:

$$\begin{cases} 0 = -s_1 \\ 0 = -s_2 \ + \ \alpha \cdot s_1 \\ 0 = -s_3 \ + \ \alpha \cdot s_2 \end{cases} \tag{3.7}$$

The only fixed point of the system of equations 3.7 can be directly inferred as being $\bar{s} = [0, 0, 0]$ and the associated eigenvalues are the following:

$$\lambda_i = \frac{-1}{\tau}, \text{ for } i = 1, 2, 3$$

The corresponding eigenvectors matrix of the system 3.7 is the following:

$$V = \begin{pmatrix} 0 & 0 & 1 \\ 0 & 1 & 0 \\ 1 & 0 & 0 \end{pmatrix} \tag{3.8}$$

Model Simulation

The behavior of the system in simulation can be seen in Figure 3.6 for the following values of parameters: $\alpha = 2,\ b = 0,\ \tau = 70$.

It can be observed that the behavior of the model is not robust to incorrect order of input sequences as the activation variable of the last dendritic compartment s_3 generates a non-null response when dendritic compartments were not activated from distal to proximal. Therefore, a system using only additive arithmetic operations leads to mitigated results. Depending on the value of delays between synaptic inputs, their width as well as the dendritic compartments' time constant, the system can reliably detect correct order of input sequences only for restrictive ranges of parameters values as it will be studied in Section 3.3.

Due to the limitations of this system, a model using both additive and multiplicative arithmetic operations will be investigated to obtain a more reliable motion detection system with broader ranges of parameters values under which the system functions optimally.

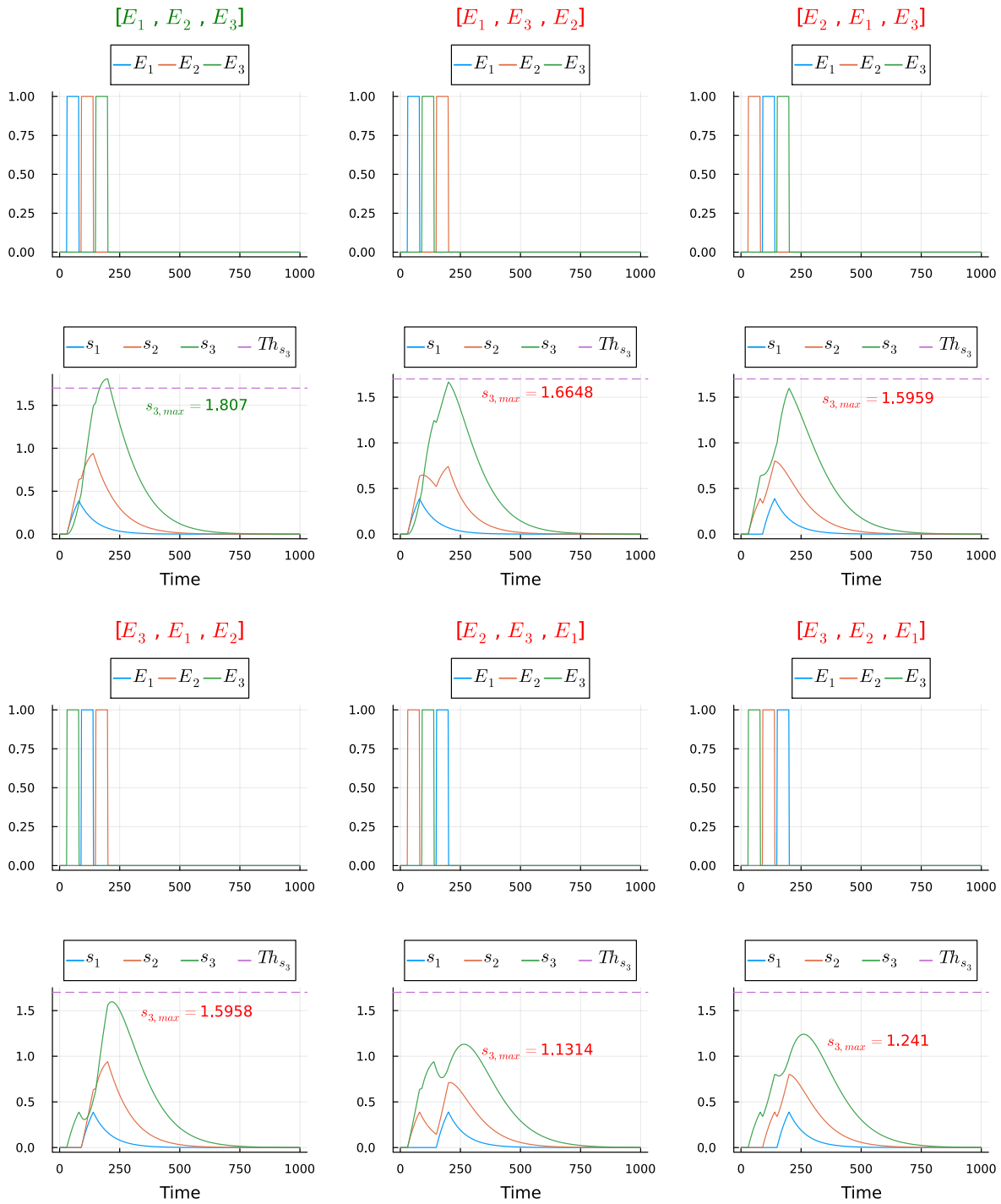

Figure 3.6.: Simulation of the model using only additive arithmetic operations for a width of synaptic input of 50 and a delay of 60 for a dendritic branch of 3 dendritic compartments. Only the correct input sequence generate a movement detection. However, incorrect input sequences generate a non-null response in the last compartment preceding the decision unit s_3.

3.2. Dendritic-inspired Approach

For the design of this dendritic-inspired system, each dendritic compartment is fed by its own synaptic input, as a feedback from its own state and receives the response of the preceding compartment.

The interconnection between the different compartments are shown in Figure 3.7.

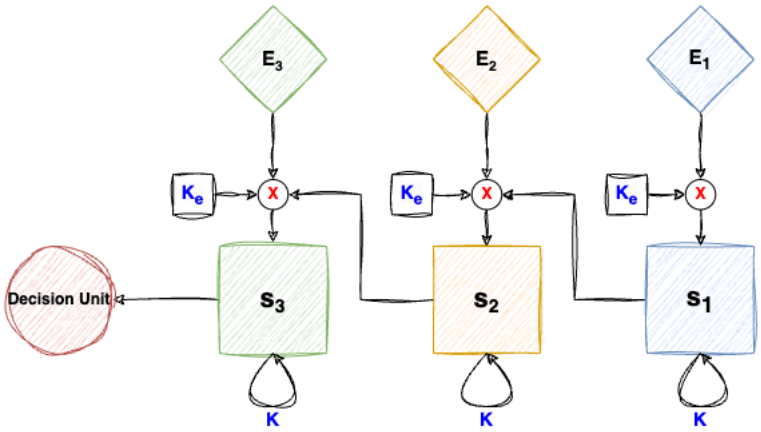

Figure 3.7.: Overview of the structure of the dendritic-inspired system for a dendritic branch composed of three dendritic compartments.

Activation Function

The activation function of a dendritic compartment is now dependent both to the synaptic input of the compartment as well as its activation variable. The expression of the activation function is the following:

$$T(x,\ K,\ K_e,\ E,\ \sigma) = \frac{\tanh\left(K \cdot x + K_e \cdot E - \sigma\right) - \tanh\left(-\sigma\right)}{1 - \tanh^2\left(\sigma\right)} \tag{3.9}$$

where K controls the contribution of the activation variable of the dendritic compartment in the activation function, K_e controls the contribution of the synaptic input of the compartment and σ is the bias of the activation function. It can be noted that the output of the activation function is null when the synaptic input is null at the initial time t_0 , $t = 0$ whatever the value of the bias.

The shape of the activation function T can be seen in Figure 3.8.

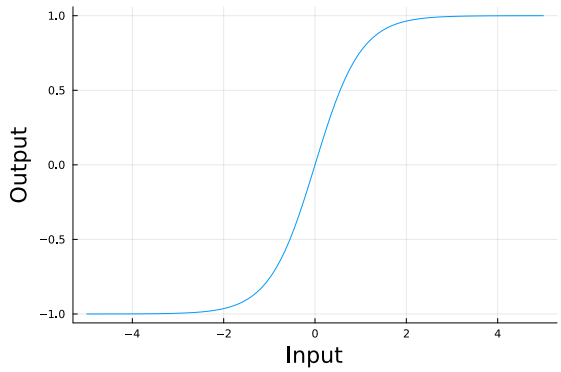

Figure 3.8.: Activation function T for $K = 1$, $K_e = 1$ and $\sigma = 0$.

The effect of the different parameters of the activation function will now be studied.

First, the effect of the bias σ on the activation function can be seen in Figure 3.9.

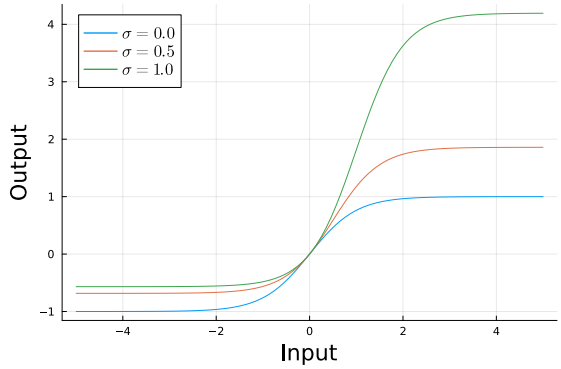

Figure 3.9.: Effect of the bias σ on the activation function T for $K = 1$ and $K_e = 1$.

As the model has to be designed to detect temporal input sequences in the preferred direction, the system will therefore be unidirectional and emphasize the response of subsequent dendritic compartments in the preferred direction only if the input sequence is correctly ordered. To achieve such a feature of the system, the value of the bias has been chosen so that the output of the activation function is slightly negative for negative synaptic inputs and is rapidly increasing for positive synaptic inputs. This allows the activation function to directly saturate for relatively small positive synaptic inputs while discarding all negative synaptic inputs (the outputs of the activation function to negative inputs being negligible compared to the ones of positive inputs). A value of $\sigma = 1$ has been chosen as it enable the system to exhibit the desired behavior.

The effect of the activation variable contribution parameter K has been studied in Figure 3.10.

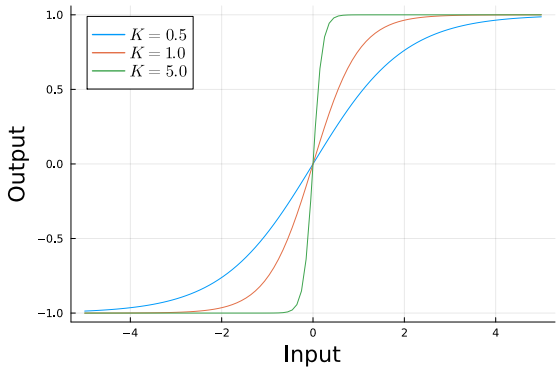

Figure 3.10.: Effect of the parameter K on the activation function T for $K_e = 1$ and $\sigma = 0$.

The parameter K is therefore responsible for the multiplicative arithmetic operations of the system as it controls the slope of the activation function as described in Section 2.5. Indeed, the parameter K tunes the amplification of the non-linearity of the I-O relationship of the activation function by controlling its neuronal gain. It can be observed in Figure 3.10 that the higher the value of the parameter K, the more the I-O relationship is similar to an AND logical operation.

The effect of the synaptic input contribution parameter K_e can be seen in Figure 3.11.

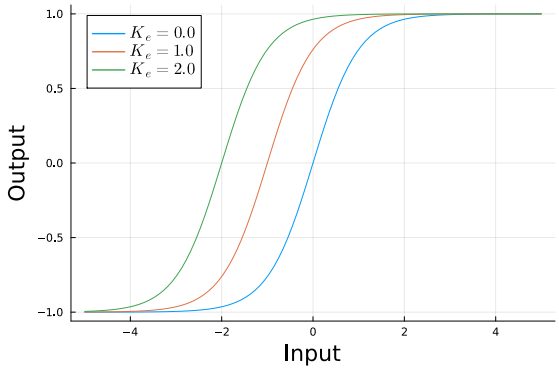

Figure 3.11.: Effect of the parameter K_e on the activation function T for $K = 1$ and $\sigma = 0$. Note that a non-zero synaptic input has been considered.

The parameter K_e is thus responsible for the additive arithmetic operations of the system as it controls the translation of the activation function along the input axis as described in

Section 2.5. It can be observed in Figure 3.11 that the higher the value of the parameter K_e, the more the I-O relationship is translated to the left therefore leading to a direct saturation of the activation function for positive inputs.

3.2.1. Basic model with multiplicative interactions

Mathematical Model

The mathematical model used for the designed system is the following:

$$\begin{cases} 1 & \tau \dot{s}_1(t) = -s_1(t) + T(s_1(t),\ K,\ K_e,\ E_1(t),\ \sigma) \\ \vdots & \\ i & \tau \dot{s}_i(t) = -s_i(t) + T(s_i(t),\ K,\ K_e \cdot s_{i-1}(t),\ E_i(t),\ \sigma) \\ \vdots & \\ n & \tau \dot{s}_n(t) = -s_n(t) + T(s_n(t),\ K,\ K_e \cdot s_{n-1}(t),\ E_n(t),\ \sigma) \end{cases} \tag{3.10}$$

In such a system, the synaptic input of each dendritic compartment acts as an excitatory driving input equivalent to voltage-dependent calcium conductance. It has to be noted that for all activation variable s_i , $\forall i > 1$, the synaptic input contribution parameter K_e is multiplied by the activation variable of the preceding dendritic compartment to either act as an additional excitatory modulatory input equivalent to voltage-dependent NMDA conductance if $s_{i-1} > 0$ either as an inhibitive modulatory input equivalent to voltage-dependent potassium conductance if $s_{i-1} = 0$.

The hypothesis of a uniform distribution of ionic conductances along the dendritic branch has been made to simplify the designed model even though such an hypothesis does not hold in biology as discussed in Section 2.5. Therefore, for all dendritic compartments, the parameters τ, K, K_e and σ have the same value respectively over the compartments.

Equilibrium Analysis

An analysis of the different equilibrium of the system with regards to the activation variable contribution parameter K has been conducted at the initial time t_0 (for a zero synaptic input) in a similar manner as performed in Section 3.1.1.

The system of equations under the conditions introduced in Section 3.1.1 is as follows:

$$\begin{cases} 1 & 0 = -s_1 + \frac{\tanh(K \cdot s_1 - \sigma) - \tanh(-\sigma)}{1 - \tanh^2(\sigma)} \\ \vdots & \\ i & 0 = -s_i + \frac{\tanh(K \cdot s_i - \sigma) - \tanh(-\sigma)}{1 - \tanh^2(\sigma)} \\ \vdots & \\ n & 0 = -s_n + \frac{\tanh(K \cdot s_n - \sigma) - \tanh(-\sigma)}{1 - \tanh^2(\sigma)} \end{cases} \tag{3.11}$$

One of the fixed point to the system of equations 3.11 can be directly inferred as being $\bar{s} = [0, \ldots, 0]$. However, other fixed points cannot be determined analytically.

The Jacobian matrix is computed using 3.2 and is the following:

$$J = \frac{1}{\tau \cdot \left[1 - \tanh^2(\sigma)\right]} \begin{pmatrix} a_1 & 0 & \ldots & 0 \\ 0 & \ddots & \ddots & \vdots \\ \vdots & \ddots & \ddots & 0 \\ 0 & \ldots & 0 & a_n \end{pmatrix} \tag{3.12}$$

where $a_i = -(1 - \tanh^2(\sigma)) + K \cdot \operatorname{sech}^2(K \cdot s_i - \sigma)$.

Evaluating the Jacobian matrix at the fixed point $\bar{s} = [0, \ldots, 0]$ and computing the determinant, one can found the following eigenvalues for the system of equations 3.11.

$$\lambda_i = \frac{K \cdot \operatorname{sech}^2(\sigma) + \tanh^2(\sigma) - 1}{\tau \cdot \left[\tanh^2(\sigma) - 1\right]} \text{ , for } i = 1, \ldots, n$$

It is direct that the system of equations 3.11 has one eigenvalue of multiplicity n for the computed fixed point. In order to study the stability of the system for different values of the parameter K, let the derivative of the activation variable of a dendritic compartment be a function of the activation variable itself and the parameter K such as $\dot{s}_i = f(s_i, K)$. The stability of the system can be directly inferred by analysing the sign of the eigenvalues of the system w.r.t. values of K.

For values of $K < 1$, the system has a negative eigenvalue of multiplicity n leading to stable fixed points for $K \in [0, 1[$ (values of $K < 0$ are not taken into account as we consider that the dendritic compartments have an inherent local positive feedback in their dynamics). It can be noted that a local bifurcation occurs at $f(0, 1)$ as the eigenvalue obtained at this point is equal to $\lambda_i = 0$, $\forall i$. For values of $K > 1$, the system has a positive eigenvalue of multiplicity n leading to unstable fixed points for $K \in]1, \infty[$

The eigenvectors are such that v_i is a vector composed of $n - 1$ zeros and a single 1 at index i. The index form of the eigenvector matrix can also be expressed as follows:

$$J_{i,j} = \begin{cases} 1 & \text{if } \; j = n - i \\ 0 & \text{otherwise} \end{cases}$$

The equilibrium analysis w.r.t. the parameter K has been conducted both with a value of $\sigma = 0$ and $\sigma = 1$ to study the classic behavior with no bias as well as the behavior of the deformed activation function.

The equilibrium analysis for a value of $\sigma = 0$ can be observed in Figure 3.12.

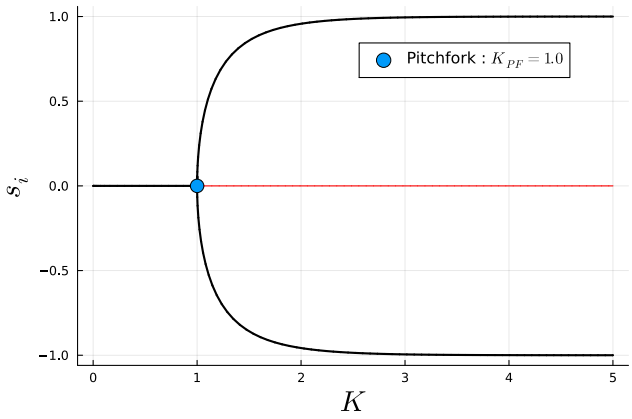

Figure 3.12.: Parameter K determination for a null bias ($\sigma = 0$) for the basic model.

It can be seen that the equilibrium analysis of the studied system is a supercritical Pitchfork-like bifurcation of co-dimension 1.

For value of $K < 1$, there is only one stable equilibrium located at $s_i = 0$. The value of $K = 1$ represents the bifurcation point of the system. For value of $K > 1$, there is an

unstable equilibrium located at $s_i = 0$ and two stable equilibrium on the upper and lower branches.

The equilibrium analysis for a value of the bias $\sigma = 1$ chosen for the system can be observed in Figure 3.13.

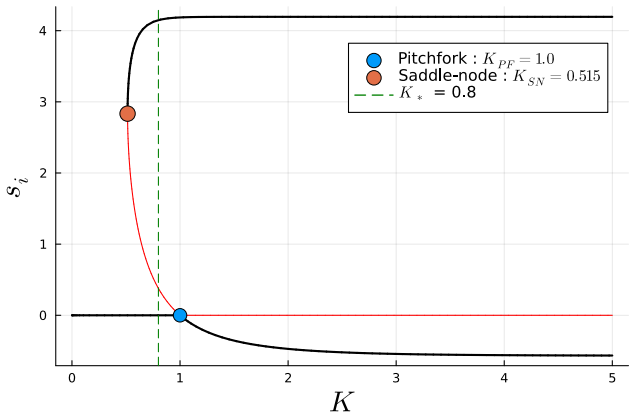

Figure 3.13.: Parameter K determination for a bias $\sigma = 1$ for the basic model.

It can be noted that the supercritical Pitchfork-like bifurcation is quite different from Figure 3.12. Indeed, since the bias of the activation function has been taken to be positive, the non-linearity of the activation function has been emphasized resulting in an upward unfolding of the Pitchfork bifurcation.

Due to the nonlinear nature of the hyperbolic tangent function in the activation function and the parameter K dependence in the equations of the system 3.11, the analytical determination of the saddle-node bifurcation K_{SN} does not lead to a general algebraic solution for this equation. Therefore, a numerical determination will be performed using the numerical continuation methods available in Julia *BifurcationKit* [28]. It has thus been computed numerically that $K_{SN} = 0.515$ for the chosen parameters values.

It can be seen in Figure 3.13 that, for $K < K_{SN}$, there is only one equilibrium located at $s_i = 0$. For $K \in]K_{SN}, 1[$, there are two stable equilibrium (one located at $s_i = 0$ and the other one in the upper branch) as well as an unstable equilibrium in-between. For $K > 1$, there is an unstable equilibrium located at $s_i = 0$ and two stable equilibrium on the upper and lower branches.

It has to be brought to attention that the value of the upper stable equilibrium branch, being about 4 in Figure 3.13, strictly depends on the value of σ. Indeed, the more the value of the bias σ increases, the higher the value of the upper stable equilibrium branch will be. This value is quite significant as it will determine the maximal value that the activation variable of a dendritic compartment will be able to reach. It is therefore direct that one can obtain a higher compartment response by using a higher bias. However, for the following simulations, a bias of $\sigma = 1$ will be used. The maximal value of the upper stable equilibrium branch can be derived from the saturation value of the activation function in Figure 3.9 for $\sigma = 1$.

The value chosen for the parameter K was therefore a value in the interval $]K_{SN}, 1[$ in order to have a stable equilibrium in the upper branch, corresponding to a positive decision, as well as a stable equilibrium for a null value of s_i, corresponding to the neutral stable branch. The value of the parameter has thus been chosen as $K = 0.8$.

This behavior was desired for the designed model as the system can either stay at the neutral stable branch either take a positive decision and jump to the upper stable branch. However, it has to be noted that the system is unable to return to its neutral stable branch once it has taken a decision.

Model Simulation

The behavior of the system in simulation can be seen in Figure 3.14 for the following values of parameters: $K = 0.8,\ K_e = 10,\ \sigma = 1,\ \tau = 40$.

It can be observed that, thanks to the modulatory input $s_{i-1}(t)$ of a compartment i, the activation variable $s_i(t)$ stays at 0 if the synaptic input $E_{i-1}(t)$ did not occur before its own synaptic input $E_i(t)$. Therefore, for these parameters values, the system is efficiently able to detect the correct input sequence.

As explained in the equilibrium analysis, the model can either decide to stay in its neutral stable branch, being $s_i = 0$, either to take a positive decision resulting in a jump from the neutral stable branch to the stable upper branch from Figure 3.13. However, as seen in

Figure 3.14, once the decision to transition from the neutral stable branch to the stable upper branch as been taken, the model is stuck in its decision and is therefore unable to return to its neutral stable branch.

One goal of the designed system being to detect consecutive input sequences temporally-separated by an in-between sequence delay, this model does not meet the requirements as the activation variable of the different dendritic compartments will never be reset after taking a decision.

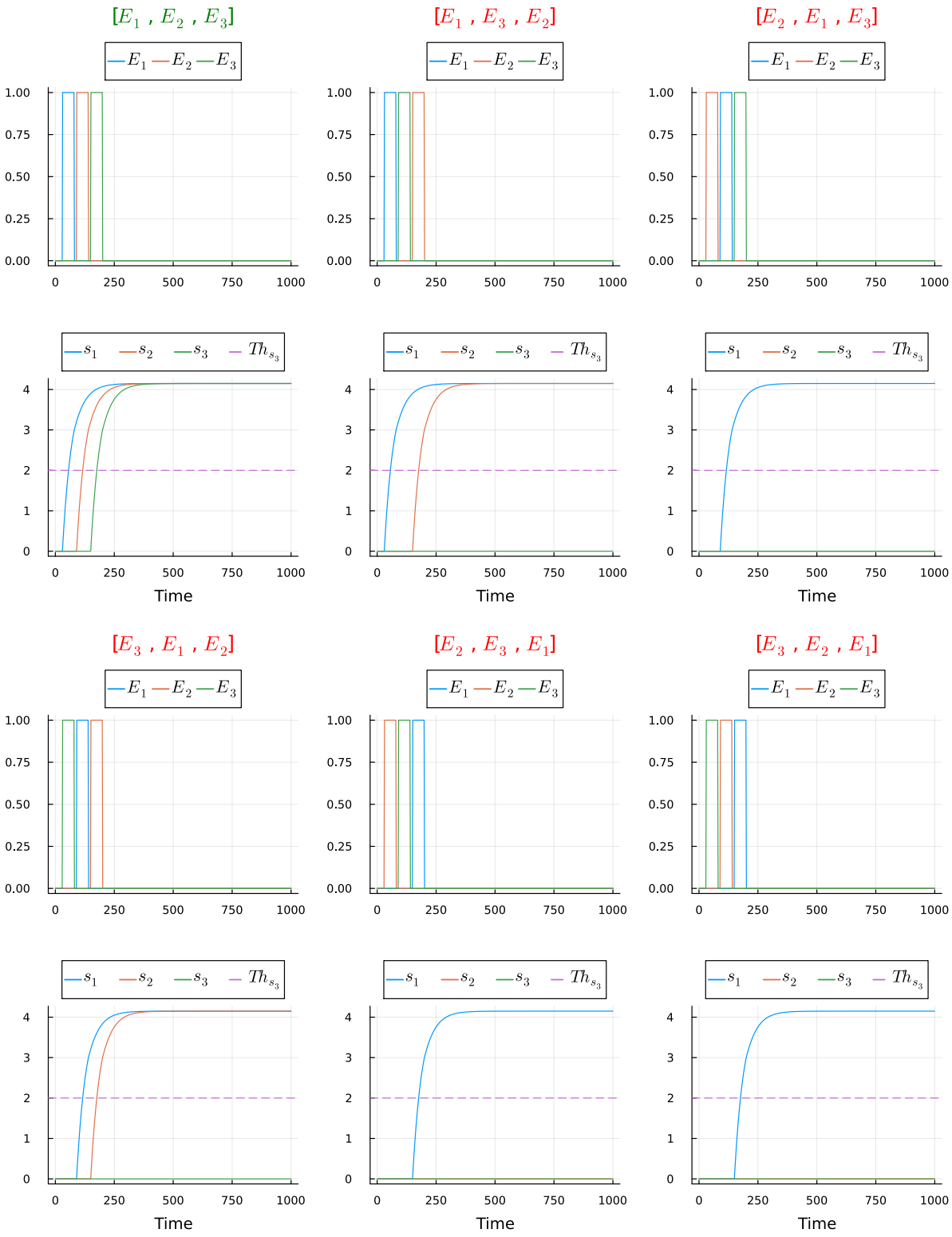

Figure 3.14.: Simulation of the basic model without the reset mechanism for a width of synaptic input of 50 and a delay of 60 for a dendritic branch of 3 dendritic compartments. Only the correct input sequence generates a movement detection. The activation variables are never reset even after a detection occurred.

3.2.2. Reset model with fast global negative feedback

To be able to detect consecutive input sequences temporally-separated by an in-between sequence delay, a reset mechanism has been incorporated in the dendritic-inspired model. Such a mechanism consists in activating a fast global negative feedback, symbolizing voltage-dependent potassium conductances, whose function is to bring the activation variable of the dendritic compartments to 0 once the response of the most proximal compartment has reach the detection threshold of the decision unit. In a system whose dendritic branch is composed of three dendritic compartments, the activation variables will thus be brought to 0 once $s_3(t)$ has reach the decision unit's threshold under the system configuration of Figure 3.7.

Mathematical Model

The mathematical model of the new system incorporating the described reset mechanism is the following:

$$\begin{cases} 1 & \tau \dot{s}_1(t) = -(1 + g_K(t)) \cdot s_1(t) + T(s_1(t),\ K - g_K(t),\ K_e,\ E_1(t),\ \sigma) \\ \vdots & \\ i & \tau \dot{s}_i(t) = -(1 + g_K(t)) \cdot s_i(t) + T(s_i(t),\ K - g_K(t),\ K_e \cdot s_{i-1}(t),\ E_i(t),\ \sigma) \\ \vdots & \\ n & \tau \dot{s}_n(t) = -(1 + g_K(t)) \cdot s_n(t) + T(s_n(t),\ K - g_K(t),\ K_e \cdot s_{n-1}(t),\ E_n(t),\ \sigma) \\ \\ \text{Reset} & \tau_{spike}\ \dot{g}_K(t) = \bar{g}_K\ \delta(t - t_{reset}) - g_K(t) \end{cases} \tag{3.13}$$

where t_{reset} is the time at which s_n reaches the decision unit's threshold, g_K is the reset memory such that $g_K(0) = 0$, τ_{spike} is the time constant of the reset variable dynamics and $\bar{g}_K$ is the reset strength.

It has to be noted that, in order for the reset mechanism to function as desired (to bring back the activation variables to 0), the time constant τ_{spike} has to be much smaller than the dendritic compartment's time constant τ as the reset acts as a fast negative feedback.

Moreover, the reset strength $\bar{g}_K$ value has to be taken relatively high for the reset to be able to bring the activation variables to 0 rapidly after the detection occurred.

The value of the parameter K is the same as in Section 3.2 since the equilibrium analysis is identical.

It can be observed in the model's system of equations 3.13 that the reset variable $g_K(t)$ appears at two different locations in the dynamics of each dendritic compartment. Firstly, it affects the inherent negative feedback of the dynamics by modifying the coefficient of the activation variable of the compartment itself following the relation $-(1+g_k(t)) \cdot s_i(t)$. Therefore, when a detection occurs, the reset variable g_K will increase and subsequently increase the inherent negative feedback of the compartment's dynamics. This thus results in a decrease of the activation variables of the compartments after a detection has been made by the decision unit.

Secondly, the reset variable affects the activation variable contribution parameter K. Similarly to the inherent negative feedback, the inherent positive feedback located inside the activation function will be reduced when a detection is made resulting in a decrease of the value of the activation variables. Another way to understand this mechanism is to look at the equilibrium analysis in Figure 3.13. It can be observed that, starting from a value of $K = 0.8$, reducing this value by g_K will bring the parameter K to a value lower than the saddle-node point K_{SN}. The consequence of this mechanism is therefore to force the system to reach a configuration where it has only a stable equilibrium located at $s_i = 0$.

Even though configurations where the reset variable only affects one location in the compartment' dynamics lead to a functioning reset mechanism, it has been preferred to use the described configuration where the reset affects both locations simultaneously as it hasten the transition between the upper stable equilibrium branch towards the neutral stable branch of the activation variables after a decision has been made.

Model Simulation

The behavior of the system in simulation can be seen in Figure 3.15 for the following values of parameters: $K = 0.8,\ K_e = 10,\ \sigma = 1,\ \tau = 40,\ \tau_{spike} = 30,\ \bar{g}_K = 2.$

As it can be observed in Figure 3.15, the role of the modulatory input $s_{i-1}(t)$ of a compartment i on its activation variable $s_i(t)$ is the same as in Section 3.2. Therefore, incorporating a reset mechanism did not prevent the system to efficiently detect the correct input sequence.

The major difference with the model 3.10 lies in the reset capacity of the system. It can indeed be seen in Figure 3.15 that, for the correct input sequence, all activation variables are brought back to their neutral stable branch as the activation variable of the most proximal compartment reached the decision unit's threshold. Therefore, an artificial transition of the model from the upper stable equilibrium branch towards the neutral stable branch has been performed. However, one flaw still exists in the system as the reset is only performed in case a correct motion was detected. Indeed, for all other input sequences than the correct one, the activation variables of the two first compartments stayed stuck in their decision.

As for the previous model, this model is unable to detect consecutive input sequences temporally-separated by an in-between sequence delay as the model will stay stuck in its decision until a correct input sequence is detected. Therefore, an incorrect input sequence might be identified as correct due to this flaw in the model when detecting consecutive input sequences.

As it has been determined in Section 2.5, dendritic action potentials generated at distal locations of the dendritic branch (in this case s_1) are attenuated when propagating to the soma (in this case the decision unit). Therefore, such a feature has been implemented using the reset mechanism as the response of the successive activation variables of the dendritic compartments are attenuated as observed in Figure 3.15 when a detection occurs.

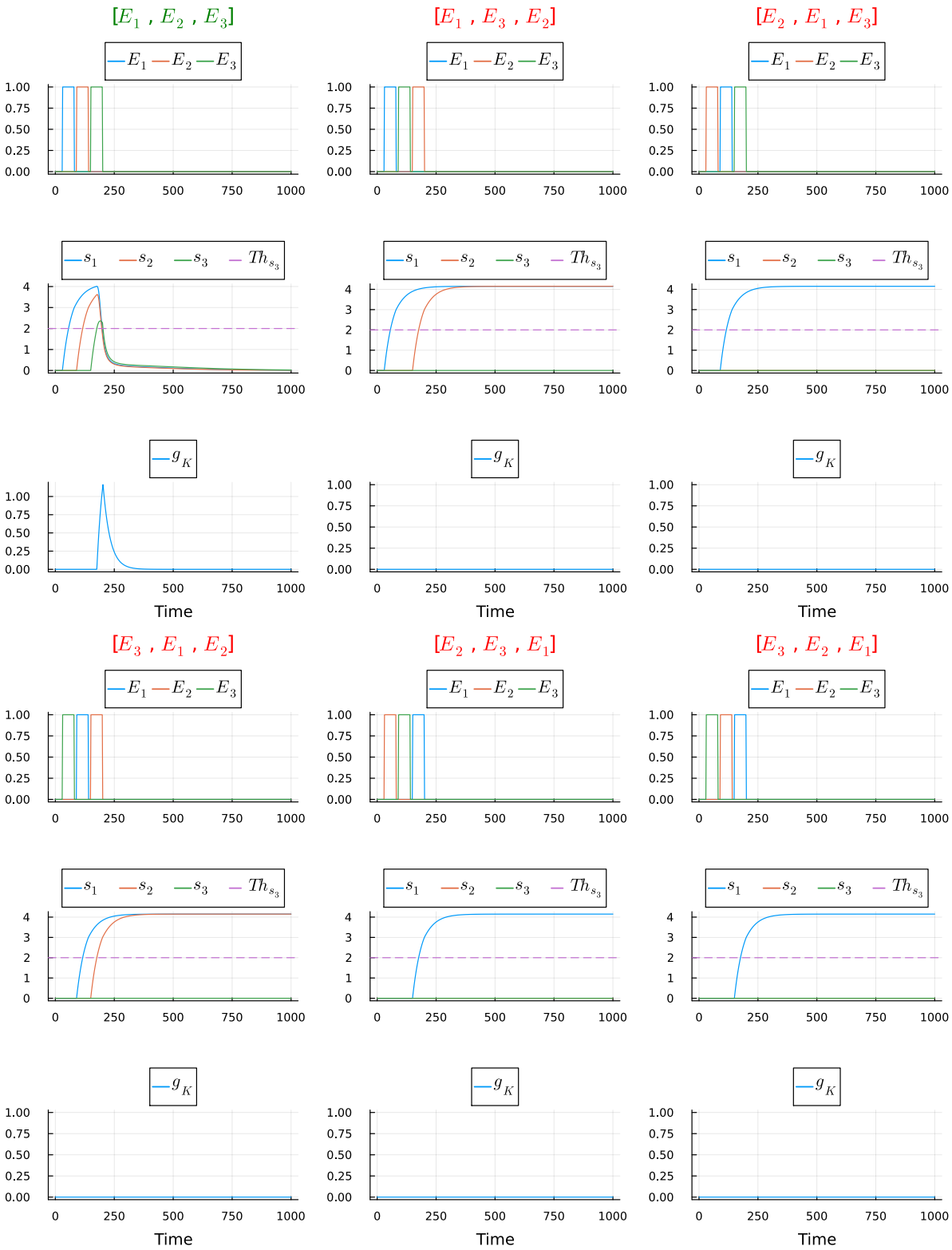

Figure 3.15.: Simulation of the basic model with the reset mechanism for a width of synaptic input of 50 and a delay of 60 for a dendritic branch of 3 dendritic compartments. Only the correct input sequence generates a movement detection. The reset mechanism efficiently resets the activation variables when a detection occurs.

3.3. Models Performances

3.3.1. Comparison of the performances of the two approaches

A comparison of the performances of the two approaches for the same parameters values, being the delay between synaptic inputs of the different dendritic compartments, the width of these synaptic inputs as well as the dendritic compartments' time constant will be performed to determine which approach is more reliable. The metric used for the performance comparison is the interval of delays' values under which the model is able to exhibit only true positive detection for a determined threshold.

The threshold determination of both approaches are performed for a time constant $\tau = 100$ and for a width of the synaptic inputs of 30. The results of the analysis can be seen in Figure 3.16.

As it can be observed in Figure 3.16, the first approach cannot detect the correct order of input sequences for all delay values between synaptic inputs of the different dendritic compartments. Indeed, using the determined threshold, the model cannot detect the correct input sequence for delays lower than 25 but exhibit only true positive detection for higher delays (see Figure 3.16a). On the other hand, the second approach exhibit only true positive detection for delays higher than about 5 with a much higher detection confidence (see Figure 3.16b).

Therefore, the second approach leads to a more reliable model to detect the correct input sequence thanks to the use of multiplicative arithmetic operations combined to additive ones to inhibit the responses of successive compartments if the order of the synaptic inputs is incorrect. A thorough analysis of the performances of the two approaches for different values of synaptic inputs width and compartments time constant will be performed in Section 3.3.2.

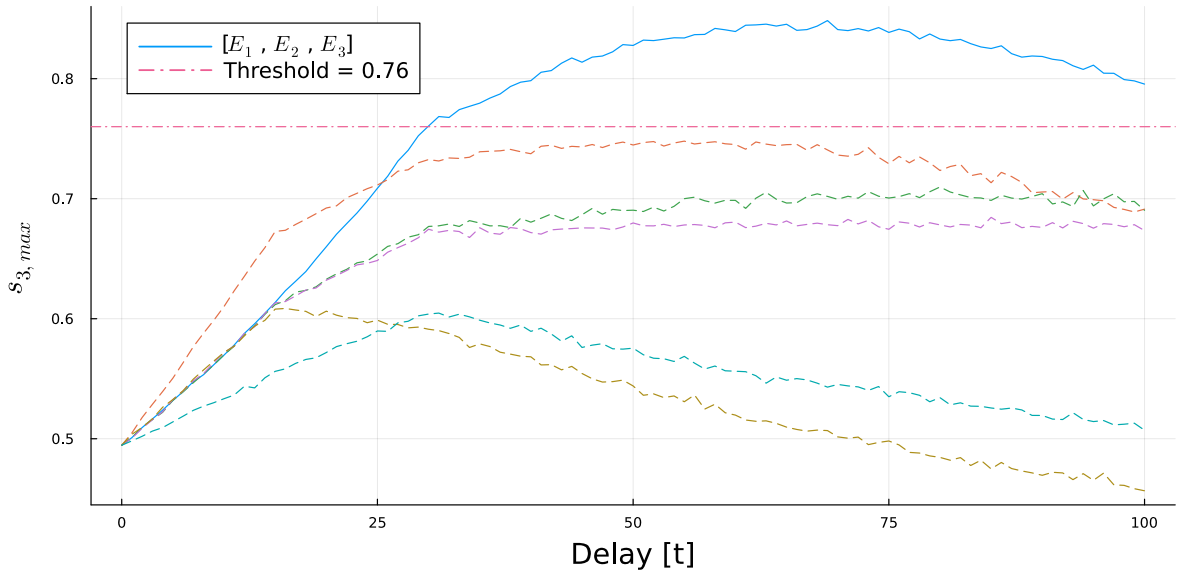

(a) Additive arithmetic operations approach.

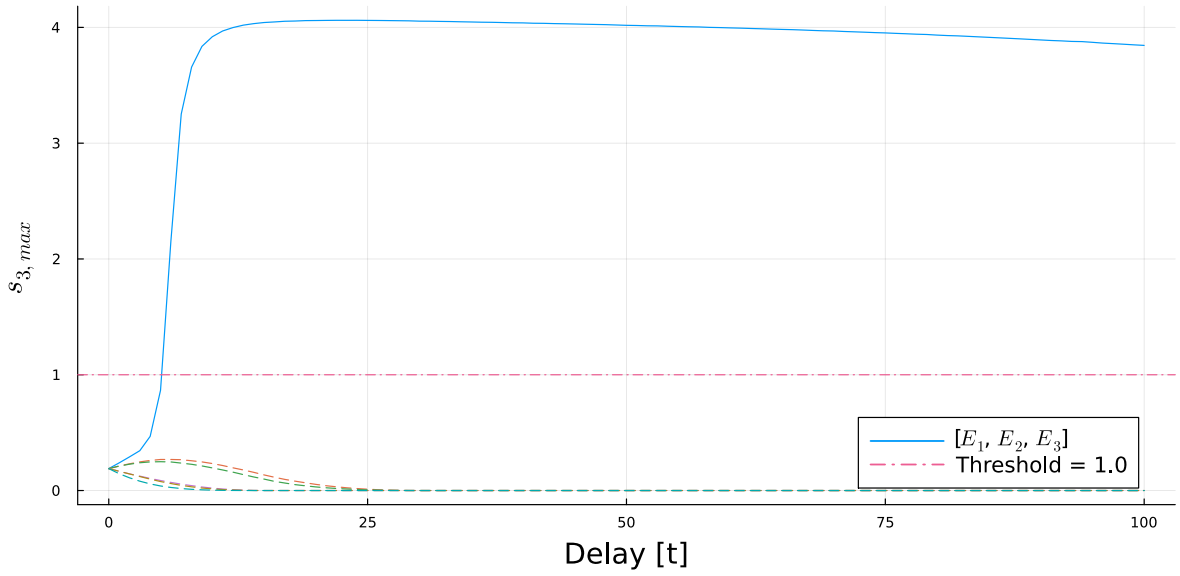

(b) Additive and multiplicative arithmetic operations approach.

Figure 3.16.: Threshold and delay interval determination for the naive and dendritic-inspired approaches. The blue line represents the maximum value of s_3 as a function of the delay between the inputs of the different compartments for the correct input sequence $[E_1, E_2, E_3]$. The dashed lines represent the same relationship for the incorrect orders of input sequences.

3.3.2. Global Analysis of the System Parameters

A global analysis of the effects of the time constant τ of the model, the delay between synaptic inputs of the different dendritic compartments and the width of these synaptic inputs will be performed to determine under which range of parameters values the system is correctly able to determine the correct order of input sequences.

Figure 3.17 shows the threshold determination of the first approach's model for different values of the time constant τ as well as for different synaptic inputs width. It can be noted that the additive model exhibits satisfying performances despite having a narrow range of delays in which the correct order of input sequences is detected. Moreover, this range of delays increases for higher values of the system's time constant as well as for small synaptic inputs width. Such a result can be understood by the fact that, using large synaptic inputs width, an overlapping of the synaptic inputs of the different compartments occurs which makes the system unable to detect the correct order of input sequences. As regards the effect of the time constant, the higher τ is, the slower the activation variable of the dendritic compartments will react to their synaptic input therefore counteracting the synaptic inputs overlap.

The interval of delays under which only true positive detection can occur gets narrower for higher values of synaptic inputs width whatever the model's time constant. Therefore, the system is found to be more reliable for higher time constant values and lower synaptic inputs width.

It can be noted in Figure 3.18 that the second approach's model exhibits more desirable performances despite a compromise of the system on its acceptance of false positive detection for small time constant values.

The same behavior as for the first approach can be observed in Figure 3.18. Indeed, the range of delays of solely true positive detection increases for higher values of the system's time constant as well as for small synaptic inputs width.

The downside of the second approach's model is its inability to work in an interval of delay values in which only true positive detection occurs for small time constant values.

Indeed, for small time constant values and large synaptic inputs width, incorrect orders of input sequences yield the same maximal value of the activation variable of the last dendritic compartment s_3 making the determination of a threshold leading to none false positive detection impossible. Therefore, a compromise on the system acceptance of false positive detection can be made which enable the system to determine a threshold yielding only true positive detection once the response of incorrect orders of input sequence falls to 0.

However, increasing the time constant τ to large values i.e. $\tau = 150$ in Figure 3.18, the system is capable to determine a threshold leading to only true positive detection for small synaptic inputs width.

It can thus be established that under small time constant values, the first approach enables the determination of a range of delay values leading to only true positive detection while the second approach is unable to. However, if a compromise is made to accept some false positive detection, the second approach leads to a larger delay interval in which the system can identify true positive detection.

For larger time constant values, the second approach is able to determine a very broad range of delay values in which only true positive detection occurs while the performances of the first approach do not improve as drastically when increasing the system time constant.

Therefore, the second approach using both additive and multiplicative arithmetic operations will be further investigated as it is more robust to variations of the system's parameters and exhibits higher confidence in the detection of the correct order of input sequences.

The detection of consecutive input sequences temporally-separated by an in-between sequence delay will thus be conducted with dendritic-inspired model.

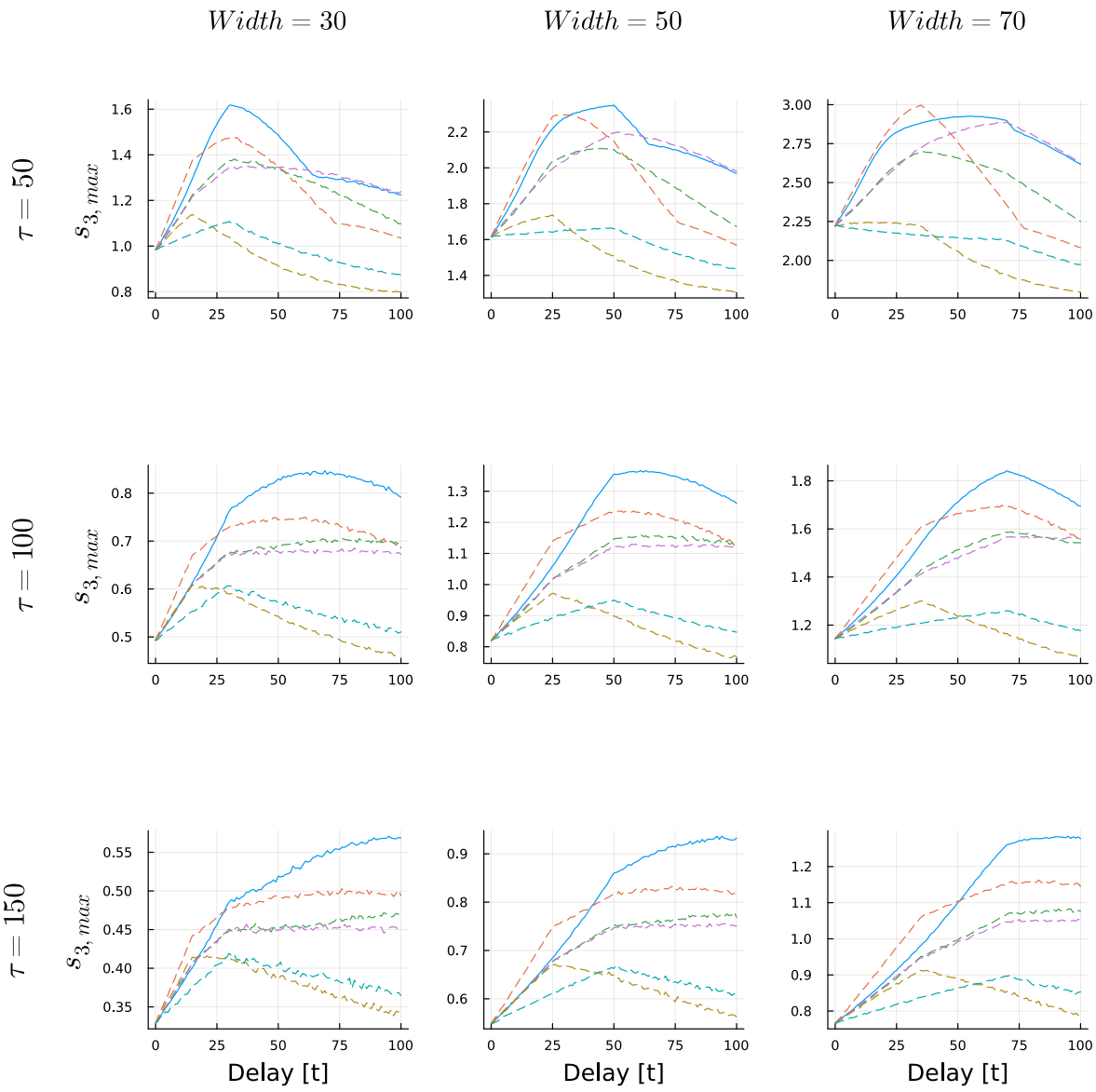

Figure 3.17.: Global analysis of the naive approach's model performances for different values of time constant τ and synaptic inputs width. The blue line represents the maximum value of s_3 as a function of the delay between the inputs of the different compartments for the correct input sequence $[E_1, E_2, E_3]$. The dashed lines represent the same relationship for the incorrect orders of input sequences.

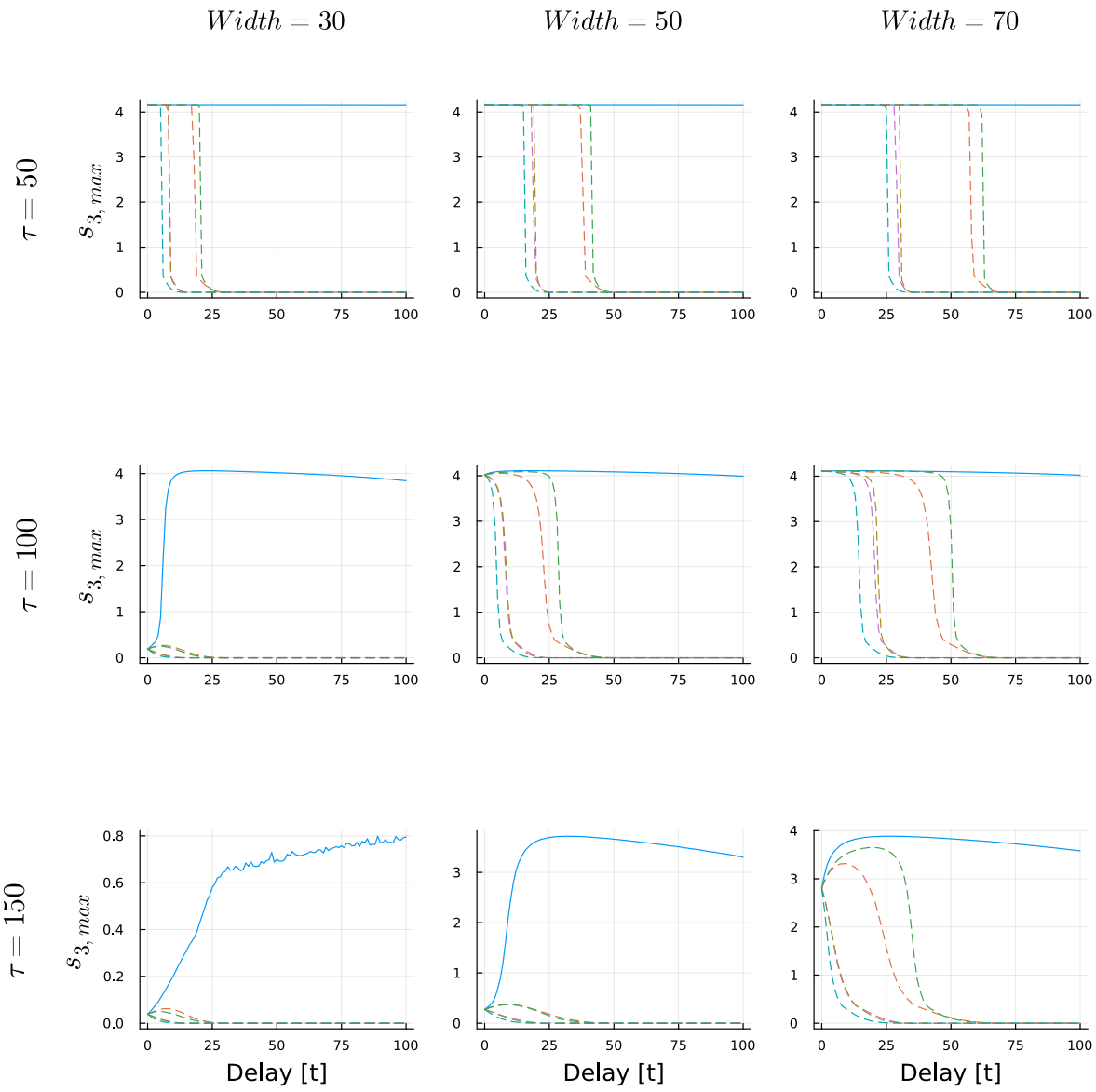

Figure 3.18.: Global analysis of the dendritic-inspired model performances for different values of time constant τ and synaptic inputs width. The blue line represents the maximum value of s_3 as a function of the delay between the inputs of the different compartments for the correct input sequence $[E_1, E_2, E_3]$. The dashed lines represent the same relationship for the incorrect orders of input sequences.

4. Improved dendritic-inspired model with slow local negative feedback

An improvement to remedy to the flaw of the model of staying stuck in its decision discussed in Section 3.2.1 consists in introducing slow local negative feedback into the model 3.13.

4.1. Activation Function

$$U(x,\ K,\ K_e,\ k_s,\ E,\ \sigma) = \frac{\tanh\left((K - k_s)\cdot x + K_e \cdot E - \sigma\right) - \tanh\left(-\sigma\right)}{1 - \tanh\left(\sigma\right)^2} \tag{4.1}$$

where k_s is the slow local negative feedback variable and all other parameters involved have already been introduced in the activation function of Section 3.2.

4.2. Mathematical Model

Using the new activation function U defined above, the mathematical model of the system with integrated slow local negative feedback with the reset mechanism is the following:

$$
\begin{cases}
1 & \tau \dot{s}_1(t) = -(1 + g_K(t)) \cdot s_1(t) + U(s_1(t),\ K - g_K(t),\ K_e,\ k_{s,1},\ E_1(t),\ \sigma) \\
 & \tau_{slow}\ \dot{k}_{s,1}(t) = g \cdot s_1^2(t) - k_{s,1}(t) \\
\vdots & \\
i & \tau \dot{s}_i(t) = -(1 + g_K(t)) \cdot s_i(t) + U(s_i(t),\ K - g_K(t),\ K_e \cdot s_{i-1}(t),\ k_{s,i},\ E_i(t),\ \sigma) \\
 & \tau_{slow}\ \dot{k}_{s,i}(t) = g \cdot s_i^2(t) - k_{s,i}(t) \\
\vdots & \\
n & \tau \dot{s}_n(t) = -(1 + g_K(t)) \cdot s_n(t) + U(s_n(t),\ K - g_K(t),\ K_e \cdot s_{n-1}(t),\ k_{s,n},\ E_n(t),\ \sigma) \\
 & \tau_{slow}\ \dot{k}_{s,n}(t) = g \cdot s_n^2(t) - k_{s,n}(t) \\
 & \\
\text{Reset} & \tau_{spike}\ \dot{g}_K(t) = \bar{g}_K\ \delta(t - t_{reset}) - g_K(t)
\end{cases}
\tag{4.2}
$$

where t_{slow} is the time constant of the slow local negative feedback variable k_s dynamics and g is the activation variable strength in the negative feedback variable k_s dynamics.

The dynamics of the slow negative feedback variable k_s are similar to the one of the activation variable of the dendritic compartments since they both are first-order ODEs. The input in the k_s dynamics is the activation variable whose strength is controlled by the parameter g. It can be directly seen that as s_i increases, $k_{s,i}$ increases linearly with a multiplicative factor g. Once $k_{s,i}$ reaches a sufficient value, its negative feedback on s_i will become ample enough to bring down s_i. Thus, as s_i decreases, $k_{s,i}$ will decrease as well and both variables will be brought down to 0.

Concerning the reset mechanism, the choice of using the reset variable g_K at two locations in the activation variable dynamics is still made as it speeds up the transition between the upper stable equilibrium branch towards the neutral stable branch of the activation variables after a decision has been made.

It has to be noted that, in order for the slow local negative feedback to function as desired, which is to bring back the activation variables to 0 naturally, the time constant τ_{slow} of the variable k_s dynamics has to be much larger than the dendritic compartment's time

constant τ as the variable k_s has to act a a slow local negative feedback. Moreover, the value of the negative feedback variable k_s strength g has to be taken relatively low for the negative feedback to be able to bring the activation variables to 0 naturally.

4.3. Equilibrium Analysis

An analysis of the different equilibrium of the system with regards to the activation variable contribution parameter K has been conducted at the initial time t_0 (for a zero synaptic input and a zero reset variable $g_K(t_0) = 0$) in a similar manner as performed in Section 3.2.1.

At the initial time t_0, the fixed points of the system can be computed for $\dot{s}_i = 0 \ , \forall i$. It comes as well that to compute the fixed points, one has to replace $k_{s,i}$ in terms of s_i in the equation $\dot{s}_i = 0$. This can be determined by setting $\dot{k}_{s,i} = 0$ which leads to $k_{s,i} = g \cdot s_i^2$.

The system obtained by taking into consideration these conditions as well as the fact that $E_i = 0 \ , \forall i$ is thus the following:

$$\begin{cases} 1 & 0 = -s_1 + \frac{\tanh\left[(K - g \cdot s_1^2) \cdot s_1 - \sigma\right] - \tanh\left(-\sigma\right)}{1 - \tanh^2\left(\sigma\right)} \\ \vdots & \\ i & 0 = -s_i + \frac{\tanh\left[(K - g \cdot s_i^2) \cdot s_i - \sigma\right] - \tanh\left(-\sigma\right)}{1 - \tanh^2\left(\sigma\right)} \\ \vdots & \\ n & 0 = -s_n + \frac{\tanh\left[(K - g \cdot s_n^2) \cdot s_n - \sigma\right] - \tanh\left(-\sigma\right)}{1 - \tanh^2\left(\sigma\right)} \end{cases} \tag{4.3}$$

One fixed to the system of equations 4.3 can be directly inferred as being $\bar{s} = [0, \ldots, 0]$. However, other fixed points cannot be determined analytically.

The Jacobian matrix is computed using 3.2 and is the following:

$$J = \frac{1}{\tau \cdot \left[1 - \tanh^2(\sigma)\right]} \begin{pmatrix} a_1 & 0 & \dots & 0 \\ 0 & \ddots & \ddots & \vdots \\ \vdots & \ddots & \ddots & 0 \\ 0 & \dots & 0 & a_n \end{pmatrix} \tag{4.4}$$

where $a_i = -(1 - \tanh^2(\sigma)) + [K - 3g \cdot s_i^2] \cdot \text{sech}^2\ [(K - g \cdot s_i) \cdot s_i - \sigma]$.

Evaluating the Jacobian matrix at the fixed point $\bar{s} = [0, \dots, 0]$ and computing the determinant, the system of equations 4.3 has the same eigenvalues as the system of equations 3.11.

The same equilibrium analysis as performed in Section 3.2 is valid for this model as the eigenvalues and the associated eigenvectors are the same for the computed fixed point.

The equilibrium analysis for the system can be observed in Figure 4.1 for parameters values $\sigma = 1,\ g = 0.1$.

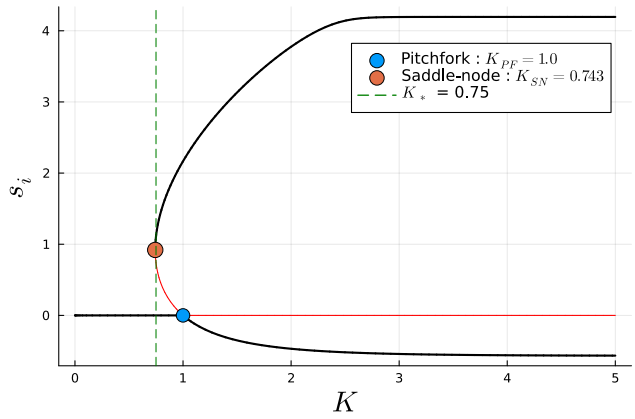

Figure 4.1.: Parameter K determination for the improved dendritic-inspired model with slow local negative feedback for $\sigma = 1$.

It can be seen in Figure 4.1 that the equilibrium analysis has a supercritical Pitchfork-like bifurcation that is even more unfolded and deformed compared to Figure 3.13. Indeed, due to both the positive bias and the additional slow local negative feedback dynamics, the non-linearity of the activation function has been emphasized resulting in a even more

deformed upward unfolding of the Pitchfork bifurcation.

As for the model 3.10, the determination of the Saddle-node bifurcation K_{SN} was performed numerically leading to $K_{SN} = 0.743$ for the chosen parameters values.

It can be seen in Figure 4.1 that, for $K < K_{SN}$, there is only one equilibrium located at $s_i = 0$. For $K \in]K_{SN}, 1[$, there are two stable equilibrium (one located at $s_i = 0$ and the other one in the upper branch) as well as an unstable equilibrium in-between. For $K > 1$, there is an unstable equilibrium located at $s_i = 0$ and two stable equilibrium on the upper and lower branches.

The same observation as in Section 3.2.1 about the maximal value of s_i can be made in Figure 4.1 and the explanation is matched
.
The value chosen for the parameter K was therefore a value in the interval $]K_{SN}, 1[$ in order to have a stable equilibrium in the upper branch, corresponding to a positive decision, as well as a stable equilibrium for a null value of s_i, corresponding to the neutral stable branch. The value of the parameter has thus been chosen as $K = 0.8$.

This behavior was desired for the designed model as the system can either stay at the neutral stable branch either take a positive decision and jump to the upper stable branch. However,the difference with the model 3.10 is that the system is now able exhibit a bistability in the interval $]K_{SN}, 1[$ between its neutral stable branch and its upper stable branch thanks to the additional slow local negative feedback.

4.4. Nullcline and Phase Plane Analysis

A nullcline and phase plane analysis of the model has been performed as it allows to determine how the dynamics of the system will behave. Such an analysis consists in studying the behavior of the system dynamics for $\dot{s}_i = 0$ and $\dot{k}_{s,i} = 0$ and analysing the geometric shape thus obtained. Moreover, it allows to determine the equilibrium points of the system which are located at the intersection of the nullclines.

As the different equations of the system 4.2 are independent w.r.t. the equations of the other dendritic compartments such that $\dot{s}_i = f(s_i, k_{s,i})$ and $\dot{k}_{s,i} = f(s_i, k_{s,i})$, the results of the analysis conducted are equivalent for all dendritic compartments as the dynamics of all compartments are identical when $E_i = \cdots = E_n = 0$.

The nullcline and phase plane analysis of the system with slow local negative feedback can be seen in Figure 4.2 for parameters values $K = 0.6,\ \sigma = 0,\ g = 0.1$.

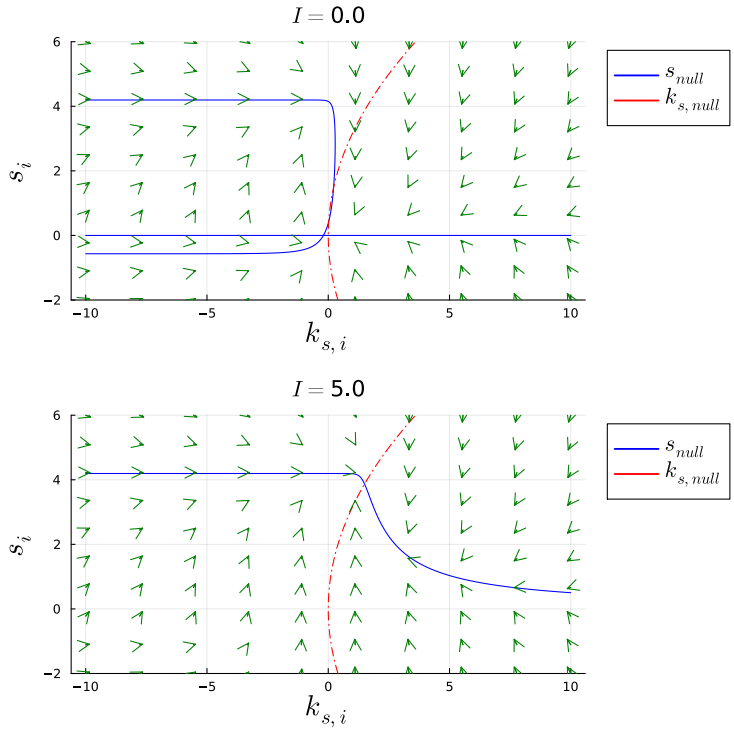

Figure 4.2.: Nullcline and phase plane analysis of the improved dendritic-inspired model with slow local negative feedback.

Figure 4.2 shows that, for a null stimulus, the only stable equilibrium point of the system is located at $(k_{s,i}\ ; s_i) = (0\ ; 0)$ as the other equilibrium points (located at the other intersections between the s_i-nullcline and the $k_{s,i}$-nullcline) are not stable. Therefore, there is an attraction towards to stable equilibrium point $(0\ ; 0)$.

When a non-null positive stimulus is fed to the dendritic compartment, the s_i-nullcline is deformed and the system only has one equilibrium point located on the upper branch

which is stable and acts as an attractor.

It can thus be understood that at the initial time $t_0 = t(0)$, the stable solution of the system is located at the stable equilibrium point $(k_{s,i}\ ; s_i) = (0\ ; 0)$ of the system. Then, when the synaptic input of the dendritic compartment is positive, the stable equilibrium point of the system is moved around on the upper stable branch of the upward-unfolded Pitchfork bifurcation of the s_i-nullcline. This results in a increase of both variables s_i and $k_{s,i}$ to reach the new equilibrium point. When the synaptic input becomes null again, the stable equilibrium point of the system returns back to $(k_{s,i}\ ; s_i) = (0\ ; 0)$ which causes both s_i and $k_{s,i}$ to decrease to reach the new stable equilibrium point.

The behavior of the system is shown by the vector field represented by the green arrows in Figure 4.2.

4.5. Model Simulation

The behavior of the improved dendritic-inspired system in simulation can be seen in Figure 4.3 for the following values of parameters: $K = 0.8,\ K_e = 10,\ \sigma = 1,\ \tau = 40,\ \tau_{spike} = 30,\ \bar{g}_K = 2,\ \tau_{slow} = 200,\ g = 0.1$.

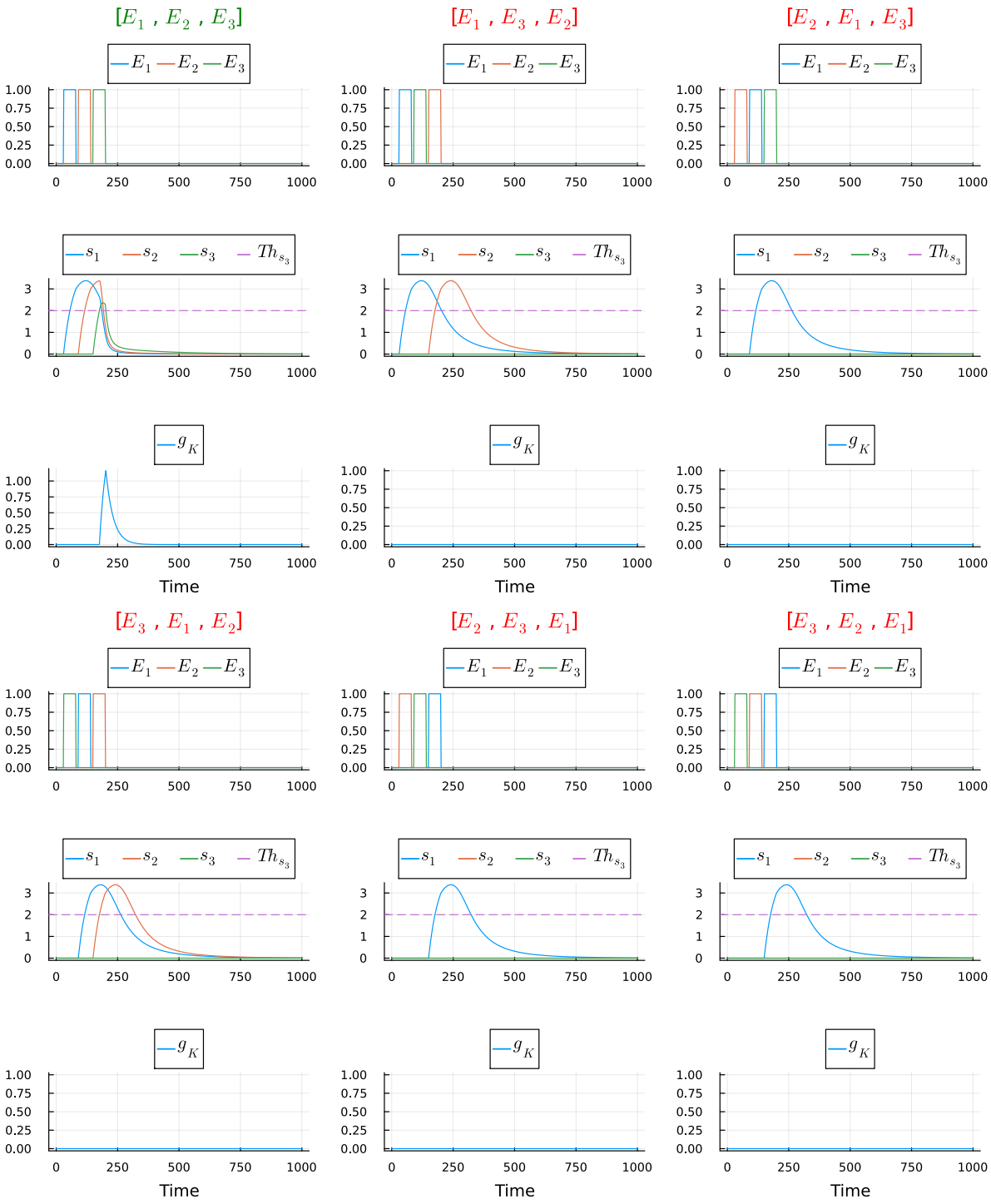

Figure 4.3.: Simulation of the improved dendritic-inspired model with the reset mechanism for a width of synaptic input of 50 and a delay of 60 for a dendritic branch of 3 dendritic compartments. Only the correct input sequence generates a movement detection. The slow local negative feedback naturally brings back the activation variables to 0. The reset mechanism speeds up the reset of the activation variables when a detection occurs.

As it can be observed in Figure 4.3, the role of the modulatory input $s_{i-1}(t)$ of a compartment i on its activation variable $s_i(t)$ is the same as in Section 3.2. Therefore, incorporating a slow local negative feedback did not prevent the system to efficiently detect the correct input sequence.

The major difference with the model 3.13 lies in the natural reset capacity of the system thanks to the slow local negative feedback of the model. It can indeed be seen in Figure 4.3 that, for the correct input sequence, all activation variables are brought back to their neutral stable branch as the activation variable of the most proximal compartment reached the decision unit's threshold. Therefore, an natural transition of the model from the upper stable equilibrium branch towards the neutral stable branch has been performed which was reinforced by the reset mechanism. The advantage of this model is that the activation variables are brought back to their neutral stable branch even when no reset is performed whatever the input sequence order. Indeed, for all other input sequences than the correct one, the activation variables of the two first compartments returned naturally to their neutral stable branch (see Figure 4.3).

Unlike the two previous models, this model is efficiently able to detect consecutive input sequences temporally- separated by an in-between sequence delay as the model does not stay stuck in its decision anymore.

However, even though the reset mechanism hasten the transition of the activation variable from the upper stable equilibrium branch towards its neutral stable branch, this models perfectly functions even without the reset mechanism implemented.

The performance of the model with integrated slow local negative feedback without the reset mechanism can be seen in Figure 4.4 with the same parameters value as in Figure 4.3.

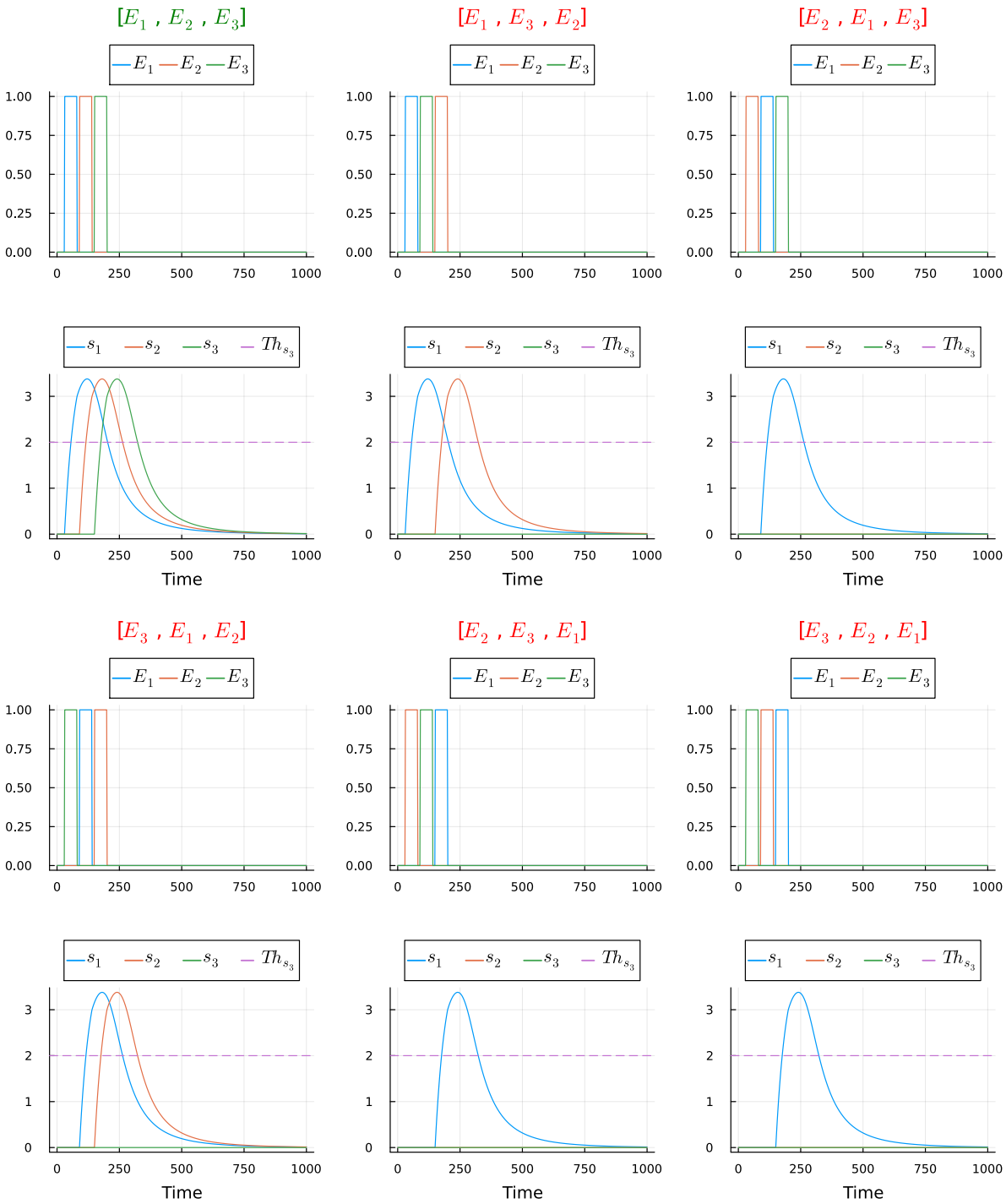

Figure 4.4.: Simulation of the improved dendritic-inspired model without the reset mechanism for a width of synaptic input of 50 and a delay of 60 for a dendritic branch of 3 dendritic compartments. Only the correct input sequence generates a movement detection. The slow local negative feedback naturally brings back the activation variables to 0 even without using the reset mechanism.

As it can be observed in Figure 4.4, the model is perfectly capable of resetting its decision naturally thanks to its additional slow local negative feedback. Therefore, both the improved model with and without the reset mechanism enable the system to correctly identify consecutive input sequences temporally-separated by an in-between sequence delay. The decision to use either one of these two models mainly depends on the in-between sequence delay. Indeed, the model without the reset mechanism will require a larger delay between consecutive input sequences as the dynamics will take longer to return to the neutral stable branch from the upper stable branch after a decision has been taken by the dendritic compartments. On the other hand, the model with the reset mechanism will see its transition from one stable branch to the other sped up by the reset variable, thus requiring a smaller delay between consecutive input sequences.

The trajectory of the model with and without reset mechanism alongside the nullclines can be seen in Figures 4.5 and 4.6.

In both Figures 4.5a and 4.6a, the trajectory initially involves an elevation of s_i while $k_{s,i}$ remains constant, followed by an increase in both variables. Subsequently, as s_i reaches its maximum value, $k_{s,i}$ continues to rise while s_i begins to decline. Eventually, when $k_{s,i}$ attains its maximum value, both variables regress back to the stable equilibrium point positioned at $(k_{s,i}\,;s_i) = (0\,;0)$. A zoom of the trajectory region in Figures 4.5a and 4.6a has been performed to clearly observe the temporal trajectories of the model and can be seen in Figures 4.5b and 4.6b.

Each cyan-colored circle represents one-tenth of the total simulation time. This visualization reveals that the rapid increase of s_i (depolarization phase) occurs on a much shorter time scale compared to its decrease (repolarization phase).

The trajectory of the model is very similar whether the reset mechanism is used or not. The only difference is the speed at which the activation variables returns to the neutral stable branch which can be seen in Figures 4.4 and 4.3.

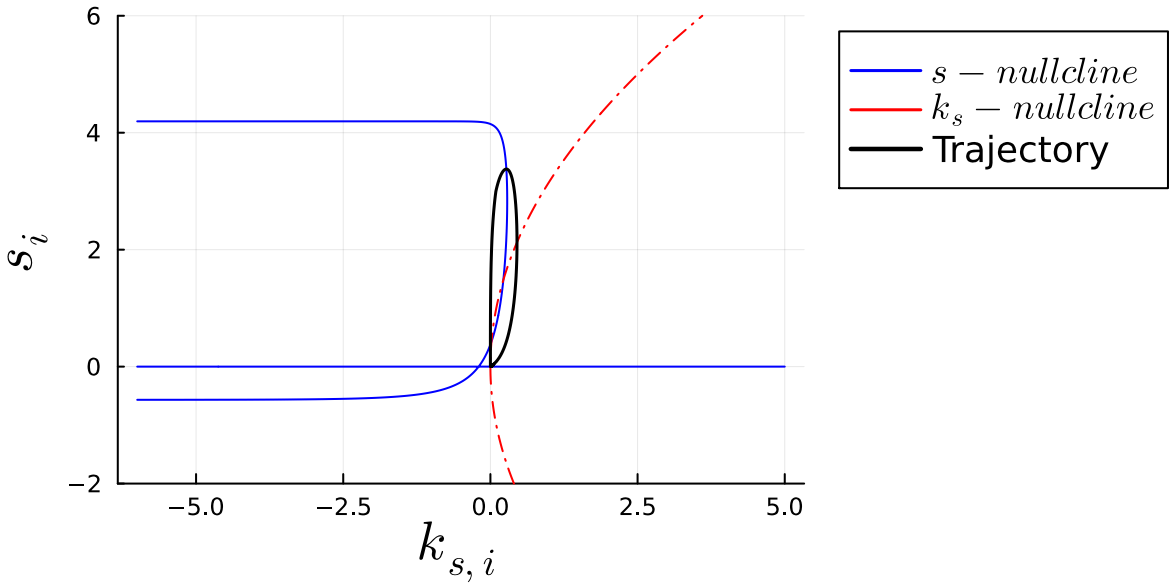

(a) Trajectory alongside nullclines.

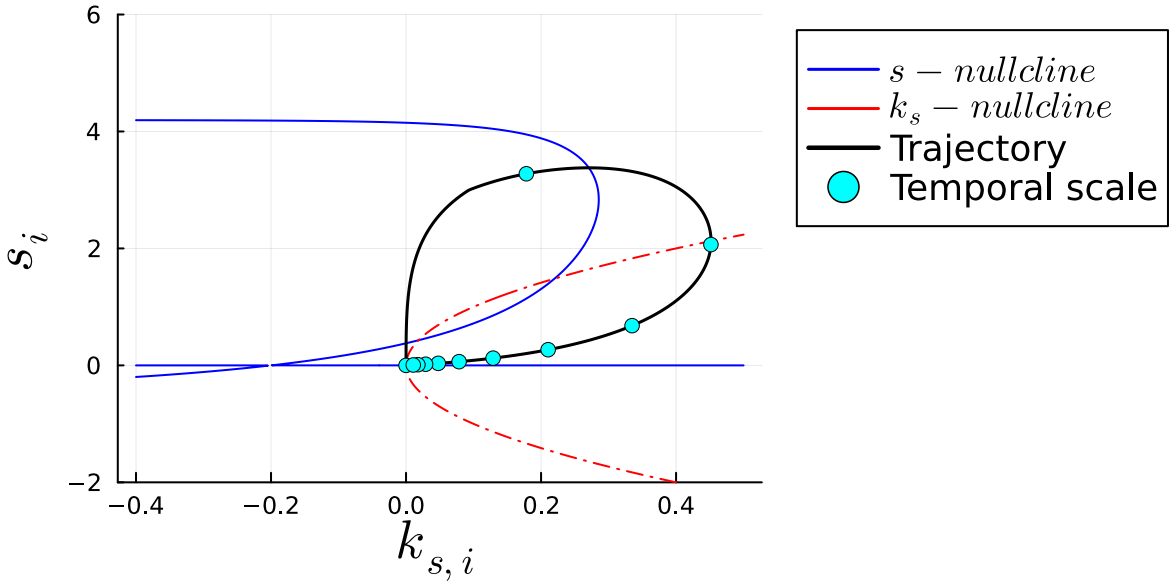

(b) Zoom in the trajectory region of Figure 4.5a.

Figure 4.5.: Trajectory of the improved dendritic-inspired model without reset mechanism alongside the nullclines. The trajectory moves from one stable fixed point to the other as expected when a synaptic input is fed. The cyan-colored circles represent the time scale of the simulation (one tenth of the simulation per circle).

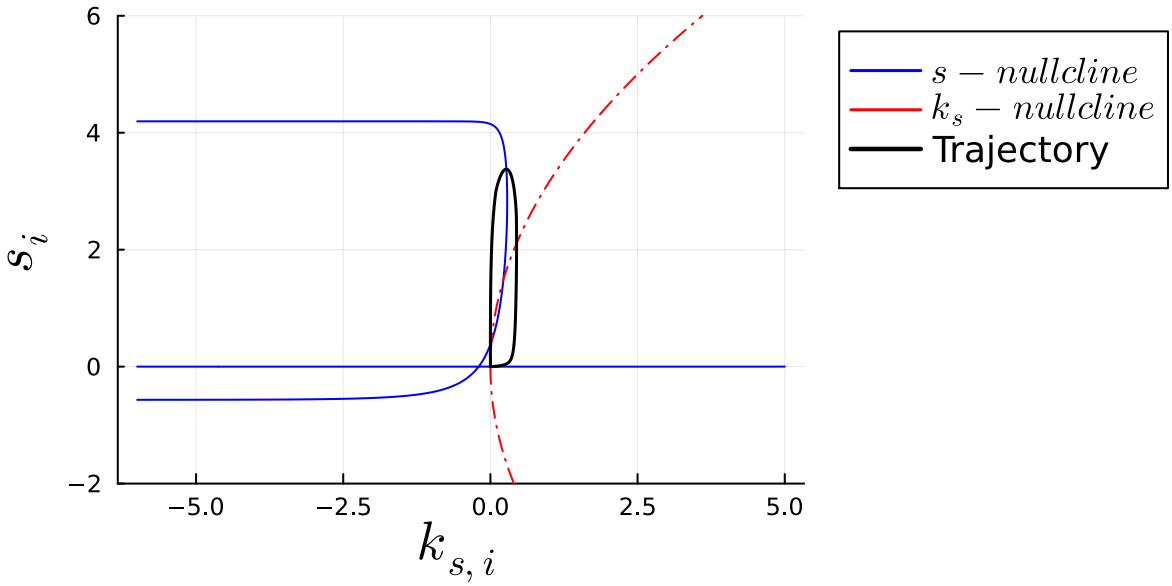

(a) Trajectory alongside nullclines.

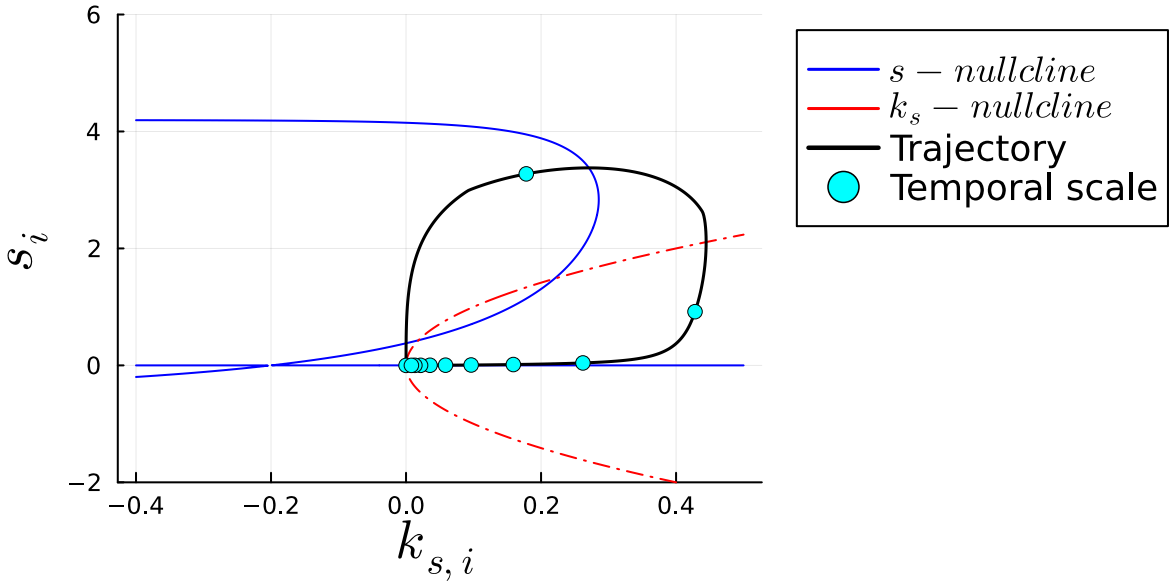

(b) Zoom in the trajectory region of Figure 4.6a.

Figure 4.6.: Trajectory of the improved dendritic-inspired model with reset mechanism alongside the nullclines. The trajectory moves from one stable fixed point to the other as expected when a synaptic input is fed. The cyan-colored circles represent the time scale of the simulation (one tenth of the simulation per circle).

5. Bidirectional movement detection

Even though it has been established in Section 2.6 that the neuron has a directional sensitivity which promotes input sequences activating dendritic compartments going from distal compartments to the soma, a model capable of detecting input sequences going both in the preferred and in the reversed direction has been implemented. The choice to develop such a model was mainly motivated for engineering purposes as such a system has more practical uses.

The implementation of a bidirectional model can be useful in many applications for movement detection although it does not make sense biologically speaking.

For the design of this system, each dendritic compartment is fed by its own synaptic input and receives the response of the preceding compartment as well as influencing the following compartment with its response.

The interconnection between the different compartments are shown in Figure 5.1.

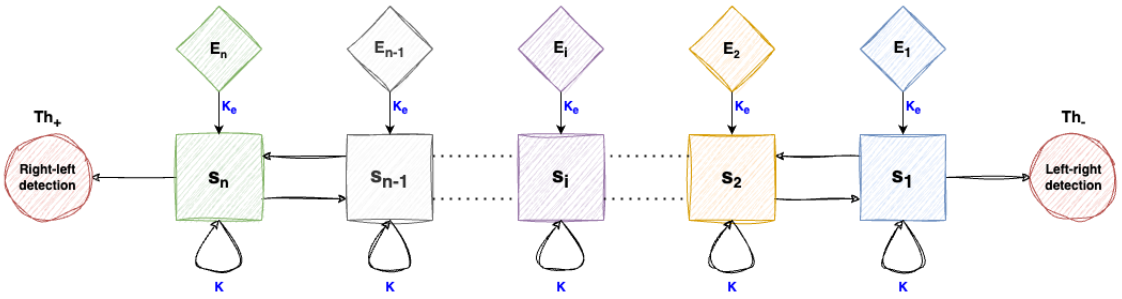

Figure 5.1.: Overview of the structure of the bidirectional system for a dendritic branch composed of n dendritic compartments.

5.1. Activation Function

$$M(x,\ K,\ K_e,\ k_s,\ E,\ \sigma) = \frac{\tanh\left((K + K_x \cdot x^2 - k_s) \cdot x + K_e \cdot E - \sigma\right) - \tanh\left(-\sigma\right)}{1 - \tanh\left(\sigma\right)^2} \quad (5.1)$$

where K_x is the strength of the reinforced local positive feedback and all other parameters involved have already been introduced in the activation function of Section 3.2.

5.2. Mathematical Model

$$\begin{cases} 1 & \tau \dot{s}_1(t) = -s_1(t) + M(s_1(t),\ K,\ K_e \cdot (\Delta + 2 \cdot s_2(t)),\ k_s + g_K(t),\ E_1(t),\ \sigma) \\ & \dot{k}_{s,1}(t) = \epsilon((g \cdot s_1(t))^4 - k_{s,1}(t)) \\ \vdots & \\ i & \tau \dot{s}_i(t) = -s_i(t) + M(s_i(t),\ K,\ K_e \cdot (s_{i-1}(t) + s_{i+1}(t)),\ k_s + g_K(t),\ E_i(t),\ \sigma) \\ & \dot{k}_{s,i}(t) = \epsilon((g \cdot s_i(t))^4 - k_{s,i}(t)) \\ \vdots & \\ n & \tau \dot{s}_n(t) = -s_n(t) + M(s_n(t),\ K,\ K_e \cdot (-\Delta + 2 \cdot s_{n-1}(t)),\ k_s + g_K(t),\ E_n(t),\ \sigma) \\ & \dot{k}_{s,n}(t) = \epsilon((g \cdot s_n(t))^4 - k_{s,n}(t)) \\ \text{Reset} & \tau_{spike}\ \dot{g}_K(t) = \bar{g}_K\ \delta(t - t_{reset}) - g_K(t) \end{cases}$$

where ϵ is the inverse time constant of the slow local negative feedback variable k_s, g is the activation variable strength in the negative feedback variable k_s dynamics and Δ is the multiplicative offset of the synaptic input.

The dynamics of the slow negative feedback variable k_s are similar to the one described in Chapter 4.

Regarding the reset mechanism, the decision to utilize the reset variable g_K at a single location in the activation variable dynamics, rather than at two locations as in previous models, is driven by the effectiveness of the slow local negative feedback introduced by k_s. This feedback is sufficiently swift to facilitate the transition from the up/down stable equilibrium branch to the neutral stable branch of the activation variables after a decision has been rendered.

It is essential to acknowledge that for the slow local negative feedback to operate effectively, the inverse time constant ϵ of the variable k_s dynamics must be substantially lower than the dendritic compartment's time constant τ, allowing k_s to function as a slow local negative feedback mechanism. Additionally, the strength g of the negative feedback variable k_s must be relatively low to naturally bring the activation variables back to 0. However, compared to the model discussed in Chapter 4, the value of g needs to be set higher.

In the bidirectional model, decisions regarding the direction of movement are made by generating positive responses for right-to-left motions and negative responses for left-to-right motions of the activation variables. Consequently, two thresholds, Th_+ and Th_-, with the same absolute value but opposite signs, are necessary in this model. Right-to-left motions are identified when the activation variable s_n exceeds the positive threshold ($s_n > Th_+$), while left-to-right motions are detected when the activation variable s_1 falls below the negative threshold ($s_1 < Th_-$). Figure 5.1 illustrates this approach.

An essential parameter for enabling this model to detect input sequences in both directions is the multiplicative offset Δ. This parameter ensures that the first and last dendritic compartments consider their synaptic input even if the subsequent or preceding compartment was not activated. In the dynamics of s_1, for instance, the offset Δ is added to the activation variable s_2, enabling s_1 to produce a positive response when E_1 occurs in a right-to-left movement scenario. Conversely, if the movement is left-to-right, s_2 will be negative when E_1 occurs, prompting s_1 to generate a negative response. A similar mechanism applies to the dynamics of s_n, with the offset having a negative sign to propagate a negative response for left-to-right movements.

It is noteworthy that the impact of the offset is counterbalanced by adding the activation variable of the preceding compartment to the offset. In the case of a right-to-left movement, for instance, the offset in the activation variable s_n dynamics is shifted by the value of s_{n-1}, and similarly, in the activation variable s_1 dynamics for left-to-right movements.

Therefore, this parameter in the model lies in the functioning of the bidirectional movement detection of the model and its value has to be taken relatively low i.e. $\Delta = 0.1$.

5.3. Equilibrium Analysis

An analysis of the different equilibrium of the system with regards to the activation variable contribution parameter K has been conducted in a similar manner as performed in Section 4.3.

Under the same conditions, the system for the fixed points determination is the following:

$$\begin{cases} 1 & 0 = -s_1 + \frac{\tanh\left[(K+K_x\cdot s_1^2-(g\cdot s_1)^4)\cdot s_1-\sigma\right]-\tanh(-\sigma)}{1-\tanh^2(\sigma)} \\ \vdots & \\ i & 0 = -s_i + \frac{\tanh\left[(K+K_x\cdot s_i^2-(g\cdot s_i)^4)\cdot s_i-\sigma\right]-\tanh(-\sigma)}{1-\tanh^2(\sigma)} \\ \vdots & \\ n & 0 = -s_n + \frac{\tanh\left[(K+K_x\cdot s_n^2-(g\cdot s_n)^4)\cdot s_n-\sigma\right]-\tanh(-\sigma)}{1-\tanh^2(\sigma)} \end{cases} \tag{5.2}$$

One fixed to the system of equations 5.2 can be directly inferred as being $\bar{s} = [0, \ldots, 0]$. However, other fixed points cannot be determined analytically.

The Jacobian matrix is computed using 3.2 and is the following:

$$J = \frac{1}{\tau \cdot \left[1 - \tanh^2(\sigma)\right]} \begin{pmatrix} a_1 & 0 & \ldots & 0 \\ 0 & \ddots & \ddots & \vdots \\ \vdots & \ddots & \ddots & 0 \\ 0 & \ldots & 0 & a_n \end{pmatrix} \tag{5.3}$$

where $a_i = -(1-\tanh^2(\sigma)) + [K + 3K_x \cdot s_i^2 - 5 \cdot (g \cdot s_i)^4] \cdot \text{sech}^2\ [(K + K_x \cdot s_i - (g \cdot s_i)^4) \cdot s_i - \sigma]$.

Evaluating the Jacobian matrix at the fixed point $\bar{s} = [0, \ldots, 0]$ and computing the determinant, the system of equations 5.2 has the same eigenvalues as the system of equations 3.11.

The same equilibrium analysis as performed in Section 3.2 is valid for this model as the eigenvalues and the associated eigenvectors are the same for the computed fixed point.

The equilibrium analysis for the system can be observed in Figure 5.2 for parameters values $\sigma = 0,\ g = 1.3,\ K_x = 3$.

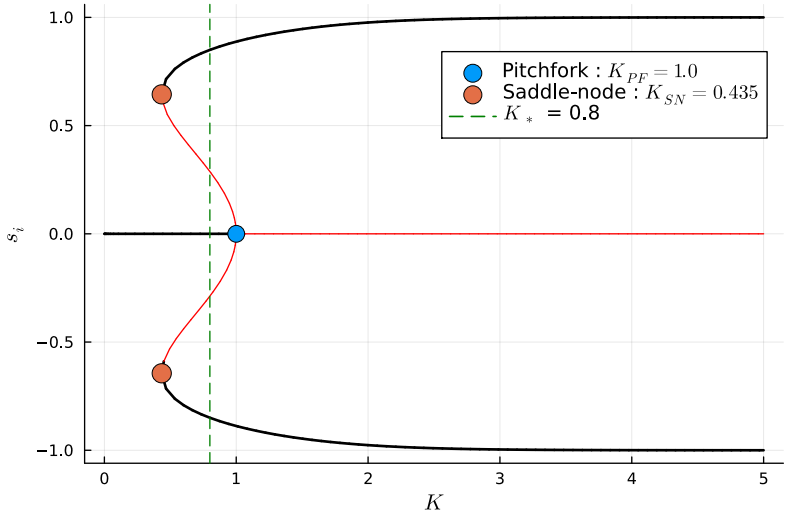

Figure 5.2.: Parameter K determination for the bidirectional model with slow local negative feedback and local reinforced positive feedback for $\sigma = 0$.

It can be seen in Figure 5.2 that the equilibrium analysis has a supercritical quintic Pitchfork-like bifurcation. Indeed, due to the reinforced positive feedback brought by $K_x \cdot s_i^2$ and the additional slow local negative feedback brought by $k_{s,i}$, the non-linearity of the activation function has been emphasized resulting in a even more deformed Pitchfork bifurcation. However, as the bias of the activation function has been taken as $\sigma = 0$, the Pitchfork bifurcation did not undergo any unfolding.

As for the model 3.10, the determination of the Saddle-node bifurcation K_{SN} was performed numerically leading to $K_{SN} = 0.435$ for the chosen parameters values.

It can be seen in Figure 5.2 that, for $K < K_{SN}$, there is only one equilibrium located at $s_i = 0$. For $K \in]K_{SN}, 1[$, there are three stable equilibrium (one located at $s_i = 0$ and the other ones in the upper and lower branches) as well as two unstable equilibrium in-between. For $K > 1$, there is an unstable equilibrium located at $s_i = 0$ and two stable equilibrium on the upper and lower branches.

The same observation as in Section 3.2.1 about the maximal value of s_i can be made in Figure 5.2 and the explanation is matched. The maximal value of the upper stable

equilibrium branch can be derived from the saturation value of the activation function in Figure 3.9 for $\sigma = 0$.

The value chosen for the parameter K was therefore a value in the interval $]K_{SN}, 1[$ in order to have a stable equilibrium in the upper branch, corresponding to a positive decision, a stable equilibrium in the lower branch, corresponding to a negative decision, as well as a stable equilibrium for a null value of s_i, corresponding to the neutral stable branch. The value of the parameter has thus been chosen as $K = 0.6$.

This behavior was desired for the designed model as the system can either stay at the neutral stable branch either take a positive/negative decision and jump to the upper/lower stable equilibrium branch. As for the model 4.2, the system is also able to exhibit a bistability in the interval $]K_{SN}, 1[$ between its neutral stable branch and its upper and lower stable branches thanks to the additional slow local negative feedback $k_{s,i}$ and reinforced positive local feedback $K_x \cdot s_i^2$.

The effect of the parameter K_x on the equilibrium curves obtained is to control the width of the region containing three stable equilibrium i.e. the width of the interval $]K_{SN}, 1[$. Therefore, K_x should be high enough for this interval to be sufficiently wide for the model to function optimally.

5.4. Nullcline and Phase Plane Analysis

A nullcline and phase plane analysis has been performed under the same conditions and hypothesis as for the model 4.2 with slow local negative feedback and can be seen in Figure 5.3 for parameters values $K = 0.6,\ \sigma = 0,\ g = 1.3,\ K_x = 3$.

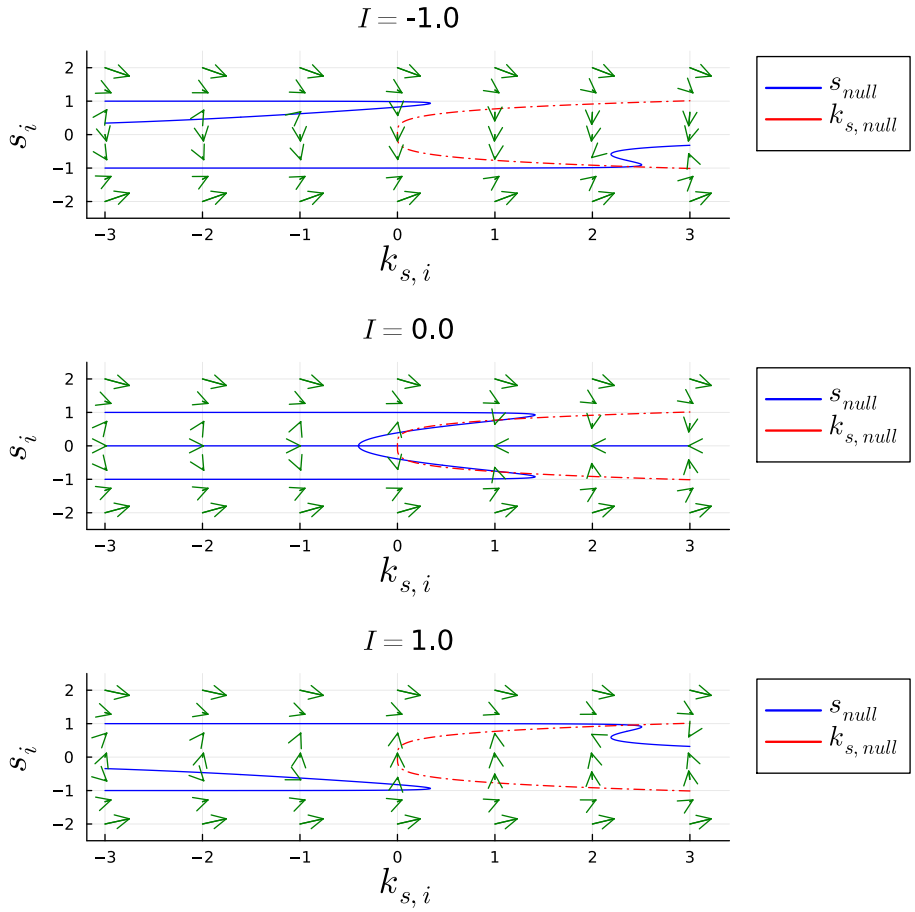

Figure 5.3.: Nullcline and phase plane analysis of the bidirectional model with slow local negative feedback and reinforced local positive feedback.

As depicted in Figure 5.3, when no stimulus is present, the system's sole stable equilibrium point is situated at $(k_{s,i}\ ; s_i) = (0\ ; 0)$. Other equilibrium points, found at the intersections between the s_i-nullcline and the $k_{s,i}$-nullcline, are unstable. Consequently, the stable equilibrium point $(0\ ; 0)$ acts as an attractor.

Upon introducing a non-null stimulus to the dendritic compartment, the s_i-nullcline undergoes deformation, resulting in a single equilibrium point situated on the upper/lower equilibrium branch. This point is stable and functions as an attractor for positive/negative stimuli.

Initially, at time $t_0 = t(0)$, the system's stable solution resides at the equilibrium point $(k_{s,i}\ ; s_i) = (0\ ; 0)$. Subsequently, when a non-null synaptic input is applied, the stable

equilibrium point of the system shifts either to the upper stable branch of the upward-unfolded quintic Pitchfork bifurcation of the s_i-nullcline (in response to a positive stimulus) or to the lower stable branch of the downward-unfolded quintic Pitchfork bifurcation (in response to a negative stimulus).

In the case of a positive stimulus, both variables s_i and $k_{s,i}$ increase to reach the new equilibrium point on the upper stable branch of the quintic Pitchfork bifurcation. Once the synaptic input returns to null, the stable equilibrium point reverts to $(k_{s,i}\ ; s_i) = (0\ ; 0)$, prompting both s_i and $k_{s,i}$ to decrease and reach the new stable equilibrium point.

Conversely, for a negative stimulus, s_i decreases while $k_{s,i}$ increases to reach the new equilibrium point situated on the lower stable branch of the quintic Pitchfork bifurcation. Upon the synaptic input becoming null again, the stable equilibrium point reverts to $(k_{s,i}\ ; s_i) = (0\ ; 0)$, causing s_i to increase and $k_{s,i}$ to decrease until reaching the new stable equilibrium point.

The behavior of the system is shown by the vector field represented by the green arrows in Figure 5.3.

5.5. Model simulation

The behavior of the system in simulation can be seen in Figure 5.4 for the following values of parameters: $K = 0.6,\ K_e = 100,\ \sigma = 0,\ \tau = 40,\ \tau_{spike} = 30,\ \bar{g}_K = 2,\ \epsilon = 5 \cdot 10^{-3},\ g = 1.3,\ K_x = 3,\ \Delta = 0.1$.

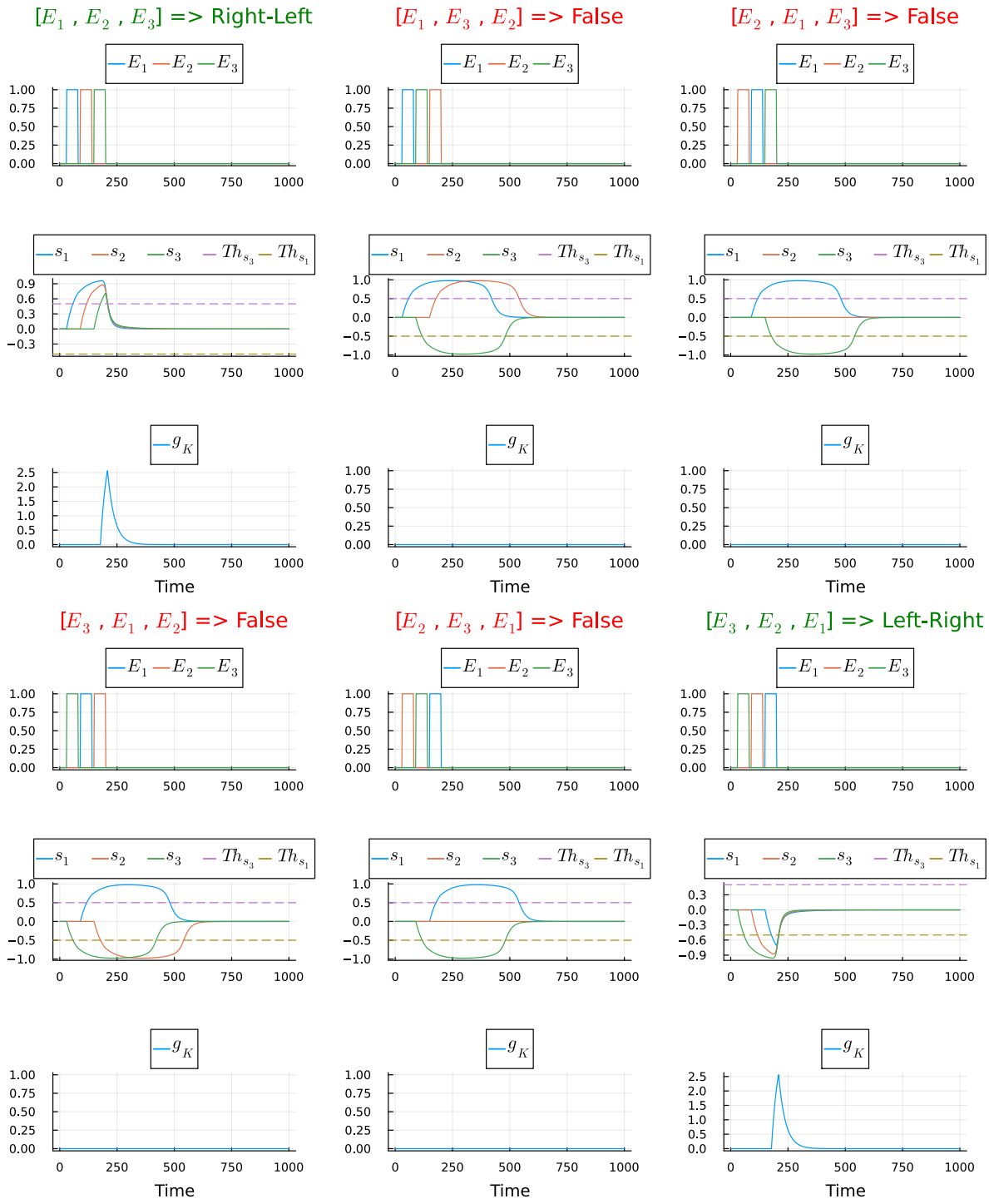

Figure 5.4.: Simulation of the bidirectional model with the reset mechanism for a width of synaptic input of 50 and a delay of 60 for a dendritic branch of 3 dendritic compartments. Both the preferred and reversed direction of movements are detected. The slow local negative feedback naturally brings back the activation variables to 0. The reset mechanism speeds up the reset of the activation variables when a detection occurs.

The performances of the bidirectional model with integrated slow local negative feedback and reinforced local positive feedback are similar to the one of the improved model of Chapter 4. It can indeed be seen in Figure 5.4 that the activation variables are brought back to their neutral stable branch whatever the input sequence order. Indeed, for all other input sequences than the correct one, the activation variables of all compartments returned naturally to their neutral stable branch. However, thanks to the parameter K_x, the positive feedback of the system is reinforced resulting in a faster transition from the neutral stable branch to the upper/lower stable branch when a decision is made.

As the improved model of Chapter 4, this model is efficiently able to detect consecutive input sequences (in this case bidirectional) temporally- separated by an in-between sequence delay as the model does not stay stuck in its decision anymore.

However, even though the reset mechanism hasten the transition of the activation variable from the upper/lower stable equilibrium branch towards its neutral stable branch, this models perfectly functions even without the reset mechanism implemented.

The performance of the bidirectional model without the reset mechanism can be seen in Figure 5.5 with the same parameters value as in Figure 5.4.

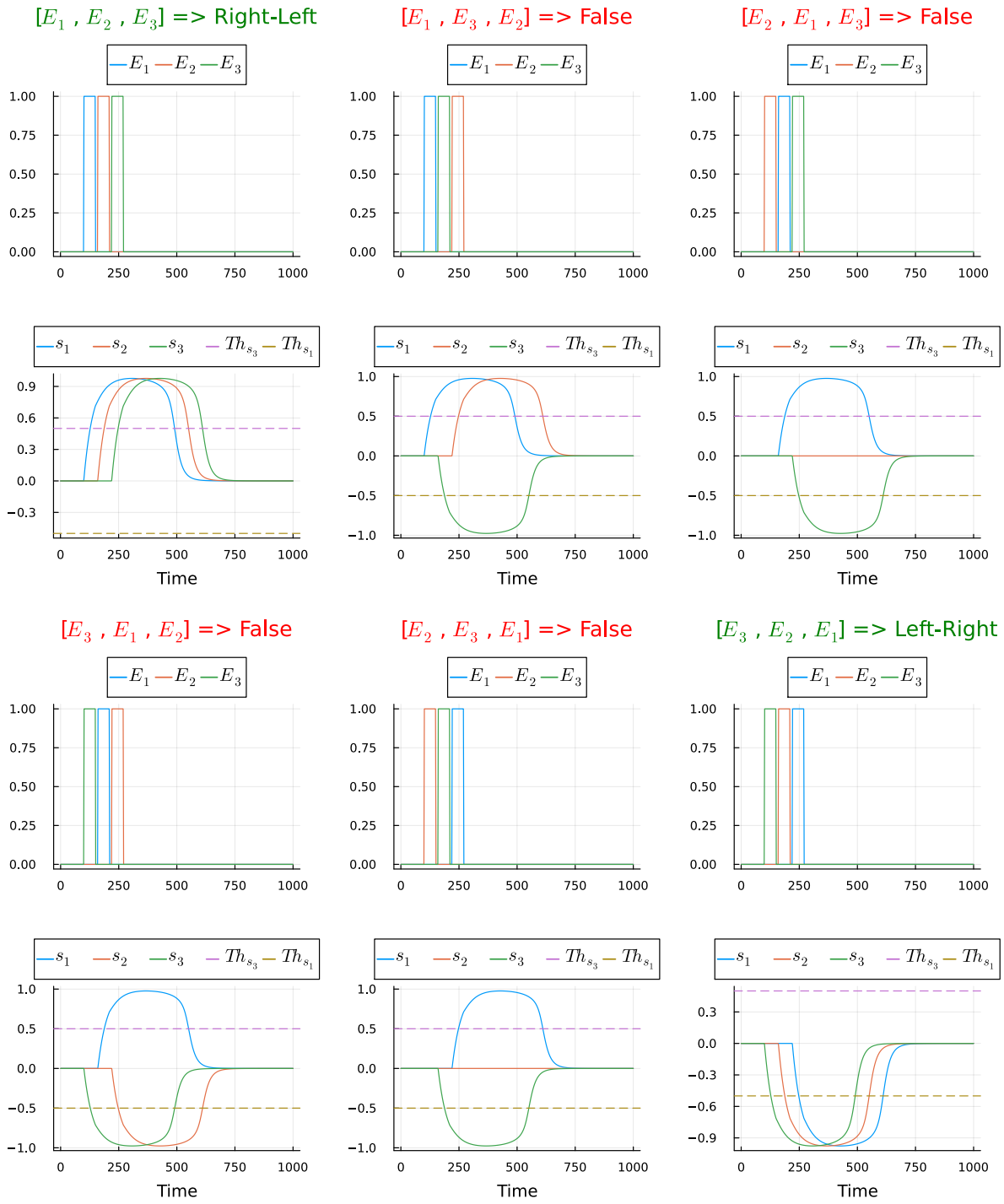

Figure 5.5.: Simulation of the bidirectional model with the reset mechanism for a width of synaptic input of 50 and a delay of 60 for a dendritic branch of 3 dendritic compartments. Both the preferred and reversed direction of movements are detected. The slow local negative feedback naturally brings back the activation variables to 0 even without using the reset mechanism.

As it can be observed in Figure 5.6a, the model is perfectly capable of resetting its decision naturally thanks to its additional slow local negative feedback. Therefore, the bidirectional model both with and without the reset mechanism enable the system to correctly identify consecutive input sequences temporally-separated by an in-between sequence delay. The same observations as for the improved model of Chapter 4 can be made about the use of the reset mechanism.

The trajectory of the model with and without the reset mechanism alongside the nullclines can be seen in Figure 5.6.

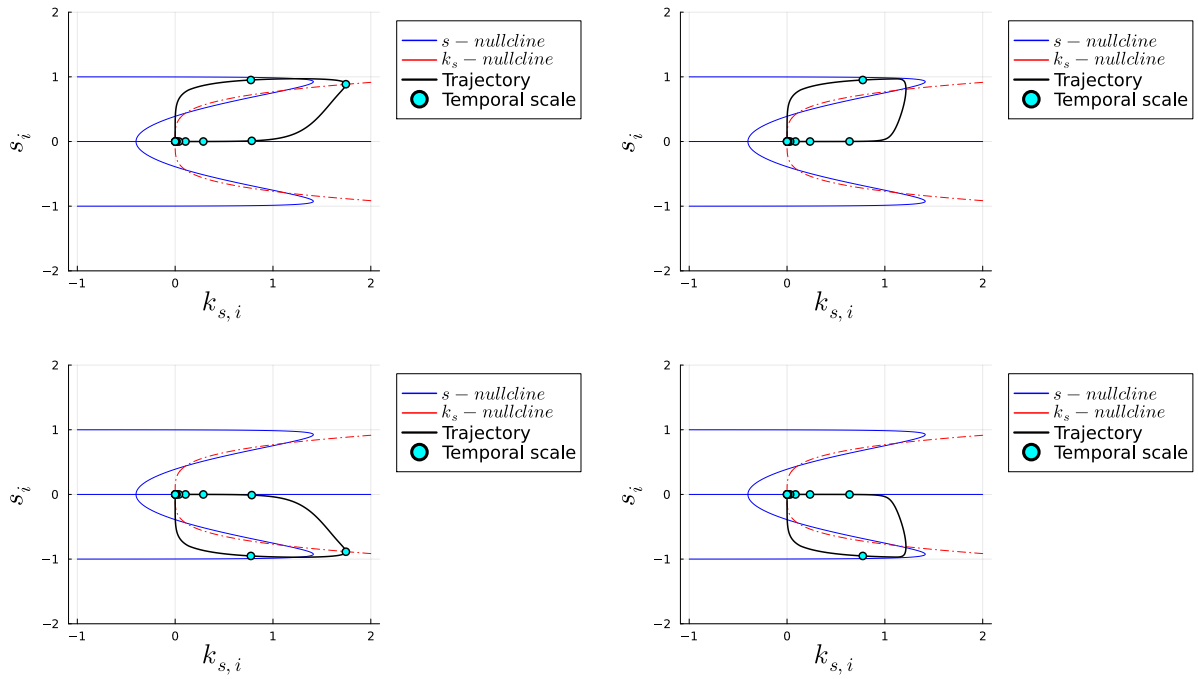

(a) Without reset mechanism.

(b) With reset mechanism.

Figure 5.6.: Trajectory of the bidirectional model alongside the nullclines. The trajectory moves from one stable fixed point to the other as expected when a synaptic input is fed. The graph in the upper part corresponds to a positive decision while the one in the lower part corresponds to a negative decision. The reset mechanism speeds up the return of the activation variable to the fixed point located at $(0, 0)$. The cyan-colored circles represent the time scale of the simulation (one tenth of the simulation per circle).

In both Figures 5.6a and 5.6b, the trajectory of the model is very similar whether the reset mechanism is used. It can be noted that whatever the sign of the stimulus, the

activation variable correctly transitions from the stable fixed point located in $(0, 0)$ to the upper/lower fixed point to finally return to the initial fixed point.

Each cyan-colored circle represents one-tenth of the total simulation time. This visualization reveals that the rapid increase/decrease of s_i (depolarization phase) occurs on a much shorter time scale compared to its decrease/increase (repolarization phase) respectively for positive and negative decisions.

6. Extension to 2-dimensional movement detection

6.1. Receptive Field Layout

The system implemented to detect 2-dimensional unidirectional movement has a predefined two-dimensional grid configuration composed of 13 dendritic compartments whose structure can be seen in Figure 6.1.

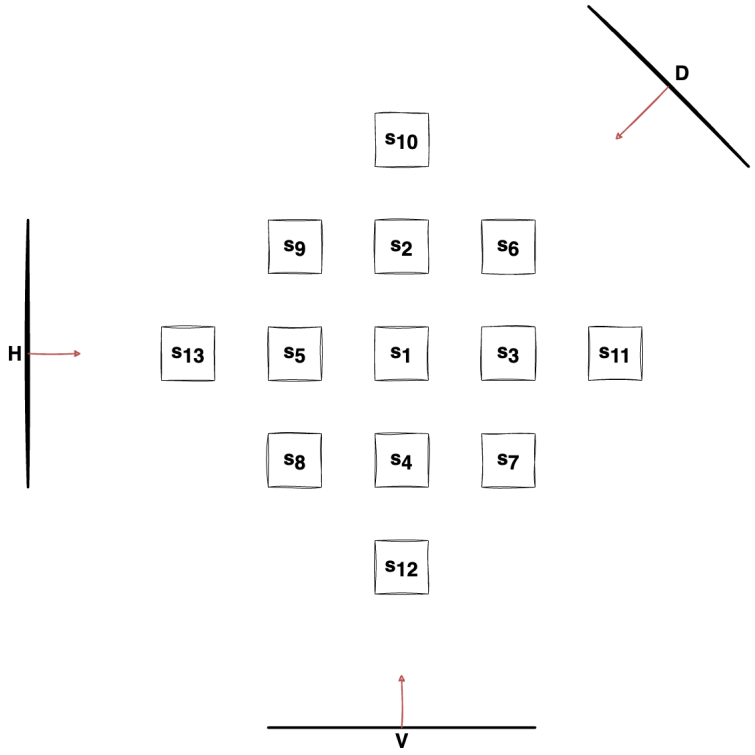

Figure 6.1.: Overview of the structure of the 2-dimensional system composed of 13 dendritic compartments.

The implemented system is capable of perceiving three primary types of 2-dimensional

movements: horizontal, vertical, and diagonal movements. It operates within a variable-sized grid of squares, with dendritic compartments occupying multiple squares arranged in a square shape and equidistant from neighboring compartments.

These perceived movements manifest as a dynamic-width bar that can be adjusted to simulate various movements within the three main types. The movement of this bar, transitioning square by square in the corresponding direction, represents the motion of the object observed within the system's receptive field.

It's important to note that only one direction of each movement has been explored, as the results remain consistent for the opposite direction due to the system's symmetry. Thus, to maintain symmetry, the midpoint of the moving bar for horizontal and vertical movements aligns respectively with the line formed by $s_{13} - s_{11}$ and the line formed by $s_{12} - s_{10}$, while for diagonal movements, it aligns with the line formed by $s_6 - s_8$.

Given the system's 2D layout, the interconnections between dendritic compartments cannot rely solely on connections with their succeeding compartments. Therefore, separate interconnection matrices are defined for each type of movement to describe how compartments interact to accurately convey perceived movement to the decision unit.

Each movement within the system is associated with a decision unit, each comparing the activation variable of a specific compartment with a predetermined threshold. For instance, the horizontal decision unit compares the activation variable s_{11}, the vertical decision unit compares s_{10}, and the diagonal decision unit compares the sum of activation variables $s_{13} + s_8 + s_{12}$.

6.2. Mathematical Model

Since generating 2-dimensional movements entails greater complexity compared to 1-dimensional motions, the designed 2-dimensional system will not be tailored to detect consecutive input sequences temporally-separated by an in-between sequence delay. Instead, the system from the improved model outlined in Chapter 4 will be employed. This decision aims to ensure that the activation variables of each dendritic compartment return

to a baseline of 0 after making a decision. Consequently, the activation function 4.1 will be utilized for the 2-dimensional model, along with the integration of a slow local negative feedback mechanism.

$$\begin{cases} 1 & \tau \dot{s}_1(t) = -s_1(t) + U(s_1(t),\ K,\ K_e \cdot [\sum (I[1] * \bar{s})]\ ,\ k_{s,1},\ E_1(t),\ \sigma) \\ & \tau_{slow}\ \dot{k}_{s,1}(t) = g \cdot s_1^2(t) - k_{s,1}(t) \\ \vdots & \\ i & \tau \dot{s}_i(t) = -s_i(t) + U(s_i(t),\ K,\ K_e \cdot [\sum (I[i] * \bar{s})]\ ,\ k_{s,i},\ E_i(t),\ \sigma) \\ & \tau_{slow}\ \dot{k}_{s,i}(t) = g \cdot s_i^2(t) - k_{s,i}(t) \\ \vdots & \\ n = 13 & \tau \dot{s}_n(t) = -s_n(t) + U(s_n(t),\ K,\ K_e \cdot [\sum (I[n] * \bar{s})]\ ,\ k_{s,n},\ E_n(t),\ \sigma) \\ & \tau_{slow}\ \dot{k}_{s,n}(t) = g \cdot s_n^2(t) - k_{s,n}(t) \end{cases} \tag{6.1}$$

where $I[i]$ is the line i of the interconnections matrix . The interconnections matrices defined for each kind of movements can be seen in Appendix A.1.

The primary distinction from model 4.2 is that the parameter K_e is no longer exclusively multiplied by the activation variable of the preceding compartment. Instead, it is multiplied by a summation of all activation variables connected to the compartment, weighted by the elements of the interconnections matrix. It is important to note that when the elements $w_{i,i}$ of the interconnections matrix are non-zero, it implies that the corresponding compartment has no interconnection, resulting in a multiplication of K_e by 1. This leads to a simplification in the expression $[\sum (I[i] * \bar{s})]$ of model 6.1, where it is considered equivalent to 1.

The equilibrium analysis of the 2-dimensional model is thus equivalent to the one performed in Chapter 4 and the same parameters values therefore apply for this model.

6.3. Model simulation

The behavior of the system in simulation can be seen in Figure 6.2 for the following values of parameters: $K = 0.8,\ K_e = 10,\ \sigma = 1,\ \tau_{slow} = 200,\ g = 0.1$.

The system's setup used in this simulation consists in a grid of squares of size 31×31, dendritic compartments of size 3×3 and a equidistant padding of 5 squares between neighboring compartments. The moving bar featuring the perceived movement has a width of 7 squares.

The results of the simulation are similar to those obtained in Chapter 4 from Figure 4.4. It can be noted that the slow local negative feedback allows the activation variables to return to 0 after taking a decision in Figure 4.2 (transition from the upper stable equilibrium branch to the fixed point $(k_{s,i},\ s_i) = (0, 0)$). Thus, the model correctly identifies the correct type of movements while generating a null response for the other types of movements.

It should be noted that for motions involving all dendritic compartments along their path, decision units other than the one corresponding to the intended movement also generate a non-null response. This makes it impossible for the system to accurately identify the correct motion direction since all decision units are fed by a non-null response from their preceding dendritic compartment.

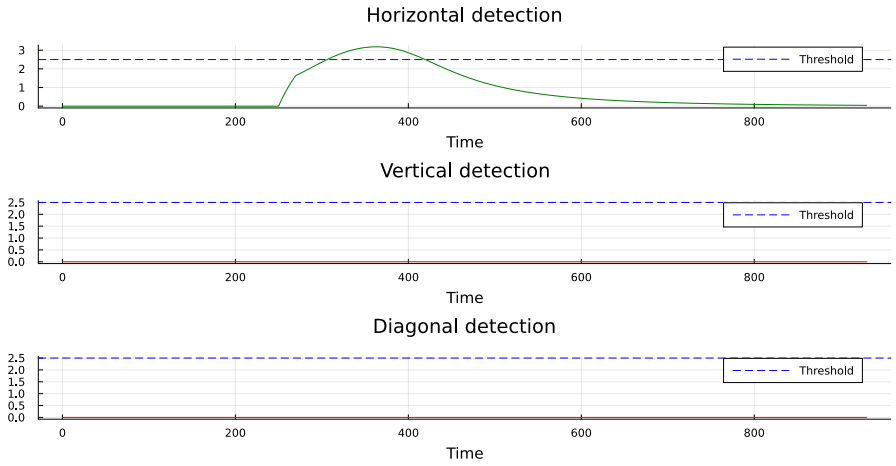

(a) Horizontal movement.

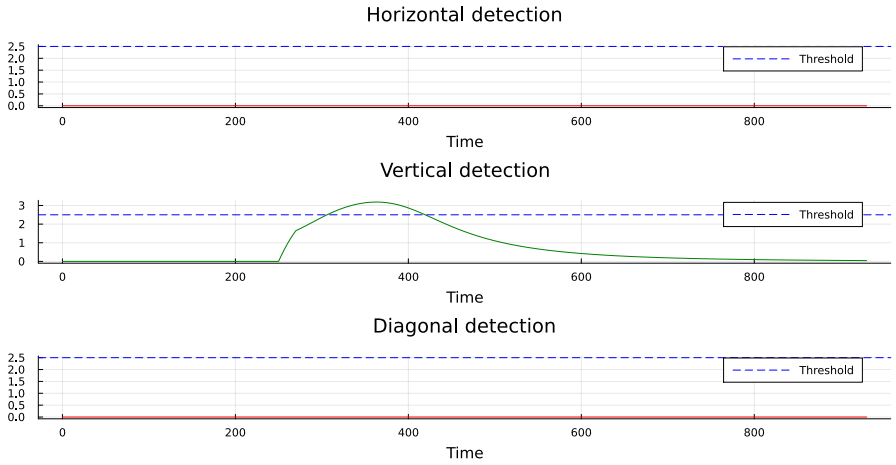

(b) Vertical movement.

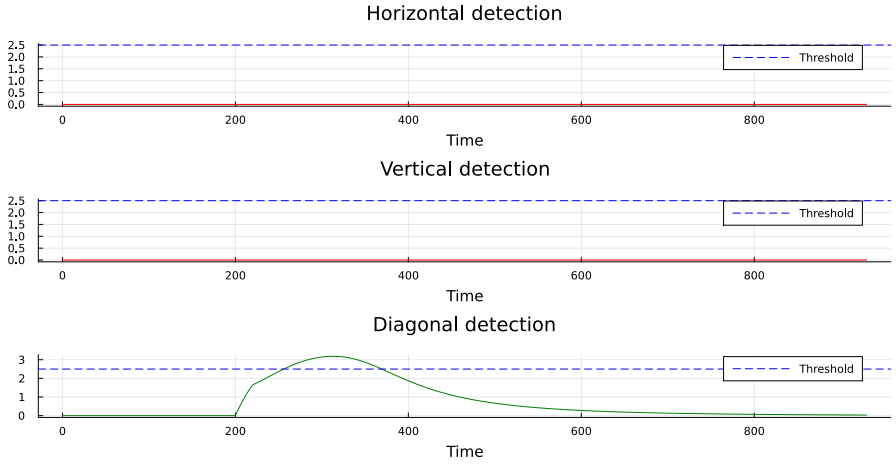

(c) Diagonal movement.

Figure 6.2.: Simulation of the 2-dimensional model for different movement directions. The model correctly identifies the correct type of movements while generating a null response for the other types of movements.

6.4. Limitations to Combined Directions

The 2-dimensional model, while demonstrating satisfactory performance in movement detection, has inherent limitations based on its configuration. To explore these limitations, a movement scenario involving a vertically moving bar has been modified, now presenting an inclination of 45°, as illustrated in Figure 6.3.

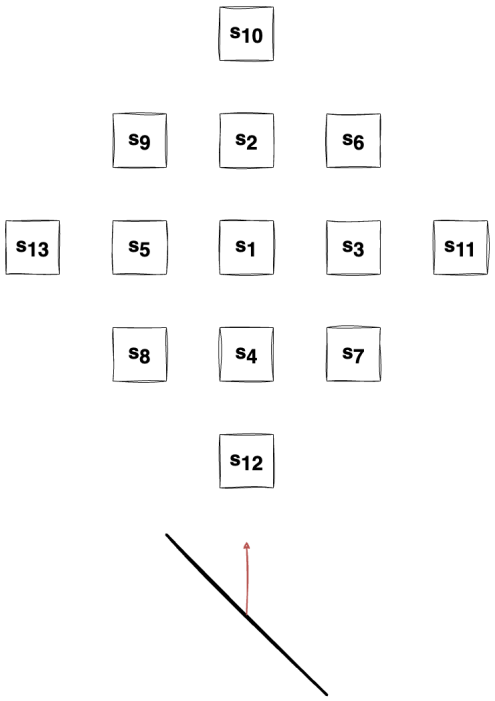

Figure 6.3.: Overview of the inclined vertical movement.

The simulation results depicting the model's response to the inclined vertical movement are illustrated in Figure 6.4. Notably, the model generates a non-null response solely for the diagonal decision unit, while both the horizontal and vertical decision units fail to detect any movement. This outcome arises because such a movement encompasses aspects of all three types of movements. Although the movement activates dendritic compartments in both horizontal and vertical configurations, the synaptic inputs are not perceived in the correct sequence by these compartments, resulting in a null response from their associated decision units. In contrast, the diagonal configuration correctly perceives the movement's sequence of activations, leading to a detection by the diagonal decision unit.

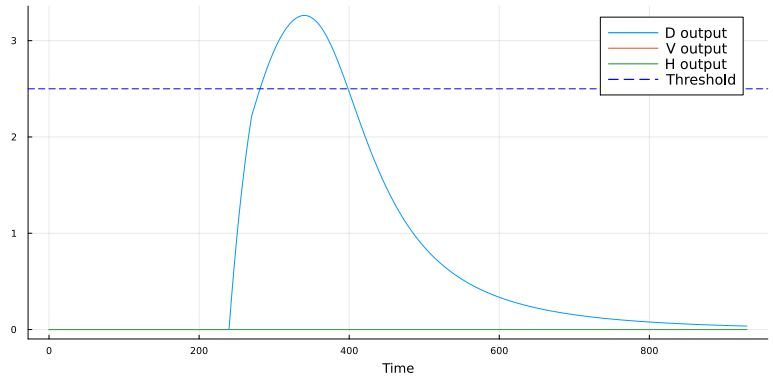

Figure 6.4.: Simulation of the 2-dimensional model for a movement propagating both diagonally and vertically. The model is only able to identify the perceived movement as diagonal and cannot detect the vertical motion simultaneously.

The implemented 2-dimensional model therefore cannot detect all information contained by a complex movement due to the limitation explained above.

7. Consecutive one-dimensional input sequences detection

The primary objective of this master's thesis was to devise a biologically-inspired system modeled after the functioning of neurons' dendrites to accurately detect the sequential activation order of synaptic inputs within dendritic compartments along the branch. The performance evaluations of the various designed systems have been detailed in Chapter 3.

The secondary aim of this thesis was to extend the movement detection model to recognize consecutive input sequences temporally-separated by an in-between sequence delay. The successful implementation of such a feature hinges on the model's ability to naturally reset its decision, thereby avoiding being stuck in a previous decision state.

The performance assessments of the models developed based on the second approach will be conducted using a configuration comprising a dendritic branch consisting of four dendritic compartments.

For the ensuing simulations, the parameter values of the different models will remain consistent with those determined in the respective analyses carried out in Chapters 3, 4, and 5. Identical consecutive input sequences will be presented to all models to facilitate the examination of their performances under the same conditions.

Additionally, the delay between the synaptic inputs of the different compartments has been taken to 120, the width of these inputs to 90 and the delay between consecutive input sequences has been set to 1500 for all following simulations.

7.1. Dendritic-inspired model

Simulations of consecutive input sequences detection for the basic model have been performed for the following values of parameters: $K = 0.8,\ K_e = 10,\ \sigma = 1,\ \tau = 40,\ \tau_{spike} = 30,\ \bar{g}_K = 2$.

Figure 7.1 shows the performances of the basic model without a reset mechanism. As analysed in Section 3.2, such a model does not possess a slow local negative feedback in its activation function. Therefore, the model is unable to reset its decision after detecting a correct movement. In this configuration, the first input sequence is a correct movement which leads the model to stay stuck in the upper stable equilibrium branch for all successive input sequences independently of the order of the input sequence.

It can thus be easily established that the basic model without a reset mechanism is not suited at all to detect consecutive input sequences.

The performances of the basic model with a reset mechanism can be observed in Figure 7.2. Compared to the basic model without the reset mechanism, the performances of the model are greatly improved as it detects correctly the two correct input sequences and generate one false positive detection out of the four incorrect sequences. It can be noted that the reset mechanism enables the system to reset its decision only after a correct input sequence has been perceived by the model. Therefore, if several incorrect input sequences are perceived consecutively, a false positive detection will occur as the activation variable will not be reset until a correct input sequence is perceived.

Even though the performances of the basic model with the reset mechanism are better than without, such a model is unable to avoid generating false positive detection.

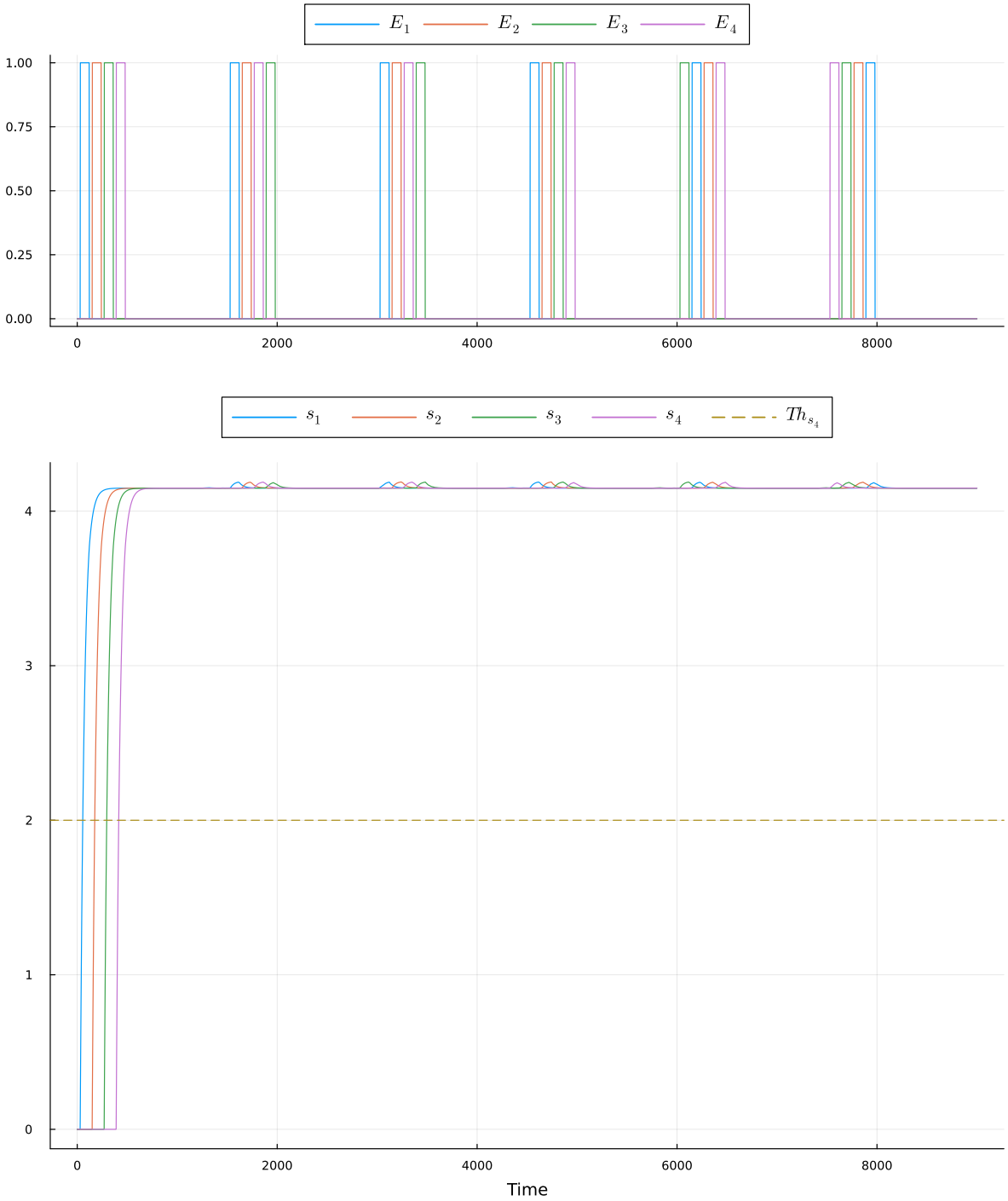

Figure 7.1.: Successive input sequences detection for a dendritic branch of 4 dendritic compartments for the basic model without reset mechanism. The different activation variables stay stuck in their decision without the capacity of resetting their values in case of an incorrect input sequence.

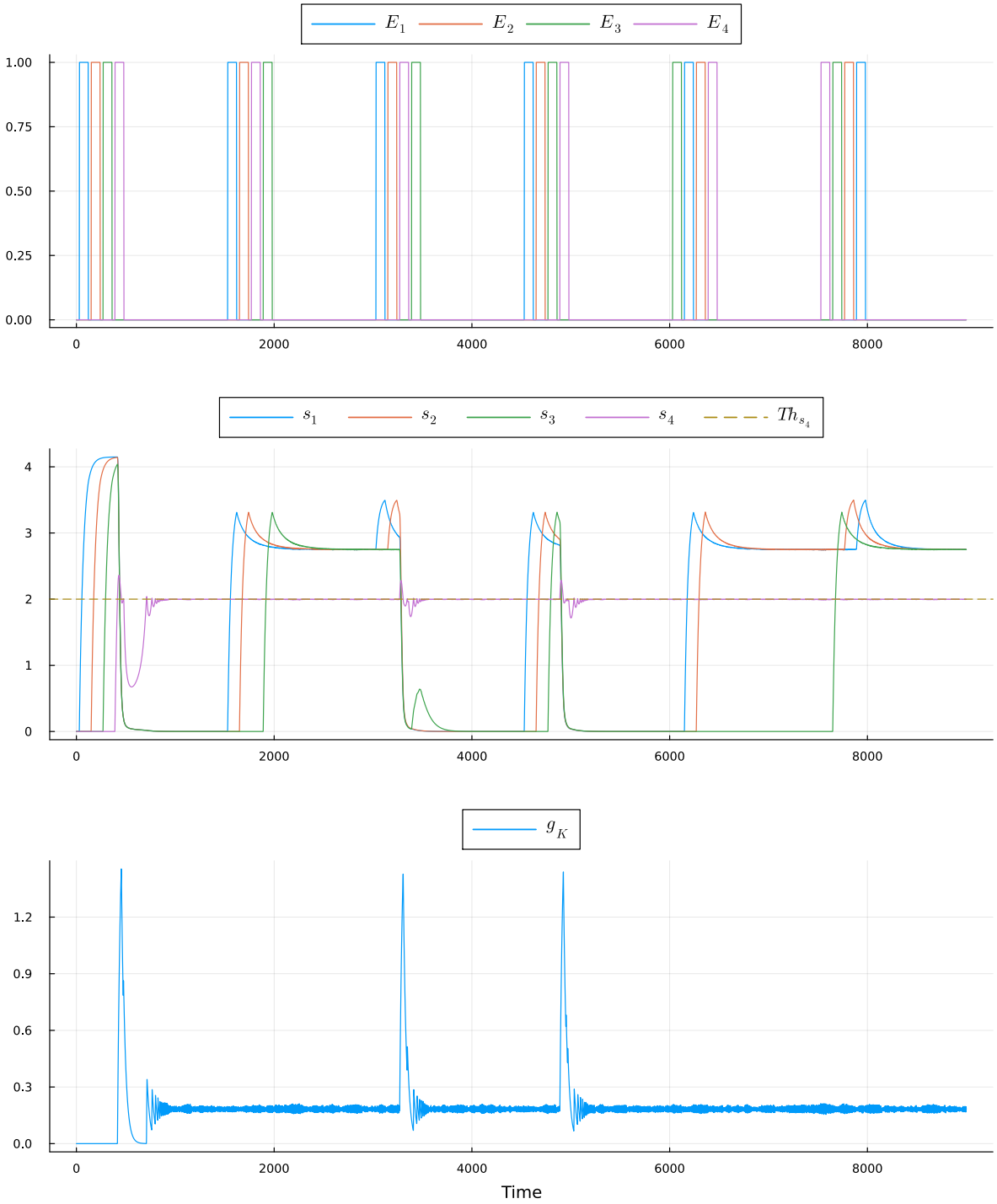

Figure 7.2.: Successive input sequences detection for a dendritic branch of 4 dendritic compartments for the basic model with reset mechanism. The different activation variables stay stuck in their decision without the capacity of resetting their values in case of an incorrect input sequence and are reset in case of a correct input sequence. The dynamics of the reset variable g_K can be seen in the third graph. Spike-like signals are generated by g_K when a detection has been made by the decision unit.

7.2. Improved dendritic-inspired model

Simulations of consecutive input sequences detection for the improved model have been performed for the following values of parameters: $K = 0.8,\ K_e = 10,\ \sigma = 1,\ \tau = 40,\ \tau_{spike} = 30,\ \bar{g}_K = 2,\ \tau_{slow} = 200,\ g = 0.1$.

Figure 7.3 shows the performances of the improved model without a reset mechanism. As analysed in Chapter 4, such a model possesses a slow local negative feedback in its activation function via the variable $k_{s,i}$. Therefore, the model is able to naturally reset its decision even without detecting a correct movement. In this configuration, all correct input sequences are detected while no response of the activation variable of the last dendritic compartment s_4 is generated for incorrect input sequences.

It can thus be easily established that the improved model without a reset mechanism is perfectly able to detect consecutive input sequences correctly.

The performances of the improved model with a reset mechanism can be observed in Figure 7.4. The performances of the model with reset is similar to the one without as the reset mechanism only speeds up the transition from the upper stable equilibrium branch to the fixed point located at $(k_{s,i},\ s_i) = (0, 0)$ from Figure 4.2.

Therefore, the improved model can accurately detect consecutive input sequences and a detection is only generated by the decision unit in case the order of the input sequence is correct.

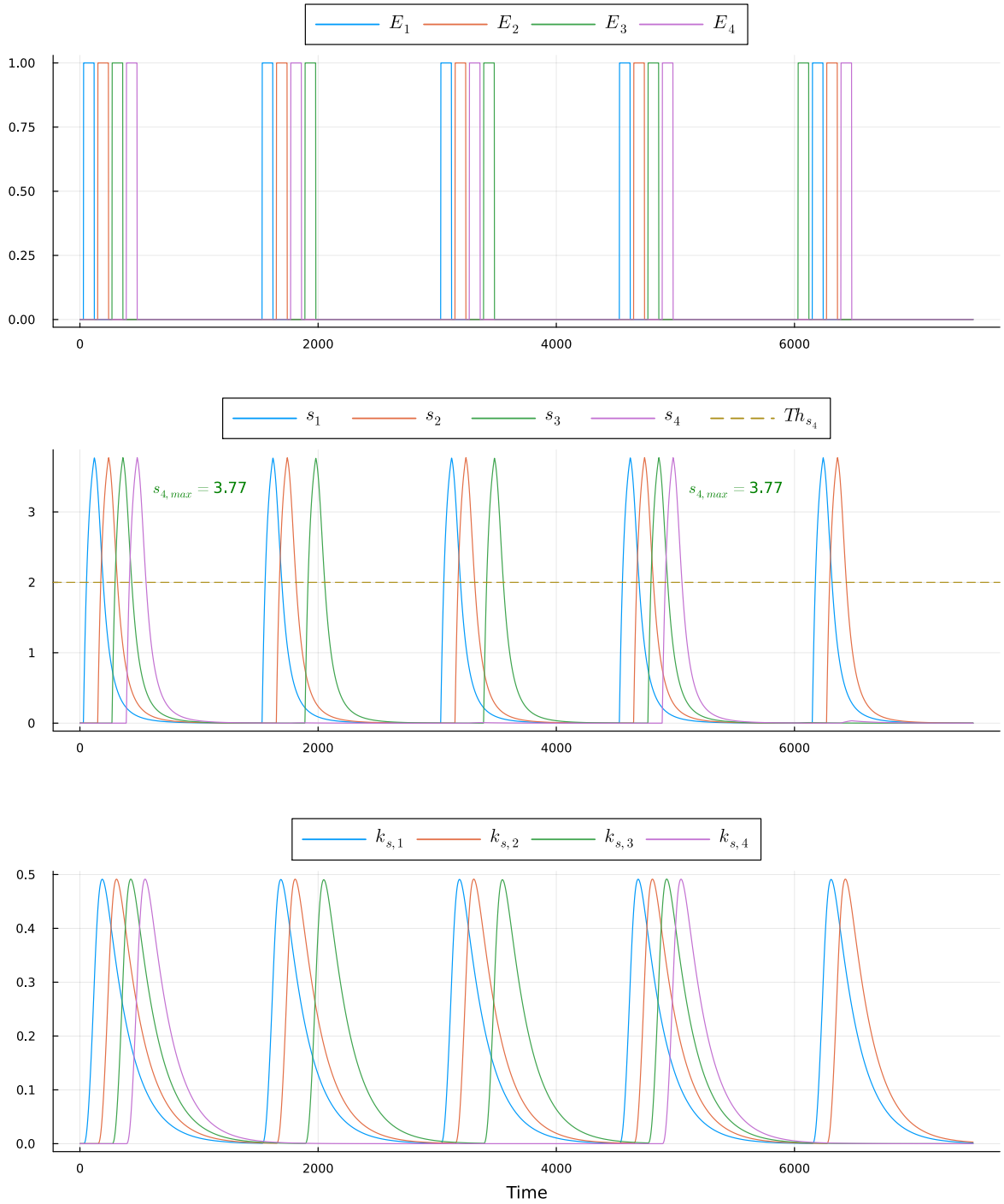

Figure 7.3.: Successive input sequences detection for a dendritic branch of 4 dendritic compartments for the improved dendritic-inspired model without reset mechanism. The negative feedback variables $k_{s,i}$ can be seen in the third graph. Thanks to the slow local negative feedback, the model is capable of resetting the activation variables naturally even without the reset mechanism.

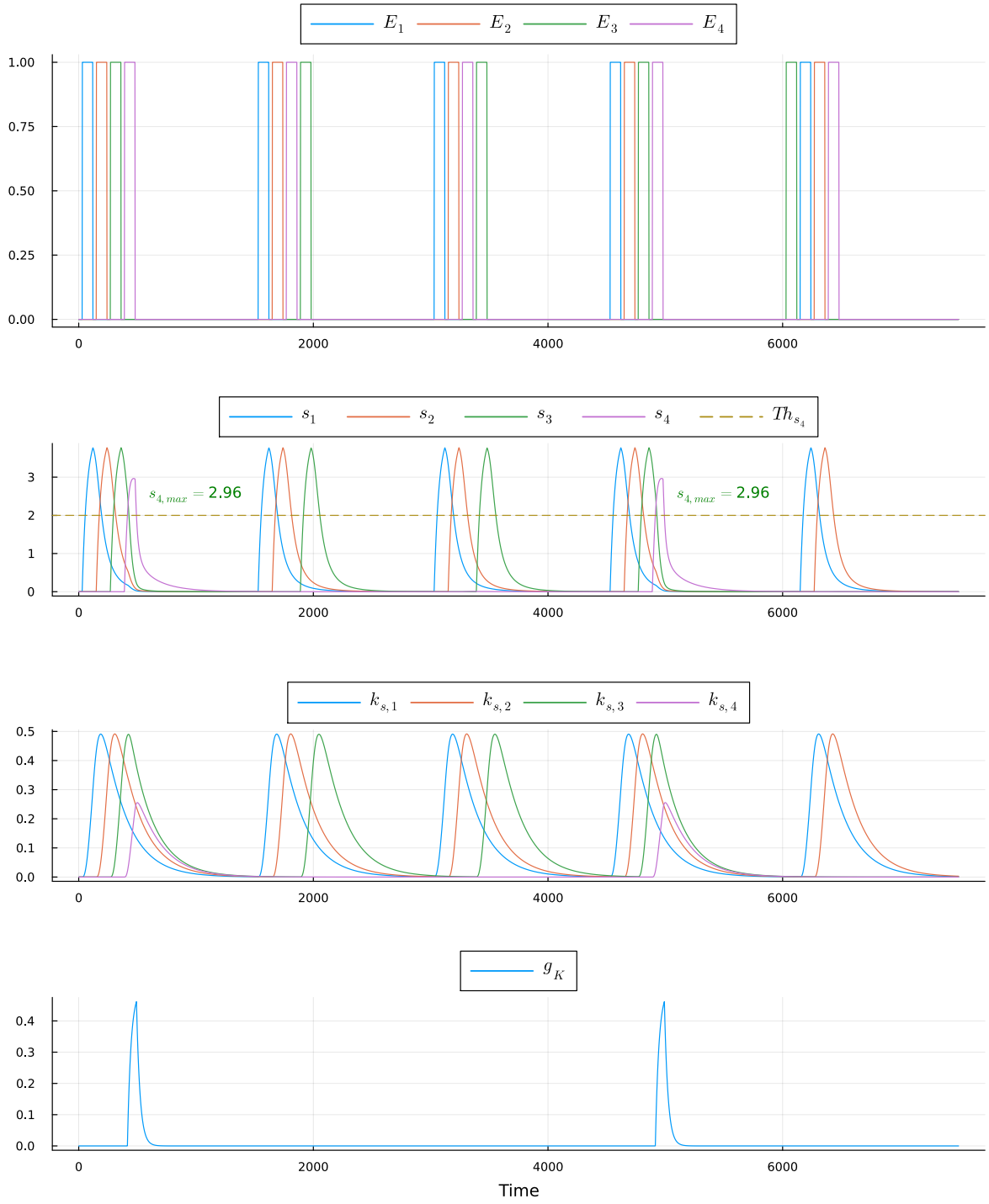

Figure 7.4.: Successive input sequences detection for a dendritic branch of 4 dendritic compartments for the improved dendritic-inspired model with reset mechanism. The negative feedback variables $k_{s,i}$ can be seen in the third graph. Thanks to the slow local negative feedback, the model is capable of resetting the activation variables naturally even without the reset mechanism. The dynamics of the reset variable g_K can be seen in the fourth graph. Spike-like signals are generated by g_K when a detection has been made by the decision unit.

7.3. Bidirectional model

Simulations of consecutive input sequences detection for the bidirectional model have been performed for the following values of parameters: $K = 0.6,\ K_e = 100,\ \sigma = 0,\ \tau = 40,\ \tau_{spike} = 30,\ \bar{g}_K = 2,\ \epsilon = 5 \cdot 10^{-3},\ g = 1.3,\ K_x = 3,\ \Delta = 0.1$.

Figure 7.5 shows the performances of the bidirectional model without a reset mechanism. As analysed in Chapter 5, such a model possesses both a slow local negative feedback in its activation function via the variable $k_{s,i}$ as well as a reinforced local positive feedback controlled by the parameter K_x. Therefore, the model is able to naturally reset its decision even without detecting a correct movement and can take both positive and negative decisions. In this configuration, all correct input sequences are detected (both right-to-left and left-to-right motions) while no response of the two decision units are generated for incorrect input sequences. The model thus successfully detects the three correct input sequences and generates a null response for the three incorrect ones.

It can thus be easily established that the bidirectional model without a reset mechanism is perfectly able to detect bidirectional consecutive input sequences correctly.

The performances of the bidirectional model with a reset mechanism can be observed in Figure 7.6. The performances of the model with reset is similar to the one without as the reset mechanism only speeds up the transition from the upper/lower stable equilibrium branch to the fixed point located at $(k_{s,i},\ s_i) = (0, 0)$ from Figure 5.3.

Therefore, the bidirectional model can accurately detect bidirectional consecutive input sequences and a detection is only generated by the decision units in case the order of the input sequence is correct (either left-to-right either right-to-left).

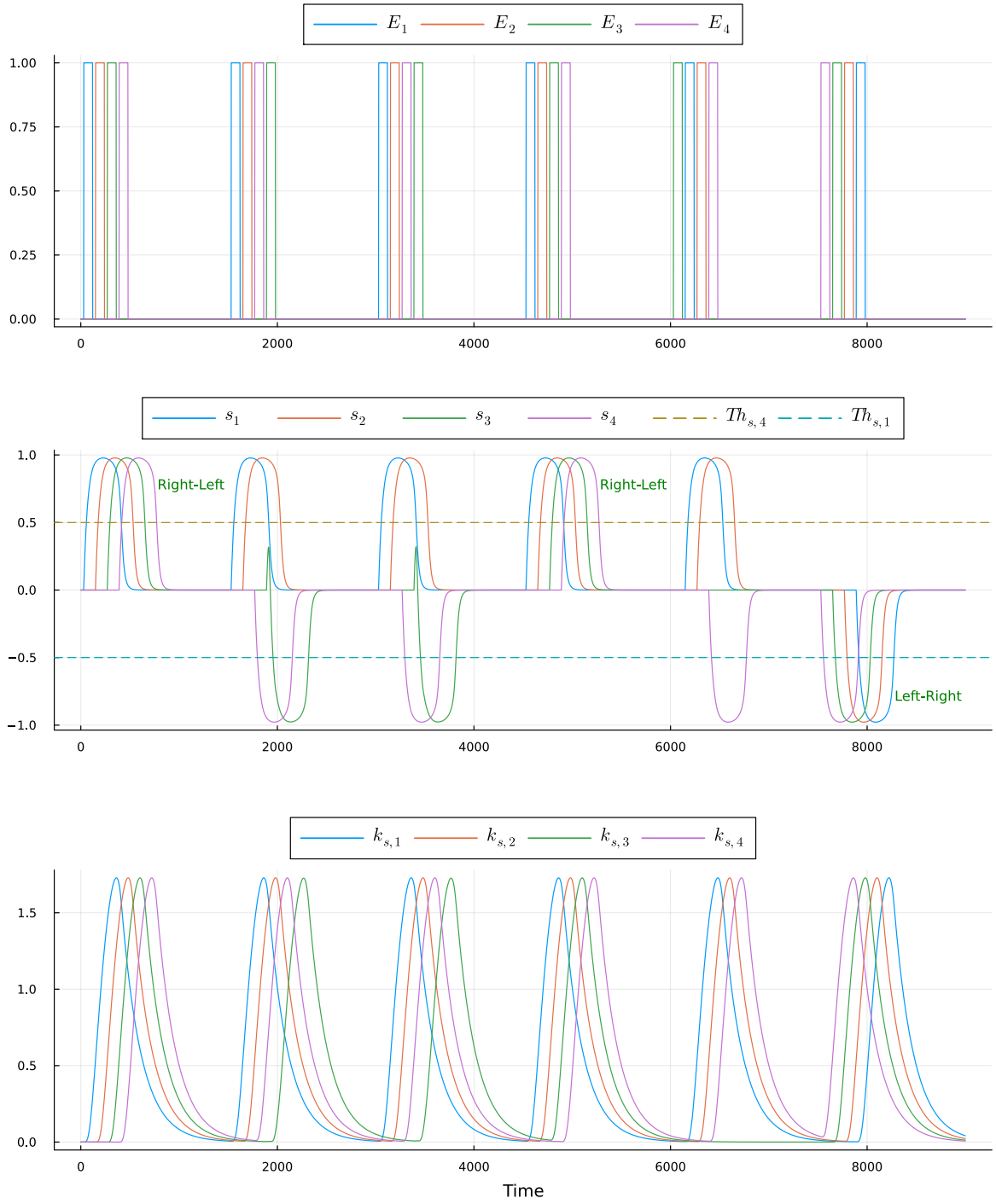

Figure 7.5.: Successive input sequences detection for a dendritic branch of 4 dendritic compartments for the bidirectional model without reset mechanism. The negative feedback variables $k_{s,i}$ can be seen in the third graph. Thanks to the slow local negative feedback, the model is capable of resetting the activation variables naturally even without the reset mechanism both for positive and negative detection.

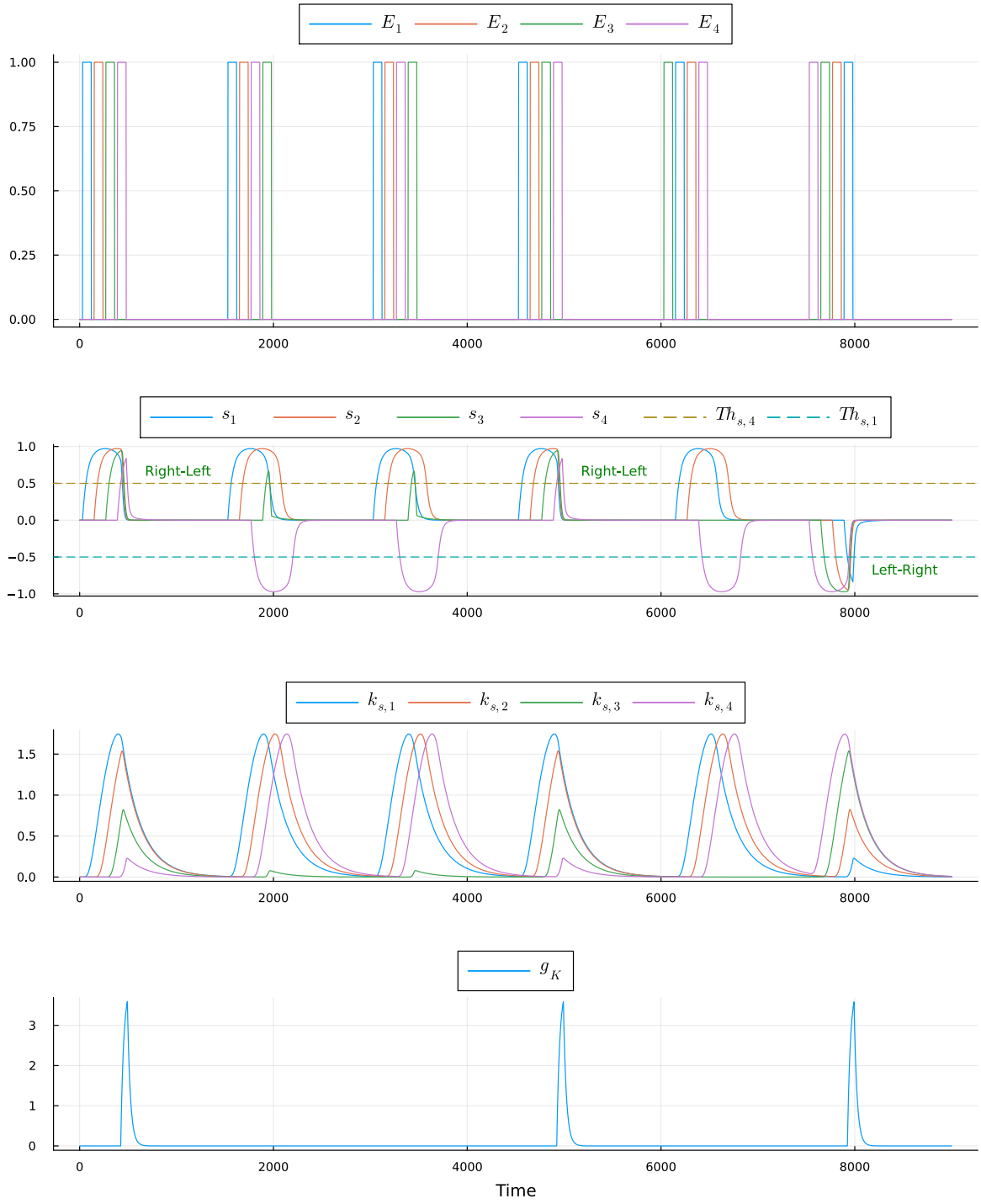

Figure 7.6.: Successive input sequences detection for a dendritic branch of 4 dendritic compartments for the bidirectional model with reset mechanism. The negative feedback variables $k_{s,i}$ can be seen in the third graph. Thanks to the slow local negative feedback, the model is capable of resetting the activation variables naturally even without the reset mechanism both for positive and negative detection.. The dynamics of the reset variable g_K can be seen in the fourth graph. Spike-like signals are generated by g_K when a detection has been made by the decision units.

8. Conclusions

8.1. Findings

The motion detection models developed in this master's thesis are inspired by the operations of neurons' dendrites and the role of various ions and molecules in generating dendritic action potentials. Excitatory driving inputs responsible for the depolarization phase of dendritic compartment activation variables are modeled after calcium-dependent conductances, while inhibitory modulatory inputs, contributing to the slow local negative feedback and the reset variable g_K for initiating the repolarization phase, are modeled after potassium-dependent conductances. To mimic the attenuation of dendritic action potentials during propagation towards the soma, a reset mechanism has been artificially incorporated in the dendritic-inspired models. Additionally, to counteract this attenuation, a reinforced positive feedback mechanism has been introduced, represented by NMDA-dependent conductances serving as excitatory modulatory inputs.

Two distinct approaches have been designed: one employing solely additive arithmetic operations and the other, dendritic-inspired, incorporating both additive and multiplicative arithmetic operations. It has been determined that the latter approach yields superior performance for the motion detection system (see Section 3.3). A comprehensive analysis of system parameters has been conducted to identify the parameter value intervals conducive to optimal system functionality. It has been found that the optimal configuration resulting in only true positive detection involves large time constants and narrow synaptic input widths.

However, as the second approach was not suited for detecting successive temporal event patterns, an enhancement has been implemented by incorporating slow local negative feedback into the activation variables of dendritic compartments. This enhancement enables the system to successfully detect consecutive input sequences. The designed system

effectively distinguishes between correct and incorrect temporal event patterns as objects move successively within the camera's field of view, leveraging the inherent bistability of the model.

A transition has been made from a biologically-inspired model tailored to detect unidirectional motion to an engineering-focused model capable of detecting bidirectional motion. Both reinforced local positive feedback and slow local negative feedback are employed to allow the model to make positive or negative decisions while being capable of resetting its decision. The implemented model accurately discerns left-to-right and right-to-left temporal event patterns from incorrect ones in consecutive input sequence configurations.

Lastly, an extension from a one-dimensional system to a two-dimensional system has been undertaken to effectively detect horizontal, vertical, and diagonal motions in a two-dimensional square grid.

8.2. Contributions

This master's thesis introduces innovative methodologies and algorithms for effectively processing the stream of events generated by event-based cameras to detect motion in both one-dimensional and two-dimensional visual scenes captured by the camera.

The developed model is applicable to systems with a variable number of pixels for the one-dimensional setup and can be extended to accommodate various two-dimensional grid configurations by adjusting the interconnections between neighboring compartments. The algorithms devised in this study present a novel approach by employing spatial filtering of the temporal events pattern, departing from the conventional temporal filtering methods. Additionally, all the models designed are easily adaptable to neuromorphic circuits, thereby fully capitalizing on the advantages offered by event-based cameras.

All implemented models operate effectively across wide parameter ranges, consistently delivering accurate detection outcomes with high confidence. Moreover, the incorporated reset mechanism offers flexibility, allowing its utilization or omission based on the specific practical constraints dictated by the application's requirements.

8.3. Applications

The motion detection system developed within this master's thesis effectively identifies the direction of motion within the event stream captured by event-based cameras, offering diverse applications like surveillance, object detection, and robotic navigation.

Milde et al. [6] demonstrated a practical implementation of a motion detection system using an alternative approach for collision-avoidance in robotic navigation. Their system accurately estimated collision-avoidance directions by converting event traversal times into bursts of spikes, achieving performance on par with conventional cameras.

Similarly, the system devised in this master's thesis, employing a unique methodology, demonstrates the capability to detect motion direction within event-based camera data in simulated environments. This versatility highlights the potential applications of such systems in various fields requiring precise motion detection and navigation capabilities.

8.4. Limitations

The designed models operate effectively across wide ranges of system parameter values, yet they may yield false positive detection in overly restrictive configurations. The system's functionality is constrained when events within a temporal events pattern occur too closely together, leading to difficulty in accurately distinguishing overlapping events. Nevertheless, the system can be manually adjusted to better align with the physical constraints imposed on it.

For two-dimensional motions involving all dendritic compartments along their path, decision units other than the one corresponding to the intended movement also generate a non-null response. Therefore, it is necessary to incorporate inhibitory and excitatory interconnections between the different decision units to reliably identify various types of motions for objects of varying sizes.

Additionally, observations indicate that the two-dimensional model has limitations in accurately detecting complex two-dimensional motions involving combined directions, such as objects moving diagonally upwards.

8.5. Further Improvements

The two-dimensional model developed in this study was not specifically designed to detect bidirectional two-dimensional motions using only one set of weight interconnections between neighboring pixels. A potential future direction following this thesis could involve implementing a model capable of detecting various types of two-dimensional motions with a single identical interconnection matrix capable of recognizing all motion patterns.

Furthermore, combining multiple two-dimensional systems could enable the detection of complex two-dimensional movements, allowing the system to identify motions combining several directions simultaneously.

Converting the designed mathematical models into neuromorphic circuits could be pursued to create a fully analog motion detection system suitable for integration into various practical movement detection applications.

List of Figures

Bibliography

[1] G. Gallego, T. Delbrück, G. Orchard, C. Bartolozzi, B. Taba, A. Censi, S. Leutenegger, A. J. Davison, J. Conradt, K. Daniilidis, *et al.*, "Event-based vision: A survey," *IEEE transactions on pattern analysis and machine intelligence*, vol. 44, no. 1, pp. 154–180, 2020.

[2] V. K. Mishra, S. Kumar, and N. Shukla, "Image acquisition and techniques to perform image acquisition," *SAMRIDDHI: A Journal of Physical Sciences, Engineering and Technology*, vol. 9, no. 01, pp. 21–24, 2017.

[3] X. Xiao, X. Chen, Z. Kang, S. Guo, and L. Wang, "A spatio-temporal event data augmentation method for dynamic vision sensor," in *Neural Information Processing* (M. Tanveer, S. Agarwal, S. Ozawa, A. Ekbal, and A. Jatowt, eds.), (Singapore), pp. 422–433, Springer Nature Singapore, 2023.

[4] C. Posch, T. Serrano-Gotarredona, B. Linares-Barranco, and T. Delbruck, "Retinomorphic event-based vision sensors: Bioinspired cameras with spiking output," *Proceedings of the IEEE*, vol. 102, no. 10, pp. 1470–1484, 2014.

[5] M. Piccardi, "Background subtraction techniques: a review," in *2004 IEEE international conference on systems, man and cybernetics (IEEE Cat. No. 04CH37583)*, vol. 4, pp. 3099–3104, IEEE, 2004.

[6] M. B. Milde, O. J. Bertrand, H. Ramachandran, M. Egelhaaf, and E. Chicca, "Spiking elementary motion detector in neuromorphic systems," *Neural computation*, vol. 30, no. 9, pp. 2384–2417, 2018.

[7] C. F. Stevens, "The neuron," *Scientific American*, vol. 241, no. 3, pp. 54–65, 1979.

[8] R. Llinas, "Neuron," *Scholarpedia*, vol. 3, no. 8, p. 1490, 2008. revision #91571.

[9] M. W. Barnett and P. M. Larkman, "The action potential," *Practical Neurology*, vol. 7, no. 3, pp. 192–197, 2007.

[10] G. Bontorin Alves, *Matrice d'électrodes intelligentes: un outil pour améliorer les performances spatiotemporelles des systèmes hybrides (vivant-artificiel), en boucle*

fermée et en temps réel. PhD thesis, 2010.

[11] Wikipedia contributors, "Action potential — Wikipedia, the free encyclopedia," 2024. [Online; accessed 1-May-2024].

[12] R. Llinás and M. Sugimori, "Electrophysiological properties of in vitro purkinje cell dendrites in mammalian cerebellar slices.," *The Journal of Physiology*, vol. 305, no. 1, pp. 197–213, 1980.

[13] J. Schiller, G. Major, H. J. Koester, and Y. Schiller, "Nmda spikes in basal dendrites of cortical pyramidal neurons," *Nature*, vol. 404, no. 6775, pp. 285–289, 2000.

[14] A. Gidon, T. A. Zolnik, P. Fidzinski, F. Bolduan, A. Papoutsi, P. Poirazi, M. Holtkamp, I. Vida, and M. E. Larkum, "Dendritic action potentials and computation in human layer 2/3 cortical neurons," *Science*, vol. 367, no. 6473, pp. 83–87, 2020.

[15] K. Boahen, "Dendrocentric learning for synthetic intelligence," *Nature*, vol. 612, no. 7938, pp. 43–50, 2022.

[16] N. L. Golding and N. Spruston, "Dendritic sodium spikes are variable triggers of axonal action potentials in hippocampal ca1 pyramidal neurons," *Neuron*, vol. 21, no. 5, pp. 1189–1200, 1998.

[17] V. S. Ramachandran, *Encyclopedia of the human brain*. Elsevier, 2002.

[18] R. A. Silver, "Neuronal arithmetic," *Nature Reviews Neuroscience*, vol. 11, no. 7, pp. 474–489, 2010.

[19] P. Poirazi and A. Papoutsi, "Illuminating dendritic function with computational models," *Nature Reviews Neuroscience*, vol. 21, no. 6, pp. 303–321, 2020.

[20] A. T. Gulledge, B. M. Kampa, and G. J. Stuart, "Synaptic integration in dendritic trees," *Journal of neurobiology*, vol. 64, no. 1, pp. 75–90, 2005.

[21] T. Branco, B. A. Clark, and M. Häusser, "Dendritic discrimination of temporal input sequences in cortical neurons," *Science*, vol. 329, no. 5999, pp. 1671–1675, 2010.

[22] H. Barlow and W. R. Levick, "The mechanism of directionally selective units in rabbit's retina.," *The Journal of physiology*, vol. 178, no. 3, p. 477, 1965.

[23] A. Brombas, X. Zhou, and S. R. Williams, "Light-evoked dendritic spikes in sustained but not transient rabbit retinal ganglion cells," *Neuron*, vol. 110, no. 17, pp. 2802–2814, 2022.

[24] M. London and M. Häusser, "Dendritic computation," *Annu. Rev. Neurosci.*, vol. 28, pp. 503–532, 2005.

[25] N. Spruston, "Pyramidal neuron," *Scholarpedia*, vol. 4, no. 5, p. 6130, 2009. revision #130430.

[26] J. Bezanson, A. Edelman, S. Karpinski, and V. B. Shah, "Julia: A fresh approach to numerical computing," *SIAM Review*, vol. 59, no. 1, pp. 65–98, 2017.

[27] C. Rackauckas and Q. Nie, "DifferentialEquations.jl–a performant and feature-rich ecosystem for solving differential equations in Julia," *Journal of Open Research Software*, vol. 5, no. 1, 2017.

[28] R. Veltz, "BifurcationKit.jl," July 2020.

A. Appendix

A.1. Extension to 2-dimensional movement detection

$$I = \begin{pmatrix} w_{1,1} & w_{1,2} & w_{1,3} & w_{1,4} & w_{1,5} & w_{1,6} & w_{1,7} & w_{1,8} & w_{1,9} & w_{1,10} & w_{1,11} & w_{1,12} & w_{1,13} \\ w_{2,1} & w_{2,2} & w_{2,3} & w_{2,4} & w_{2,5} & w_{2,6} & w_{2,7} & w_{2,8} & w_{2,9} & w_{2,10} & w_{2,11} & w_{2,12} & w_{2,13} \\ w_{3,1} & w_{3,2} & w_{3,3} & w_{3,4} & w_{3,5} & w_{3,6} & w_{3,7} & w_{3,8} & w_{3,9} & w_{3,10} & w_{3,11} & w_{3,12} & w_{3,13} \\ w_{4,1} & w_{4,2} & w_{4,3} & w_{4,4} & w_{4,5} & w_{4,6} & w_{4,7} & w_{4,8} & w_{4,9} & w_{4,10} & w_{4,11} & w_{4,12} & w_{4,13} \\ w_{5,1} & w_{5,2} & w_{5,3} & w_{5,4} & w_{5,5} & w_{5,6} & w_{5,7} & w_{5,8} & w_{5,9} & w_{5,10} & w_{5,11} & w_{5,12} & w_{5,13} \\ w_{6,1} & w_{6,2} & w_{6,3} & w_{6,4} & w_{6,5} & w_{6,6} & w_{6,7} & w_{6,8} & w_{6,9} & w_{6,10} & w_{6,11} & w_{6,12} & w_{6,13} \\ w_{7,1} & w_{7,2} & w_{7,3} & w_{7,4} & w_{7,5} & w_{7,6} & w_{7,7} & w_{7,8} & w_{7,9} & w_{7,10} & w_{7,11} & w_{7,12} & w_{7,13} \\ w_{8,1} & w_{8,2} & w_{8,3} & w_{8,4} & w_{8,5} & w_{8,6} & w_{8,7} & w_{8,8} & w_{8,9} & w_{8,10} & w_{8,11} & w_{8,12} & w_{8,13} \\ w_{9,1} & w_{9,2} & w_{9,3} & w_{9,4} & w_{9,5} & w_{9,6} & w_{9,7} & w_{9,8} & w_{9,9} & w_{9,10} & w_{9,11} & w_{9,12} & w_{9,13} \\ w_{10,1} & w_{10,2} & w_{10,3} & w_{10,4} & w_{10,5} & w_{10,6} & w_{10,7} & w_{10,8} & w_{10,9} & w_{10,10} & w_{10,11} & w_{10,12} & w_{10,13} \\ w_{11,1} & w_{11,2} & w_{11,3} & w_{11,4} & w_{11,5} & w_{11,6} & w_{11,7} & w_{11,8} & w_{11,9} & w_{11,10} & w_{11,11} & w_{11,12} & w_{11,13} \\ w_{12,1} & w_{12,2} & w_{12,3} & w_{12,4} & w_{12,5} & w_{12,6} & w_{12,7} & w_{12,8} & w_{12,9} & w_{12,10} & w_{12,11} & w_{12,12} & w_{12,13} \\ w_{13,1} & w_{13,2} & w_{13,3} & w_{13,4} & w_{13,5} & w_{13,6} & w_{13,7} & w_{13,8} & w_{13,9} & w_{13,10} & w_{13,11} & w_{13,12} & w_{13,13} \end{pmatrix} \tag{A.1}$$

A.1.1. Horizontal Interconnection Matrix

$$I_H = \begin{pmatrix} 0 & 0 & 0 & 0 & 1.75 & 0 & 0 & 1.5 & 1.5 & 0 & 0 & 0 & 0 \\ 0 & 0 & 0 & 0 & 1.25 & 0 & 0 & 0 & 1.5 & 0 & 0 & 0 & 0 \\ 1.75 & 1.25 & 0 & 1.25 & 0 & 0 & 0 & 0 & 0 & 0 & 0 & 0 & 0 \\ 0 & 0 & 0 & 0 & 1.25 & 0 & 0 & 1.5 & 0 & 0 & 0 & 0 & 0 \\ 0 & 0 & 0 & 0 & 0 & 0 & 0 & 0 & 0 & 0 & 0 & 0 & 1.75 \\ 1.25 & 1.5 & 0 & 0 & 0 & 0 & 0 & 0 & 0 & 1.25 & 0 & 0 & 0 \\ 1.25 & 0 & 0 & 1.75 & 0 & 0 & 0 & 0 & 0 & 0 & 0 & 1.25 & 0 \\ 0 & 0 & 0 & 0 & 0 & 0 & 0 & 0 & 0 & 0 & 0 & 0 & 1.5 \\ 0 & 0 & 0 & 0 & 0 & 0 & 0 & 0 & 0 & 0 & 0 & 0 & 1.5 \\ 0 & 0 & 0 & 0 & 0 & 0 & 0 & 0 & 1.25 & 0 & 0 & 0 & 0 \\ 0 & 0 & 1.75 & 0 & 0 & 1.5 & 1.5 & 0 & 0 & 0 & 0 & 0 & 0 \\ 0 & 0 & 0 & 0 & 0 & 0 & 0 & 1.25 & 0 & 0 & 0 & 0 & 0 \\ 0 & 0 & 0 & 0 & 0 & 0 & 0 & 0 & 0 & 0 & 0 & 0 & 1 \end{pmatrix} \quad \text{(A.2)}$$

A.1.2. Vertical Interconnection Matrix

$$I_V = \begin{pmatrix} 0 & 0 & 0 & 1.75 & 0 & 0 & 1.5 & 1.5 & 0 & 0 & 0 & 0 & 0 \\ 1.75 & 0 & 1.25 & 0 & 1.25 & 0 & 0 & 0 & 0 & 0 & 0 & 0 & 0 \\ 0 & 0 & 0 & 1.25 & 0 & 0 & 1.5 & 0 & 0 & 0 & 0 & 0 & 0 \\ 0 & 0 & 0 & 0 & 0 & 0 & 0 & 0 & 0 & 0 & 0 & 1.75 & 0 \\ 0 & 0 & 0 & 1.25 & 0 & 0 & 0 & 1.5 & 0 & 0 & 0 & 0 & 0 \\ 1.25 & 0 & 1.75 & 0 & 0 & 0 & 0 & 0 & 0 & 0 & 1.25 & 0 & 0 \\ 0 & 0 & 0 & 0 & 0 & 0 & 0 & 0 & 0 & 0 & 0 & 1.5 & 0 \\ 0 & 0 & 0 & 0 & 0 & 0 & 0 & 0 & 0 & 0 & 0 & 1.5 & 0 \\ 1.25 & 0 & 0 & 0 & 1.75 & 0 & 0 & 0 & 0 & 0 & 0 & 0 & 1.25 \\ 0 & 1.75 & 0 & 0 & 0 & 1.5 & 0 & 0 & 1.5 & 0 & 0 & 0 & 0 \\ 0 & 0 & 0 & 0 & 0 & 0 & 1.25 & 0 & 0 & 0 & 0 & 0 & 0 \\ 0 & 0 & 0 & 0 & 0 & 0 & 0 & 0 & 0 & 0 & 0 & 1 & 0 \\ 0 & 0 & 0 & 0 & 0 & 0 & 0 & 1.25 & 0 & 0 & 0 & 0 & 0 \end{pmatrix} \quad \text{(A.3)}$$

A.1.3. Diagonal Interconnection Matrix

$$I_D = \begin{pmatrix} 0 & 1.5 & 1.5 & 0 & 0 & 1.75 & 0 & 0 & 0 & 0 & 0 & 0 & 0 \\ 0 & 0 & 0 & 0 & 0 & 1.5 & 0 & 0 & 0 & 1.5 & 0 & 0 & 0 \\ 0 & 0 & 0 & 0 & 0 & 1.5 & 0 & 0 & 0 & 0 & 1.5 & 0 & 0 \\ 0 & 0 & 1.75 & 0 & 0 & 0 & 0 & 0 & 0 & 0 & 0 & 0 & 0 \\ 0 & 1.75 & 0 & 0 & 0 & 0 & 0 & 0 & 0 & 0 & 0 & 0 & 0 \\ 0 & 0 & 0 & 0 & 0 & 1 & 0 & 0 & 0 & 0 & 0 & 0 & 0 \\ 0 & 0 & 0 & 0 & 0 & 0 & 0 & 0 & 0 & 0 & 1.75 & 0 & 0 \\ 1.75 & 0 & 0 & 1.5 & 1.5 & 0 & 0 & 0 & 0 & 0 & 0 & 0 & 0 \\ 0 & 0 & 0 & 0 & 0 & 0 & 0 & 0 & 0 & 1.75 & 0 & 0 & 0 \\ 0 & 0 & 0 & 0 & 0 & 0 & 0 & 0 & 0 & 1 & 0 & 0 & 0 \\ 0 & 0 & 0 & 0 & 0 & 0 & 0 & 0 & 0 & 0 & 1 & 0 & 0 \\ 0 & 0 & 0 & 0 & 0 & 0 & 1.75 & 0 & 0 & 0 & 0 & 0 & 0 \\ 0 & 0 & 0 & 0 & 0 & 0 & 0 & 0 & 1.75 & 0 & 0 & 0 & 0 \end{pmatrix} \quad \text{(A.4)}$$